Optimal Active Control of Flexible Structures Applying Piezoelectric Actuators

by

Neda Darivandi Shoushtari

A thesis
presented to the University of Waterloo
in fulfillment of the
thesis requirement for the degree of
Doctor of Philosophy
in
Mechanical Engineering

Waterloo, Ontario, Canada, 2013

I hereby declare that I am the sole author of this thesis. This is a true copy of the thesis, including any required final revisions, as accepted by my examiners.

I understand that my thesis may be made electronically available to the public.

Neda Darivandi Shoushtari

Abstract

Piezoelectric actuators have proven to be useful in suppressing disturbances and shape control of flexible structures. Large space structures such as solar arrays are susceptible to large amplitude vibrations while in orbit. Moreover, Shape control of many high precision structures such as large membrane mirrors and space antenna is of great importance. Since most of these structures need to be ultra-light-weight, only a limited number of actuators can be used. Consequently, in order to obtain the most efficient control system, the locations of the piezoelectric elements as well as the feedback gain should be optimized. These optimization problems are generally non-convex. In addition, the models for these systems typically have a large number of degrees of freedom.

Researchers have used numerous optimization criteria and optimization techniques to find the optimal actuator locations in structural shape and vibration control. Due to the non-convex nature of the problem, evolutionary optimization techniques are extensively used. However, One drawback of these methods is that they do not use the gradient information and so convergence can be very slow. Classical gradient-based techniques, on the other hand, have the advantage of accurate computation; however, they may be computationally expensive, particularly since multiple initial conditions are typically needed to ensure that a global optimum is found. Consequently, a fast, yet global optimization method applicable to systems with a large number of degrees of freedom is needed.

In this study, the feedback control is chosen to be an optimal linear quadratic regulator. The optimal actuator location problem is reformulated as a convex optimization problem. A subgradient-based optimization scheme which leads to the global solution of the problem is introduced to optimize the actuator locations. The optimization algorithm is applied to optimize the placement of piezoelectric actuators in vibration control of flexible structures. This method is compared with a genetic algorithm, and is observed to be faster in finding the global optimum.

Moreover, by expanding the desired shape into the structure's modes of vibration, a methodology for shape control of structures is presented. Applying this method, locations of piezoelectric actuators on flexible structures are optimized.

Very few experimental studies exist on shape and vibration control of structures. To the best knowledge of the author, optimal actuator placement in shape control has not been experimentally studied in the past. In this work, vibration control of a cantilever beam is investigated for various actuator locations and the effect of optimal actuator placement is studied on suppressing disturbances to the beam. Also using the proposed shape control method, the effect of optimal actuator placement is studied on the same beam. The final shape of the beam and input voltages of actuators are compared for various actuator placements.

Acknowledgements

Completing this dissertation would not have occurred but for the support patience, and guidance of my supervisors Professor Amir Khajepour and Professor Kirsten Morris. They reached out to me during all the difficult times in the dissertation process.

I would also like to express my gratitude to the examining committee members Professor Hamid Jahed, Professor Baris Fidan, Professor Stephen Vavasis whose comments and suggestions were extremely helpful in improving my manuscript. Special thanks to Professor Donatus Oguamanam from Ryerson University for accepting to be my external examiner.

Over the last four years I have been privileged to work with and learn from my colleagues Masood Ansari, Saman Mohammadi, Mohammad Basirinia, Negar Rasti, Babak Ebrahimi, Dhanaraja Kasinathan and Soroosh Hassanpour. Especially I would like to thank my lovely husband Mohammad Pournazeri for his endless support, patience and dedication during my research. He has been my best friend and colleague.

I wish to express thanks to all my family members, Sadugh Dorri, Mohammad Darivandi and Navid Darivandi for their constant support and love.

Dedication

For Mohammad Pournazeri my dear husband and Sadugh Dorri, Mohammad Darivandi, Navid Darivandi, my lovely family, whose unconditional love and support empowered me through all the stages in my life.

Table of Contents

List of Tables **xv**

List of Figures **xvii**

1 Introduction **1**

1.1 Modeling and Analysis of Piezoelectrically Actuated Structures 4

1.1.1 Characteristic Equations of Piezoelectric Materials 4

1.1.2 Modeling and Analysis of Smart Structures 5

1.2 Control Method 6

1.3 Active Vibration Control of Flexible Structures 7

1.4 Active Shape Control of Flexible Structures 8

1.5 Optimal Actuator Placement 8

1.5.1 Optimization Criteria 10

1.5.2 Optimization Method 14

1.6 Experimental Study 16

1.7 Summary 17

2 Optimization Scheme **19**

2.1 Problem Formulation 20

2.2 Optimization Method 23

2.3 Integer Optimization Algorithm 26

2.3.1 Branch and Bound Method 26

2.3.2 Minimax Optimization Method 28

2.3.3 Example 30

2.4 Summary 32

3 Optimal Actuator Placement in Vibration Control **35**

3.1 Vibration Control with piezoelectric actuator patches 36

3.2 Energy Realization 38

3.3 Optimal Actuator Placement in Structures 39

3.3.1 Beams with pinned end conditions 41

3.3.2 Optimal Actuator Locations on Cantilever Beams 46

3.3.3 Optimal Actuator Locations on the beam with fixed-pinned boundary conditions 47

3.3.4 Comparison with a genetic algorithm 49

3.3.5 Optimal actuator locations in plates and comparison with a genetic algorithm 51

3.4 Summary 58

4 Optimal Actuator Placement in Shape Control **61**

4.1 Shape Control Method 62

4.2 Optimal Actuator Placement in Structures 68

4.2.1 Optimal Actuator Locations on a Cantilever Beam 72

4.2.2 Optimal Actuator Locations on a Simply Supported Beam 78

4.2.3 Optimal Actuator Locations on Plates 83

5 Experimental Study of Optimal Shape and Vibration Control **93**

5.1 Experimental Setup 94

5.2 Damping Estimation 98

5.3 Verification of Finite Element Model 100

5.4 State Estimation 102

5.5 Optimal Sensor Location 104

5.6 Vibration Control 107

5.7 Shape Control 112

6 Summary and Future Work **123**

6.1 Key Contributions 123

6.2 Future Work 126

References **127**

List of Tables

2.1 Comparison of proposed optimization method and genetic algorithm on simple example (2.16). A population size of 20 was used for the genetic algorithm. . . 32

3.1 Material Properties 40

3.2 Optimal actuator locations on a beam with pinned end conditions 44

3.3 Optimal actuator locations on a beam with pinned end conditions 48

3.4 Optimal actuator locations on a fixed-pinned beam 50

3.5 Optimal location of 10 actuators on a beam with pinned end conditions 51

3.6 Comparison of GA and the introduced algorithm for the cantilevered plate . . . 53

3.7 Comparison of GA and the introduced algorithm for the plate with pinned end conditions 56

4.1 Material properties of steel and piezoelectric materials 71

4.2 Optimal actuator locations on a 3m long cantilever beam for desired shape s_{d3} . 78

4.3 Optimal locations of 10 actuators on a 3m long simply supported beam for desired shape s_{d5} 82

5.1 Dimensions of the beam and the piezoelectric patches 95

5.2 Material Properties 96

5.3 Specifications of non-contact laser sensors 98

5.4 Decay ratio in the beam's vibration amplitude in 10 seconds 99

5.5 The first three natural frequencies of the beam with and without actuators . . . 101

5.6 Suppression time for various actuating positions 108

5.7 Suppression time for various actuating positions 111

5.8 Actuator input voltages for various actuator locations 117

List of Figures

2.1 Branch Tree 27

2.2 Function $\sigma(p)$ 31

3.1 Structure with a piezoelectric patch 36

3.2 Optimal location of 1 actuator on a 0.5 m long beam with pinned end conditions 42

3.3 The beam's response at the mid-point to an impulse at one fourth of the beam's length for optimal and non-optimal actuator locations on a 0.5m long beam with pinned end conditions 43

3.4 Optimal location of 5 actuators on a beam with pinned end conditions 43

3.5 First Modal Strain Energy for the beam with pinned ends 45

3.6 Second Modal Strain Energy for the beam with pinned ends 45

3.7 Number of modes required to accurately calculate the optimal location of actuators 46

3.8 Optimal location of one actuator on a 0.5 m long cantilever beam 47

3.9 Optimal location of one actuator on a 0.5 m long cantilever beam 47

3.10 First Modal Strain Energy for a cantilever beam 48

3.11 Optimal location of one actuator on a beam with pinned-fixed end conditions . 49

3.12 Optimal location of 5 actuators on a beam with pinned-fixed end conditions . . 49

3.13 First Modal Strain Energy for a beam with pinned-fixed end conditions 50

3.14 Optimal Location of one Actuator on a cantilever steel plate 52

3.15 Non-optimal actuator locations 52

3.16 Displacements at the plate tip subjected to a vertical impulse at its tip 53

3.17 Optimal Location of 10 actuators on a cantilever plate 54

3.18 Non-optimal Actuator Locations 55

3.19 Displacements at the plate tip for ten actuators 55

3.20 Optimal location of actuators on a plate with pinned end conditions 56

3.21 Optimal location of actuators on a plate with pinned end conditions applying GA 57

3.22 First modal strain energy of the plate with pinned end conditions on its two opposite edges 57

3.23 Second modal strain energy of the plate with pinned end conditions on its two opposite edges 58

3.24 Third modal strain energy of the plate with pinned end conditions on its two opposite edges 59

3.25 Optimal location of actuators on a plate with pinned end conditions applying only the first three modes of plate to model it 59

4.1 Structure with a piezoelectric patch 69

4.2 A 0.5m long cantilever beam divided into 15 finite elements 72

4.3 Third and fifth modes of vibration for a cantilever beam 73

4.4 Optimal actuator locations for a 0.5m long cantilever beam for desired shape s_{d1} 74

4.5 Comparison between achieved shapes and desired shape s_{d1} for a 0.5m long cantilever beam 75

4.6 Optimal actuator locations for a 0.5m long cantilever beam for desired shape s_{d2} 76

4.7 Comparison between achieved shapes and desired shape s_{d2} on a 0.5m long cantilever beam 77

4.8 Comparison between desired shape s_{d2} and achieved shapes with 6 actuators on a 0.5m long cantilever beam 78

4.9 Comparison between desired shape s_{d3} and achieved shapes on a 3m long cantilever beam with 10 actuators 79

4.10 A simply supported beam 79

4.11 Optimal actuator locations for a 0.5 m long simply supported beam for desired shape s_{d4} 80

4.12 Comparison between desired shape s_{d4} and achieved shapes on a 0.5m long simply supported beam 81

4.13 Comparing desired shape s_{d5} and achieved shapes on a 3m long simply supported beam with 10 actuators 82

4.14 A cantilever plate 84

4.15 Optimal actuator locations on a cantilever plate for desired shape s_{d6} applying two different optimization schemes 85

4.16 The achieved and desired shapes with 10 actuators on a cantilever plate 87

4.17 The errors between achieved and desired shape s_{d6} on a cantilever plate 88

4.18 A plate with pinned boundary conditions on its two opposite edges 89

4.19 Optimal actuator locations for desired shape s_{d7} on a cantilever plate applying two different optimization schemes 89

4.20 The achieved and desired shape s_{d7} on a plate with pinned boundary conditions on its two opposite edges 90

4.21 The errors between achieved and desired shape s_{d7} on a plate with pinned boundary conditions on its two opposite edges 91

5.1 Experimental setup for vibration control and shape control of a steel cantilever beam 94

5.2 Piezoelectric patch bonded to the beam's surface 95

5.3 The beam, actuators and sensors 96

5.4 Experimental beam model and the actuator and sensor positions 98

5.5 Block diagram of the experimental setup 99

5.6 Frequency response of the beam without actuators 100

5.7 Frequency response of the beam with actuators 101

5.8 Possible sensor locations 106

5.9 Optimal sensor locations 107

5.10 Beam's tip displacement to compare experimental and analytical results 108

5.11 Beam's near tip displacement with different actuating locations in vibration control experiment 109

5.12 Input voltage of actuators 110
5.13 Beam's tip displacement with different actuating locations in vibration control . 111
5.14 Input voltage of actuators at positions 1 and 2 112
5.15 Input voltage of actuators at positions 1 and 2 113
5.16 The desired shape for the beam 113
5.17 Unfiltered displacement with actuators at positions 1 and 3 114
5.18 Actuators at positions 1 and 2 in shape control 116
5.19 Achieved displacement in repeated experiments 118
5.20 Displacement with actuators at positions 1 and 3 in shape control 119
5.21 Input voltages of actuators at positions 1 and 3 in shape control 119
5.22 Displacement with actuators at positions 2 and 3 in shape control 120
5.23 Input voltages of actuators at positions 2 and 3 in shape control 120
5.24 Comparison of displacements for various actuator placements 121

Chapter 1

Introduction

Active shape and vibration control of flexible structures has recently become a popular research interest in modern space industries. In vibration control, it is desired to suppress the effect of external disturbances and keep the structure in its equilibrium position. In shape control it is intended to deform the structure to a desired shape and position and maintain the structure in the desired shape. For instance, ultra-light-weight large-scale space structures such as solar sails and solar arrays are susceptible to large amplitude vibrations while in orbit. In extreme cases, these disturbances may lead to instability of the overall structure [1]. Moreover, shape control of some high-precision structures, such as space antennas and reflectors, is an issue of concern [2].

In the past few decades, application of piezoelectric actuators in active control of structures has raised interest in modeling and control of smart structures. These actuators are inexpensive and available in various shapes and sizes and can be easily bonded to any structure [3]. In addition, membranes can now be used as surfaces for satellites and reflectors [4]. The small thickness of these key components makes it necessary to apply actuators with the least impact on

the system's dynamics. Consequently, their light weight, make piezoelectric materials suitable to be applied as sensors and/or actuators in space structures.

While considerable research has been focused on active vibration suppression of flexible structures, less effort has been dedicated to the use of smart structures for shape control. However, shape control, arises in many applications, especially when precise tolerances of structure surfaces are necessary [2].

One essential factor in designing these active control systems is suitable placement of the actuators (and sensors) since misplaced sensors and actuators lead to degradation of performance [5]. Judicious selection of actuator locations can be particularly challenging when there are multiple actuators because an ad hoc procedure is not feasible. Researchers have used numerous optimization criteria and optimization techniques to find the optimal actuator locations in vibration control. Different results can be achieved with different cost functions. A numerical challenge with any criterion is that the resulting optimization problem is generally non-convex. Moreover, for simulation and controller design, distributed parameter systems are approximated, for instance by finite elements methods. For complex systems with several state space variables a large number of elements is required for accurate modeling. As the number of elements increases, calculation of the optimal actuator placement can be computationally costly, particularly due to the non-convexity of the actuator location problem. Consequently, there is a need for a fast and accurate optimization algorithm that can be used for structures where there is a large number of degrees of freedom.

Some new studies have focused on applying evolutionary algorithms to find the optimal locations. A major drawback of these methods is their low convergence speed since they do not use the gradient information. This is particularly an issue for control of systems, such as structures where a large number of state variables are needed for accuracy, due to high computational time of the genetic algorithms as the number of design variables increases. Classical

gradient-based techniques, on the other hand, have the advantage of using the gradient information. However, multiple initial conditions are typically needed to ensure that a global optimum is found. Consequently, despite the non-convex nature of this optimization problem, it is quite helpful to seek methods that use gradient-based information. Consequently, a fast, yet global optimization method applicable to systems with a large number of degrees of freedom is needed.

The aim of this study is to investigate the optimal shape and vibration control of flexible structures augmented with piezoelectric actuator patches. In this study, a linear quadratic cost function for multi-input systems is considered. It is desired to optimize the locations of control devices on flexible structures. The optimal linear quadratic cost is taken as the objective function. It has been shown that by mapping actuator locations into zero-one vectors and projecting the solution of the Riccati equation, to a space of design parameters, the cost function becomes convex in the new topology [6]. This approach has been used to develop a gradient-based optimization algorithm that finds the optimal actuator locations. Note that due to the reformulation of the problem as a convex problem, the calculated locations are globally optimal. The optimization scheme is discussed in detail in Chapter 2.

The optimal actuator placement is studied in detail for shape control and vibration control and the results are compared with a genetic algorithm to verify accuracy. Chapter 3 discusses the optimal actuator placement in vibration control. In Chapter 4 a methodology is introduced for shape control of structures. Further, the optimal actuator placement in shape control is investigated.

Chapter 5 includes experimental studies on both optimal vibration control and shape control. The importance of optimal actuator placement is discussed in this Chapter. Chapter 6 includes the summary of this study and suggests future works to complete the optimal shape and vibration control topics.

1.1 Modeling and Analysis of Piezoelectrically Actuated Structures

Piezoelectric materials are among the most commonly used smart materials. They have the ability to generate an electric charge proportional to their externally applied load in a certain direction, a characteristic known as direct piezoelectric effect [3]. Conversely, an electric field induces deformation in a piezoelectric material - the inverse piezoelectric effect. This effect is used in piezoelectric actuators' design.

Ceramics and polymers are the two classes of piezoelectric materials primarily used in vibration control. Lead zirconate titanate also called PZT is a piezoceramic that can be used as an actuator and sensor for a wide range of frequencies. PZT materials can withstand high strain energies and can be easily bonded to a structure. Piezopolymers are used mainly as sensors; Polyvinylidene fluoride (PVDF), for example is one member of this material category [7].

1.1.1 Characteristic Equations of Piezoelectric Materials

The constitutive equations of piezoelectric materials can be written as

$$\sigma = C_E S + e\nabla\phi \tag{1.1a}$$

$$D = eS - \epsilon\nabla\phi, \tag{1.1b}$$

where, σ is the stress vector, S is the strain vector, ϕ is the electric potential, C_E is the matrix of elastic constants under constant electric field (dependent on modulus of elasticity and Poisson's ration), ϵ is the electric permittivity matrix under constant mechanical strain, $e = dC$ contains the piezoelectric coupling constants, d is the dielectric constant matrix, and D is the electric displacement vector [8].

The elastic strain tensor and the electric field vector can be written as functions of displacement vector u and electric potential ϕ

$$S = \frac{1}{2}(\nabla u + u\nabla),$$

$$E = -\nabla\phi.$$

1.1.2 Modeling and Analysis of Smart Structures

Many authors have modeled piezolaminated beams analytically. Pan *et al.* modeled the dynamic response of a pure bending Euler-Bernoulli beam with one set of collocated sensor and actuator [9]. This modeling was corrected and extended by Rivory and Hansen [10]. The authors neglected the effect of mass and stiffness of the piezoelectric patches. At the same time, Yang and Lee studied the effect of mass and stiffness of piezoelectric layers on the natural frequencies and mode shapes of a beam structure [11].

Kim and Jones studied the dynamics of a finite dimensional beam with symmetric and asymmetric piezoelectric configurations [12]. The beam was entirely covered by the piezoelectric layer. Basak *et al.* modeled the finite beam with one set of symmetric and asymmetric patches which covered a part of the beam [13]. Khalatkar *et al.* used ANSYS finite element software to three-dimensionally model a cantilever plate augmented with piezoelectric actuator patches [14]. The authors studied the effect of actuator placement in efficiency of the control system. In [15] a finite element formulation was developed for modeling the dynamic and static response of laminated plates containing discrete piezoelectric ceramics subjected to both mechanical and electrical loadings.

For systems with more complicated boundary conditions and multiple piezoelectric patches, numerical methods are applied. Few authors have applied the finite difference method to model

the base structure and piezoelectric patches [16, 17, 18]. Due to its simplicity, the finite element method has gained more popularity. This method has been applied by many researchers [19, 20, 21] and has been a major area of research [22].

The electric potential at the upper and lower surfaces of a piezoelectric structure can be treated as electrical degrees of freedom in the finite element modeling. Through several simplifications, some researchers have deduced these quantities from finite element modeling . Some authors have used the mechanical finite element for very small piezoelectric patches, ignoring the electrical degrees of freedom [23, 24]. However, Bruant *et al.* mentioned that in the case of embedded piezoelectric or when large piezoelectric patches are used it is necessary to take the electrical degrees of freedom into account [25].

1.2 Control Method

Various control laws are applied to control active structures. In [26], three laws, direct proportional feedback, constant gain negative velocity feedback and linear quadratic regulator (LQR) optimal control laws are compared. It was concluded that since the negative velocity feedback adds damping to the system, it is much more effective than the direct proportional feedback which only adds stiffness to the system; however, the LQR optimal control scheme is even more effective than the other control laws. A review of the existing control measures in active and semi-active control of structures can be found in [27].

The LQR control law is applied in various studies. Bruant *et al.* employed a LQR control method which includes a state observer to compute the optimal control [25]. LQR control was also employed in [28]. Roy and Chakraborti used a genetic algorithm to find the optimum Q and R matrices in designing a LQR controller [21]. This control law is also used in this thesis.

1.3 Active Vibration Control of Flexible Structures

Since space structures are highly flexible, their performance is strongly affected external disturbances. In vibration control, the goal is to nullify the effect of external disturbances by applying a proper control actuation. Several active control methods have been used for structural vibration suppression.

Zabihollah *et al.* studied the concept of vibration suppression of layered laminated beams [20]. In [29], the influence of laminate configurations and locations of sensors/actuators on vibration responses of smart laminated beams under random loading was studied. In this paper the LQR was used to calculate the closed loop feedback control. Ruggiero and Inman studied vibration control of an active membrane mirror [30].

In [31] the authors studied active vibration control of an Euler-Bernoulli beam with piezoelectric actuators bonded to the top and bottom surfaces. They used optimal control theory to control the beam. Kwak *et al.* studied active vibration control of shells [32]. The paper focused on active vibration controller design. Through experiments, it was verified that piezoelectric actuators are effective in vibration control. In [33] vibration control of piezoelectric light weight structures was studied analytically and numerically. Modal truncation was applied and the controller was designed to suppress the first two flexural vibrations of the beam. In [34], Li *et al.* studied active vibration control of large flexible spacecrafts via the use of piezoelectric actuator stacks. The control devices were active tuned mass dampers which utilized piezoelectric materials. Butta *et al.* experimentally studied vibration control of gas turbine blades. Their aim was to minimize the vibrations and increase the fatigue life of gas turbine [35].

1.4 Active Shape Control of Flexible Structures

In a structural shape control, it is desired to deform a structure to a certain configuration. The need for shape control arises in many applications, such as membrane mirrors to improve their imaging quality [2]. The shape of some flexible structures needs to be precisely regulated to achieve the desired operation. This allows the weight of these structures to be reduced by replacing rigidizing members with active control devices. Irschik [36] reviewed some applications of static and dynamic shape control of structures by piezoelectrics.

In [37], Binette *et al.* analytically studied the shape control of composite structures with MFC actuators. These structures are subjected to temperature gradients throughout their thickness. Chellabi *et al.* designed an optimal tracking controller to shape the surface of a flexible mirror used in an adaptive optic system [38]. The authors took into account the dynamics of the mirror and included piezoelectric actuators as a control measure. Shaik Dawood *et al.* used a weighted shape control method to study the required input voltages of piezo-actuators in static shape control of composite plates [39]. Hu and Vukovich designed an LQR controller to keep the structure in a specified shape and reject disturbances [40]. Luo and Tong studied dynamic shape tracking in piezoelectric actuated structures [41]. Punahi developed a closed loop control method for dynamic shape control of a PVDF laminated plate with simply supported boundary conditions [42].

1.5 Optimal Actuator Placement

One essential factor in designing these active control systems is proper placement of the actuators (and sensors) since misplaced sensors and actuators lead to lack of controllability and observability in the system. Researchers have used numerous optimization criteria and tech-

niques to find the optimal actuator locations in vibration control of structures; see in particular the papers [43, 44, 45, 46, 47]. Different results can be achieved with different cost functions. A numerical challenge with any criterion is that the resulting optimization problem is generally non-convex.

Kumar and Narayanan studied the optimal location of collocated piezoelectric sensor/actuator patches to control vibrations on an Euler-Bernoulli cantilever beam [48]. The authors minimized the linear quadratic cost as the optimization objective function. Daraji and Hale optimized the location of piezoelectric sensor-actuator pairs on plates. The authors applied a genetic algorithm as the optimization method. The objective was to minimize the optimal linear quadratic control [49]. Li *et al.* studied optimal actuator placement in vibration control of satellite antenna reflector [50]. Piezoelectric actuator locations were optimized based on controllability and observability of the system. The authors employed a genetic algorithm as the optimization technique. Tianbing and Fei optimized piezoelectric sensors and actuators sizes and locations on beams. The authors applied chaos particle swarm algorithm for the optimization. The optimization was based on minimization of the stored and required control energy [51].

Marinova formulated the dynamics of a thin plate and studied the effectiveness of piezoelectric layers for plate shape control [52]. A genetic algorithm was finally used to find the optimal voltages for some preselected locations of piezoelectric actuators. Luo and Tong also optimized the piezo-stiffeners voltages in a plate shape control using the linear least squares method [53]. Liu *et al.* applied piezoelectric stiffeners to control the shape of a plate structure [47]. By the minimization of the square of the error between the actuated and desired shapes, their goal was to optimize the size and voltages of actuators. Chee *et al.* optimized the orientation of piezoelectric actuators for static shape control of composite plates [54]. Andoh *et al.* expanded the reference shape as a set of eigen functions and optimized the actuators' locations based on con-

trollability of the system [55]. Bruch *et al.* optimized the location and length of piezo-actuators for static shape control of beams [16]. Their objective was to find the minimum control effort for the maximum deflection of the beam. Applying a genetic algorithm, Yu *et al.* optimized the applied voltages to laminated piezoelectric actuators in static shape control of a cantilever beam structure [56]. Marinova formulated the dynamics of a thin plate and studied the effectiveness of piezoelectric layers on the plate shape control [52]. A genetic algorithm was applied to find the optimal voltages for some preselected locations of piezoelectric actuators. Kudikala *et al.* optimized the location of actuators and their input voltages in static shape control of plates [43]. They applied genetic algorithm to solve this multi-objective optimization problem. Sun and Tong studied the optimal location of piezoelectric patches in static shape control of composite plates [57]. The authors applied an evolutionary actuator location optimization method in which actuators with smallest voltages are removed sequentially until a desired error is reached.

Lui and Lin optimized voltage channel distribution and voltage of each channel for tracking dynamic shapes of the structure [58]. The authors applied a two-level optimization method based on a simulated annealing algorithm. In [59] a genetic algorithm is applied to optimize the location and input voltages of piezoelectric actuators for steering a parabolic antenna. In [60], the authors optimized the distribution of single channel input voltages in static shape control of structures.

1.5.1 Optimization Criteria

Over the past decade, researchers have applied numerous optimization criteria to find the optimal location of piezoelectric sensors and actuators. The most popular optimization criteria are controllability measures and linear quadratic control. In this section, these criteria and some other optimization criteria are reviewed.

Controllability Measures

To locate actuators in a linear time-invariant system

$$\begin{aligned} \dot{x}(t) = Ax(t) + Bu(t), \quad x(0) = x_0 \\ y(t) = Cx(t) \end{aligned},$$

where $x(t)$ and $u(t)$ are state and input vectors respectively, it is desirable to minimize the required control energy, J_c, to bring the system to a final state x_f. Consequently, this optimization problem can be defined as

$$min_u J_c = \int_0^{t_f} u^T(t)u(t)dt,$$

subjected to the system dynamics with given initial and final conditions. The solution to this problem is

$$u_0(t) = -B^T e^{A(t_f - t)} W^{-1}(t)(e^{At_f} x_0 - x_f),$$

where $W(t)$ is called the controllability grammian of the system, stated as

$$W(t) = \int_0^t e^{A\tau} BB^T e^{A^T \tau} d\tau.$$

As a result, the minimum eigenvalue of the grammian matrix can be applied to estimate controllability of the system [61]. In [62], the objective function is defined based on the maximization of the trace of the grammian and to ensure that all eigenvalues of the grammian are large, the product of all eigenvalues is included in the objective function.

In [63], the authors applied modal controllability by investigating the product of the singular values of the normalized matrix B. The authors studied the piezoelectric locations based on maximum controllability while having the minimal change in the system's natural frequencies. In [19], they applied genetic algorithm to find the piezoelectric locations based on maximum controllability and minimum change in natural frequencies. The maximization of the product

of the singular values of the normalized matrix B is also considered in [64]. Many authors optimized actuator locations based on maximization of observability and controllability in active control methods [58, 65, 66, 67, 68].

Linear Quadratic Control

Linear quadratic control is a commonly used strategy for controller design which minimizes both the control and output energies simultaneously. It is intended to find the input $u(t)$ to minimize the quadratic cost function

$$J = \int_0^\infty (x^T(t)Qx(t) + u^T(t)Ru(t))dt,$$

where Q and R are positive semi-definite and positive definite matrices, respectively. The solution to this problem is

$$u_{opt}(t) = -R^{-1}B^T Px(t),$$

and the optimal cost is

$$J_{opt} = x_0^T Px_0,$$

where x_0 indicates the initial condition and P is the solution of algebraic Riccati equation (ARE)

$$A^T P + PA - PBR^{-1}B^T P + Q = 0.$$

Several studies are focused on the minimization of the linear quadratic cost e.g. [5, 48, 69, 70]. Kumar and Narayanan applied the optimal quadratic regulator controller to find the optimal placement of collocated piezoelectric sensor/actuator pairs [5]. They minimized the LQR performance as the objective function of a zero-one optimization problem, and solved it by applying a genetic algorithm. Ruggiero and Inman developed an LQR controller to suppress vibrations in a Kapton membrane with a PZT biomorph [30].

As a performance index, LQR has proved to be effective for placing and sizing actuators. Specifically, for an optimal actuator location problem, Geromel showed that by mapping actuator locations into zero-one vectors and projecting the solution of Riccati equation to a special space of design parameters, the minimum cost shows convexity properties [6]. A formulation to find the global solution of this problem was presented. Based on this formulation Geromel described an optimization method which made it possible to find the optimal location of actuators. Moreover, the optimal control equation cannot be solved unless, finite-rank approximations are made, which lead to solving a finite-dimensional ARE. In [71], Morris developed conditions for convergence of the approximated optimal cost to its exact value and mentioned that the sequence of Riccati operators need to converge uniformly to the exact operators.

Other Objective Functions

Ning applied an eigenvalue distribution of energy correlative matrix of control input force to determine the optimal number of actuators and the genetic algorithm with the objective of active vibration control effects to find the optimum actuators location [72]. In [73], Barboni *et al.* tried to find the optimal placement of piezoelectric sensor/actuator pairs on a flexible beam by maximizing the dynamic influence function of the beam's deflection under the action of PZT patches. Kang *et al.* used the structural damping index which can be defined as the product of modal damping and mode shape function as the optimization objective function in laminated beams [74]. Yang *et al.* calculated the optimal size and location of collocated piezoelectric sensors/actuators as well as the optimal feedback control gain in a beam applying the genetic algorithm [75]. This optimization criterion was based on maximization of dissipated energy by the active controller. Seeger and Gabbert minimized the H_2 norm of the transfer function between an external excitation disturbance and the plate vibration amplitude to find the optimal positioning of collocated sensor/actuators on a simply supported plate [76]. Silva and Lopez

calculated the optimal location of actuators by using the H_∞ norm to excite the desired modes most effectively [77]. Kasinathan and Morris also used H_∞ norm as the performance index in optimal actuator placement [78].

In [79], the authors located piezoelectric actuators to maximize the harvested strain energy in piezoceramic materials. The objective in [80] was to minimize the vibration amplitude. In [81], actuators and sensors are located in buildings based on two objective functions, the number of sensors and actuators and the inter-story drifts. In [21], the optimization criterion was to maximize closed-loop damping ratio.

Kondoh *et al.* [82] proposed an optimization criterion based on minimization of the sum of the integrated square regulating error and the integrated square input.

1.5.2 Optimization Method

Most researchers have used evolutionary optimization techniques. In a number of studies, [19, 48, 83, 84, 85, 86], the authors used genetic algorithms. In [81] the authors optimized the location of sensors and actuators as well as the inter-story drifts of large civil structures applying a multi-objective genetic algorithm.

Some studies have applied particle swarm methods [68, 87, 88]. In [68], two swarm intelligence algorithms, the artificial bee colony and glow worm swarm optimization algorithms, were considered to obtain the optimal location of sensors and actuators. These algorithms mimic the behavior of insect swarms. Swarm methods are different from genetic algorithms since they are based on cooperation rather than competition. In [89, 90] an invasive weed optimization technique was applied, which is a new numerical stochastic technique and is inspired from the colonizing behavior of weeds.

In [91], the authors optimized sensor locations in structural health monitoring. They applied a new intelligent algorithm called monkey algorithm. In this method, the diversity of the monkeys is increased by introducing Hamming distance in the initial location, in order to improve the capacity of global search, and the random disturbance mechanism of Harmony search is introduced in the process of climbing to improve the capacity of local search. Harmony search is a metaheuristic algorithm that finds the best solution to a given problem without using the gradient function [92]. It is inspired by improvisation process of musicians. In [93], placement of sensors is optimized for detecting damages in composite structures. The problem is formulated as a minimax optimization in which the goal is to find the coordinates of a given number of sensors so that the worst (maximum) probability of non detection of the sensor network is made as good as possible (minimized). The authors used *fminimax* algorithm in MATLAB which applies sequential quadratic programming for the solution.

One drawback of many of these methods is that they do not use gradient information and so convergence can be very slow. This is particularly a problem when controlling structures where a large number of state variables are needed for accuracy. That is because genetic algorithms have a dramatic increase in computation time as the number of design variables increases. Classical gradient-based techniques, on the other hand, have the advantage of using gradient information; however, they may be computationally expensive [94, 95, 96]. Gradient-based optimization algorithms may lead to local minima. Consequently, multiple initial conditions are typically needed to ensure that a global optimum is found. Lee and Chen for instance, solved the optimal actuator location problem, using the gradient-based quasi-Newtonian algorithm [97]. To assure a global solution, the authors ran the algorithm with 380 different initial conditions and chose the best design.

A fast, yet accurate optimization method applicable to systems with a large number of degrees of freedom is needed. In [6] a gradient based optimization algorithm was introduced

by mapping the optimization objective into a convex function in a binary space of actuator locations. This optimization algorithm is extended in this thesis to be applicable to placement of arbitrary number of actuators on structures.

1.6 Experimental Study

Many experimental works on piezoelectric active structures so far has been conducted on aluminum or Kapton materials. Suhariono *et al.*, experimentally compared the efficiency of different types of piezoelectric patches on a cantilever aluminum beam [98]. The authors applied a laser displacement device to measure the displacement at the tip of the beam. Lou and Tong studied the dynamic shape tracking of piezoelectric smart structures. They validated their approach on an aluminum cantilever beam with two sets of piezo-actuators and applied eddy probes as displacement transducers [53]. Agrawal and Treanor carried out two phases of experiments on an aluminum cantilever beam with four groups of two piezoelectric patches attached to one side of the beam [99]. The authors investigated the performance of each actuator and also verified their analytical model for static shape control. They noticed some residual displacement on all measurement runs and a nonlinear relation between the actuator input voltage and the beam tip displacement. Roggiero experimentally verified the results of the derived dynamic model of a Kapton membrane strip with a PZT biomorph [30]. In this study, a vacuum chamber was used to minimize the effect of ambient air pressure, and, due to the excessively small thickness of the model, a laser vibrometer was used to measure the beam's response. The SigLab data acquisition board was used to excite the attached PZT biomorph. The same experimental setup was used in [2]. Yocum and Abramorich [100] experimentally studied the static behavior of a cantilever beam actuated using piezoceramic patches. In [101] switching control schemes were studied on an aluminum steel plate augmented with piezoelectric patches

as sensors and actuators. In this study the aim was to compare the performance of the proposed control scheme with traditional non-switched control schemes.

1.7 Summary

Many authors investigated optimal actuator placement in vibration control. In optimal vibration control, the actuators are placed to optimally suppress external disturbances. Relatively a smaller number of studies were focused on optimal shape control, where the actuator locations are calculated to optimally achieve a desired position for the structure. As can be anticipated from Section 1.5.1 various optimization criteria have been considered in optimal actuator placement. Different optimization criteria might lead to different results. Applying the linear quadratic regulator as the control law and optimizing the control effort with respect to actuator locations, also minimizes the control energy. This criteria is applied here to minimize actuator locations.

Moreover, as mentioned in Section 1.5.2, due to the non-convex nature of the objective function, many authors have used evolutionary techniques to solve the problem, which have their own difficulties for large host structures with a large number of degrees of freedom. Hence, in subsequent chapters of this thesis, a fast and accurate convex optimization algorithm is presented for structural shape and vibration control and its results are experimentally verified.

Chapter 2

Optimization Scheme

In this chapter, an optimization scheme is presented to optimize actuators' placement in flexible structures. This optimization algorithm is applicable to actuator placement problems in vibration and shape control. In Section 2.1 the optimization problem is formulated. An objective function is presented and a mapping algorithm introduced in [6] is used to transform the optimal actuator placement problem into a convex optimization problem. The applied objective function is not smooth. Consequently, an optimization scheme is presented in Section 2.2 which is applicable to a non-smooth objective function.

The formulation of the optimization method requires an integer optimization scheme for the solution. The optimization algorithm is composed of branch and bound technique for the integer part and a minimax optimization for the relaxation part. It is explained in Section 2.3. This section includes two parts. In the first part, the branch and bound method is explained in detail. In the second part, the minimax optimization is explained and sequential quadratic programming is presented to solve the minimax optimization.

2.1 Problem Formulation

Consider a linear time-invariant system,

$$\begin{aligned} \dot{x}(t) &= Ax(t) + Bu(t), \quad x(0) = x_0, \\ y(t) &= Cx(t). \end{aligned} \tag{2.1}$$

The control $u(t)$ is chosen to minimize a quadratic performance index

$$J = \int_0^\infty (x(t)^T Q x(t) + u(t)^T R u(t)) dt, \tag{2.2}$$

where Q and R are positive semi-definite and positive definite weighting matrices, respectively. For stabilizable (A, B) and detectable $(Q^{1/2}, A)$, the optimal cost is [102]

$$J_{opt} = x_0^T P x_0 \tag{2.3}$$

where P is the unique positive semi-definite solution of the algebraic Riccati equation (ARE)

$$A^T P + PA - PBR^{-1}B^T P + Q = 0. \tag{2.4}$$

The optimal control is

$$u(t) = -R^{-1}B^T P x(t) = -Gx(t).$$

The optimal cost (2.3) depends on the initial condition. This dependency can be handled in several ways, depending on the application. Most commonly, the initial condition that has the worst effect on the cost or else a random initial condition is considered. In this study, we optimize the actuator location by considering the worst initial condition. The cost is [71]

$$\max_{\|x_0\|=1} x_0^T P x_0 = \|P\|.$$

Letting λ_i indicate the eigenvalues of P,

$$\|P\| = \max_i \lambda_i.$$

Now consider the situation where there are a number of possible actuator locations. The control operator B in (2.1) is dependent on the actuator locations. This yields a cost $\|P\|$ that varies with actuator location. This cost function in general is a non-convex function of the actuator locations. However, in [6] the problem is re-formulated into a convex optimization problem. The formulation relies on considering a discrete set of N possible actuator locations. In some situations, the number of possible actuator locations is finite due to engineering constraints. In other cases, the region of possible actuator needs to be discretized. Since each actuator occupies a non-zero amount of space, this does not present a practical constraint on possible actuator locations.

Suppose that there are M_N actuators and N possible actuator locations. Define a set of possible control operators B_j by considering a single actuator at the j^{th} location. Define similarly R_j by considering one actuator at the j^{th} location. Following the approach in [6], let π be a vector of N logical elements where the j^{th} entry has a 1 when an actuator exists in that location and a value of 0 otherwise. Note that π has exactly M_N non-zero elements so

$$\sum_{j=1}^{N} \pi_j = M_N.$$

Each such vector π defines a possible set of actuator locations. The B and R matrices are then defined by

$$B \equiv [\pi_1 B_1, \ldots, \pi_N B_N]$$

$$R \equiv blockdiag\{\pi_1 R_1, \ldots, \pi_N R_N\},$$

The column $\pi_j B_j$ is a column of the B matrix, and $\pi_j R_j$ is a blockdiagonal part of the R matrix, which both take zero values if there is no actuator on the j^{th} finite element. As an example, if there is only one actuator ($M_N = 1$), and it is placed at the j^{th} position then $B = B_j$ and $R = R_j$.

The joint actuator placement and control problem is

$$\begin{gathered} \min_{\pi,u} J = \min_{\pi,u} \tfrac{1}{2} \int_0^\infty \{x^T Q x + \textstyle\sum_{j=1}^N u_j^T \pi_j R_j u_j\} dt \\ s.t. \\ \dot{x} = Ax + \textstyle\sum_{j=1}^N \pi_j B_j u_j \\ y = Cx. \end{gathered} \tag{2.5}$$

For each possible set of actuator locations, π, there is a different cost, obtained by solving the ARE (4.10) and so the the objective function is

$$\sigma_m(\pi) = \|P(\pi)\|. \tag{2.6}$$

The optimization problem is

$$\begin{gathered} \min\{\sigma_m(\pi); \pi \in \Phi\}, \\ s.t. \\ \Phi = \{\pi \in \mathbb{R}^N \quad s.t. \quad \pi_j \in \{0,1\}; \textstyle\sum_{j=1}^N \pi_j = M_N\}, \end{gathered} \tag{2.7}$$

where M_N indicates the number of actuators.

Theorem [6] : On the convex set $\Phi_c = \{\pi \in R^N s.t. \quad \pi \geq 0\}$, $\sigma_m(\pi) : \Phi_c \to R$ is convex. For $\pi_0 \in \Phi_c$, a subgradient μ of $\sigma(\pi_0)$ can be defined as

$$\begin{gathered} \mu(\pi_0) = [\mu_1(\pi_0) \ldots \mu_N(\pi_0)], \\ \mu_j(\pi_0) = Tr\{L_j S(\pi_0)\} \\ L_j = B_j R_j^{-1} B_j^T \qquad j = 1, \ldots, N \\ S(\pi_0) = -\tfrac{1}{2} P(\pi_0) \theta(\pi_0) P(\pi_0) \end{gathered} \tag{2.8}$$

where, with $Z = z.z'$ and z as the normalized eigenvector associated with the maximum eigenvalue of $P(\pi_0)$, $\theta(\pi_0)$ is the solution of the Lyapunov equation

$$(A - BG(\pi_0))\theta(\pi_0) + \theta(\pi_0)(A - BG(\pi_0))' + Z = 0.$$

2.2 Optimization Method

For a convex optimization problem, any gradient-based optimization method will converge to a global minimum. This is true when the optimization cost function is a smooth function of the design variables. Here, however, $\sigma(\pi)$ is not a smooth function of π, and the usual gradient-based algorithms may not lead to a correct result. This problem can be resolved by using $\mu(\pi)$ which is a subgradient of $\sigma(\pi)$.

Since $\sigma(\pi)$ is a convex function of π,

$$\sigma(\pi) - \sigma(\pi_0) \geq \langle \mu(\pi_0), \pi - \pi_0 \rangle \qquad for\ all \quad \pi \in \Phi_c \tag{2.9}$$

where, μ is defined in (2.8) and $\langle \mu(\pi_0), \pi - \pi_0 \rangle$ denotes the usual inner product of $\mu(\pi_0)$ and $\pi - \pi_0$. To optimize the actuator locations, we should look for the smallest $\sigma(\pi)$ that satisfies (2.9). In [6], an optimization scheme is proposed as follows. Equation (2.9) is rewritten as

$$\sigma(\pi) \geq \sigma(\pi_0) + \langle \mu(\pi_0), \pi - \pi_0 \rangle. \tag{2.10}$$

To solve the optimization, $\sigma(\pi)$ in (2.10) can be replaced with θ that can take any real value and the optimization problem written as

$$\begin{gathered} \min_{\pi} \theta \\ s.t. \quad \theta \geq \sigma(\pi_0) + \langle \mu(\pi_0), \pi - \pi_0 \rangle \\ \pi \in \Phi_c \end{gathered} \tag{2.11}$$

Letting π^* indicate the optimizer of (2.11), $\theta(\pi^*)$ is not restricted to be equal to $\sigma(\pi^*)$. Consequently, (2.11) is called a relaxation of the original optimization problem [103]. Since (2.11) is a linear optimization problem, the solution falls on the boundary of the inequality constraint and

$$\theta_{opt} = \min_{\pi} \sigma(\pi_0) + \langle \mu(\pi_0), \pi - \pi_0 \rangle.$$

If the solution of this relaxed problem, π^*, has an objective value $\theta(\pi^*)$ which equals $\sigma(\pi^*)$ then

$$\sigma(\pi^*) = \sigma(\pi_0) + \langle \mu(\pi_0), \pi^* - \pi_0 \rangle.$$

Since σ is a convex function of π, for all $\pi \in \Phi, \pi \neq \pi^*$,

$$\sigma(\pi) \geq \sigma(\pi_0) + \langle \mu(\pi_0), \pi^* - \pi_0 \rangle$$

and so for all $\pi \neq \pi^*$

$$\sigma(\pi) \geq \sigma(\pi^*).$$

Hence, $\sigma(\pi^*)$ is the global minimum for the actuator location problem. If $\sigma(\pi^*) \neq \theta$, then define $\sigma_1 = \sigma(\pi^*)$ and $\mu_1 = \mu(\pi^*)$, another constraint

$$\theta \geq \sigma(\pi_1) + \langle \mu(\pi_1), \pi - \pi_1 \rangle$$

is added to (2.11). Continuing this way, a series of linear optimization problems

$$\begin{aligned} &\min_{\pi} \theta \\ &s.t. \quad \theta \geq \sigma(\pi_i) + \langle \mu(\pi_i), \pi - \pi_i \rangle \qquad i = 1, \ldots, n \end{aligned}$$

is obtained. Since the optimization problem is linear, θ_{opt} at each iteration is on one of the constraint boundaries. From (2.9) ,

$$\sigma(\pi) \geq \sigma_i + \langle \mu_i, \pi - \pi_i \rangle \quad for\ all \quad \pi \in \Phi.$$

Therefore, in (2.11)

$$\sigma(\pi) \geq \theta_{opt} \qquad for\ all \quad \pi \in \Phi.$$

If $\theta_{opt} = \sigma(\pi_{opt})$, then π_{opt} is the global solution of the problem. As the number of constraints for this problem increases, its feasibility space gets smaller and finally converge to the optimal actuator locations.

This algorithm can be summarized as follows:

A Assume $\pi_0 \in \Phi$ and calculate $\sigma(\pi_0)$ and $\mu(\pi_0)$. Set $k = 1$ and choose a sufficiently small value $\varepsilon > 0$.

B Choose an initial location for actuators $\pi_0 \in \Phi$ and calculate $\sigma(\pi_0)$ and $\mu(\pi_0)$.

C Equation (2.9) can be relaxed as

$$\begin{gathered} \min_{\pi \in \Phi} \theta \\ s.t. \quad \theta \geq \sigma(\pi_i) + \langle \mu(\pi_i), \pi - \pi_i \rangle \quad i = 1, \ldots, k \end{gathered} \tag{2.12}$$

D Using π_{k+1}, calculate σ_{k+1}. If $(\sigma_{k+1} - \theta_{k+1}) \leq \varepsilon$, terminate. If not, calculate μ_{k+1} and return to step C.

For a single actuator, the relaxed problem (2.12) in step C can be simply solved, since the linear constraint in this problem is a scalar equation. However, for multiple actuators, solution of the relaxed master problem (2.12) is challenging, especially for large N and M_N.

The relaxed master problem (2.12) in step C, can be written

$$\min_{\pi \in \Phi} \max_i \sigma(\pi_i) + \langle \mu(\pi_i), \pi - \pi_i \rangle \qquad i = 1, \ldots, k,$$

which minimizes the largest value of a set of functions. Thus, (**??**) can be written as

$$\begin{gathered} \min_{\pi \in \Phi} \max_i \sigma(\pi_i) - \langle \mu(\pi_i), \pi_i \rangle + \langle \mu(\pi_i), \pi \rangle \qquad i = 1, \ldots, k \\ s.t. \quad \Phi = \{\pi \in \mathbb{R}^{\mathbb{N}} \quad s.t. \quad \pi_j \in \{0, 1\}; \textstyle\sum_{j=1}^{N} \pi_j = M_N\} \end{gathered} \tag{2.13}$$

The variable π in this problem is a vector of binary components. Consequently, an integer optimization algorithm is required for the solution.

2.3 Integer Optimization Algorithm

A number of integer optimization schemes are presented and used in literature. A few of them are Branch and bound methods, cutting plane methods and decomposition methods [104]. The objective function in (2.13) is a linear function of π and can be easily calculated in a considerably short time. For such an objective function, the branch and bound optimization method is a suitable algorithm. In this study, branch and bound technique is used to solve the integer part of the problem. The relaxed master problem is then a minimax optimization problem with upper and lower bounds on each variable.

2.3.1 Branch and Bound Method

In this method a binary tree is first applied to represent 0-1 variable combinations. At first, all the integer boundaries are removed. According to the binary tree, the feasible region is partitioned into sub-domains and valid upper and lower bounds are imposed to the relaxed problem. Figure 2.1 shows a binary tree for a three element vector X. Each branch of this tree is called a candidate subproblem.

In this method, first the relaxation of the original problem is solved. Consequently, for our optimization problem (2.13) can be relaxed to

$$\begin{aligned} &\min_{\pi\in\Phi_i} \max_i \sigma(\pi_i) - \langle \mu(\pi_i), \pi_i \rangle + \langle \mu(\pi_i), \pi \rangle \qquad i = 1, \ldots, k \\ &s.t. \quad \Phi_i = \{\pi \in \mathbb{R}^{\mathbb{N}} \quad s.t. \quad 0 \leq \pi_j \leq 1; \textstyle\sum_{j=1}^{N} \pi_j = M_N\} \end{aligned} \tag{2.14}$$

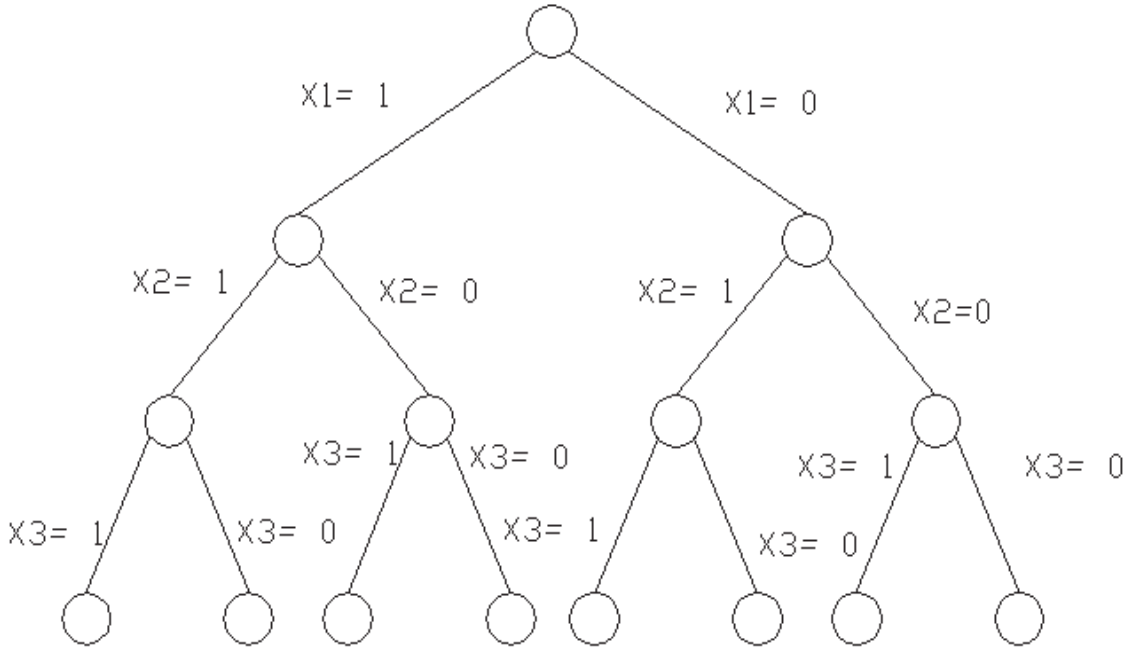

Figure 2.1: Branch Tree

.

This relaxation of the original problem is then solved. If it does not result in a binary solution, an element of the π is chosen and equality binary constraints are imposed on this element and the relaxed problem is solved once again. These added constraints form the branches of a binary tree similar to the one in Figure 2.1. Each branch of this tree is called a candidate subproblem.

At each level, the root node can be divided into two or more candidate subproblems. If the solution of a candidate subproblem is binary, the algorithm returns to the list of candidate subproblems and selects a new subproblem to solve. Otherwise, it separates the subproblem into

two or more candidate subproblems and repeats the procedure. These iterations are continued until the list of candidate subproblems is empty.

Fathoming tests should be applied to avoid enumeration of all candidate subproblems. A candidate subproblem can be fathomed if one of these 3 criteria is met:

Criterion 1: If the relaxed candidate subproblem does not have a feasible solution then the optimization subproblem is infeasible.

Criterion 2: If the optimal solution of the relaxed subproblem is greater or equal to the best feasible solution so far.

Criterion 3: If the optimal solution of the subproblem's relaxation proves to be a feasible solution of the candidate subproblem.

In the next level, the current subproblem is separated and its children are added to the list of candidate subproblems. The optimization is terminated if all the feasible subproblems are studied. The details of Branch and bound method can be found in [104].

2.3.2 Minimax Optimization Method

The optimization problem is the relaxation of the original minimax optimization in (2.13). In the relaxed master problem the binary constraints on elements in π vector are changed into inequality constraints. The minimax problem can be treated as a goal attainment problem. Consequently, for simplicity let's define the relaxed master problem in the form of,

$$\begin{gathered} \min_{\pi\in\Phi} \theta \\ s.t. \quad \theta \geq \sigma(\pi_i) + \langle \mu(\pi_i), \pi - \pi_i \rangle \quad i = 1, \ldots, k \\ \sum_{j=1}^{N} \pi_j = M_N \\ 0 \leq \pi_j \leq 1, \qquad j = 1, ..., N \end{gathered} , \tag{2.15}$$

where π_j is the j^{th} element of a vector π, N is the number of possible actuator positions and M_N indicates the number of actuators. In each candidate subproblem a binary constraint is added to this relaxed problem. Since the objective function is linear and the constraints are linear, the optimization problem is convex.

The objective functions in minimax optimization can be written as

$$F_i(\pi) = U_i + Y_i.\pi$$

where

$$U_i = \sigma(\pi_i) - \langle \mu(\pi_i), \pi_i \rangle$$

and

$$Y_i = \mu(\pi_i).$$

Each function F_i is a linear function of π. The constraints are also linear functions of π.

In this problem, the equality and inequality constrains can be written as

$$\begin{aligned} g_1(\pi) &= 0 \\ g_j(\pi) \leq 0, \quad j &= 2, ..., m+1 \\ g_i(\pi) \leq 0, \quad i &= m+2, ..., m+l+1 \end{aligned} \quad ,$$

where $g_1(\pi) = \sum_{j=1}^{N} \pi_j - M_N$. As the branch and bound algorithm proceeds binary constraints are imposed on the π vector. Therefore the number of equality constraints increases. The variable m is the number of inequality constraints $-\pi_j \leq 0$ and $\pi_i - 1 \leq 0$. The variable l is the number of F_i functions and each member of this group of constraints can be written as $g_i(\pi) = F_i(\pi) - \theta$. To solve this problem a line search algorithm can be used. A line search procedure updates the π variable for the new iteration,

$$\pi_{k+1} = \pi_k + p_k.$$

The vector p_k is the trial step which can be chosen as $-\nabla\theta(\pi_k)$ [103]. These iterations should continue until the convergence criterion is satisfied.

Further, some times the trial step p_k cannot be accepted due to violation of the original constraints. The step size needs to be controlled. For each step k a variable α_k can be defined such that

$$\pi_{k+1} = \pi_k + \alpha_k p_k.$$

Line search methods use merit functions to calculate α_k. In [105], it is mentioned that it should be searched along p_k to minimize the merit function

$$\Psi = \theta + \sum_{i=1}^{m+1} r_i g_i(x) + \sum_{i=m+2}^{m+k+1} r_i.max(0, F_i(\pi) - \theta).$$

The definitions to calculate the multipliers r_i are given in detail in [105].

The *fminimax* code, from the MATLAB optimization toolbox is applicable to such minimax optimization problems. In this study, the *fminimax* code is combined with a branch and bound method to solve the problem. All the codes are written in MATLAB.

2.3.3 Example

To illustrate the method, consider the following simple example [6]:

$$\begin{gathered} \sigma(p) = \min_u \int_0^\infty (x^2 + \phi^2) dt \\ s.t. \quad \dot{x} = -x + b(p)\phi, \\ b(\pi) = exp(p).\sin(2\pi p), \quad p \in D = [0, 1]. \end{gathered} \tag{2.16}$$

Figure 2.2 shows the variation of $\sigma(p)$ with p. This figure shows that there are two local minima in this problem, one at $p = 0.28$ and another, which is the global minimum, at $p = 0.78$.

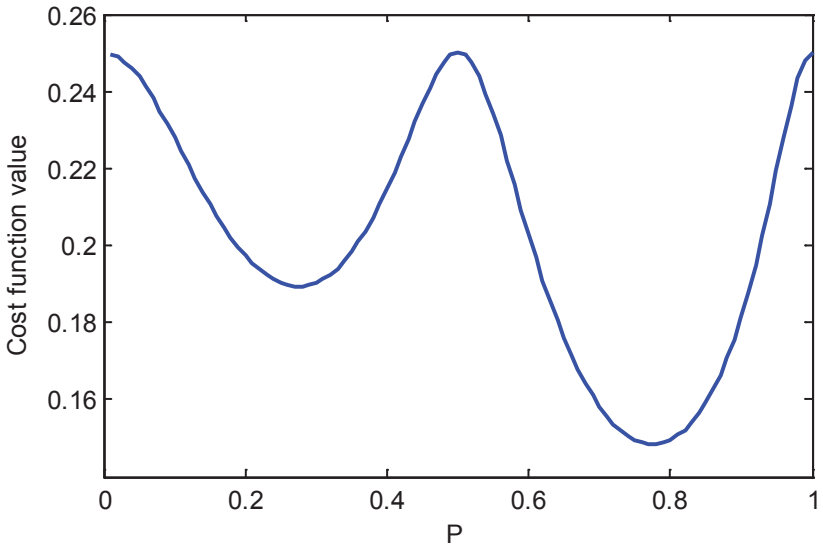

Figure 2.2: Function $\sigma(p)$

The interval D is divided into 100 possible actuator locations and so $N = 100$ and $M_N = 1$. Two different initial values, 0.01 and 0.99, were used. In both cases, the algorithm described above converged to $p = 0.78$. This problem was also solved with a genetic algorithm. The 'ga' optimization package in MATLAB was used. The population size was chosen as 20, where every member of population was a chromosome of length 100 (composed of binary genes). The optimization constraint was taken into account by assigning a very large number to the fitness value when the number of ones in binary genes of each chromosome goes higher than $M_N = 1$. The results and calculation of these two methods are compared in Table 2.1. The genetic algorithm is not as accurate or as fast as the proposed method presented here. By increasing the population size to 100, the correct result, 0.78, is calculated. However, it takes 85 seconds which is far more than the 8.5 seconds taken by the proposed method.

Proposed Algorithm			Genetic Algorithm		
Initial point	Result	Calc. Time (s)	Initial pop'n	Result	Calc. Time (s)
0.01	0.78	8.5	random	0.76	29.
0.99	0.78	6.7	random	0.75	25.

Table 2.1: Comparison of proposed optimization method and genetic algorithm on simple example (2.16). A population size of 20 was used for the genetic algorithm.

2.4 Summary

An integer optimization algorithm was developed in this chapter to optimize actuator locations on flexible structures. A MATLAB code is written based on the developed algorithm. In this code, first an initial position is assumed for the actuators and an integer optimization problem is formed. The main advantage of this integer problem is its convexity. For the integer optimization, a function is written. The integer objective function is linear. Hence, the integer problem can be solved in a short time. The code calls the integer optimization function in each iteration. The integer optimization function, uses the branch and bound technique for the optimization. In the branch and bound algorithm, the minimax optimization function in MATLAB is called to solve the relaxation.

Once the integer optimization is solved and a new position is found for the actuators, convergence conditions are checked and if the calculated position is not the optimizer, the code starts a new iteration. In each new iteration, using the function value and subgradient vector of the location calculated in the previous iteration, a new linear constraint is added to the integer problem. The code continues iterating until convergence is achieved.

It should be mentioned that the introduced optimization scheme is applicable to linear models. The stiffness and mass matrices should remain unchanged. There is no limitation on the

type and shape of the structure as long as it is linear. The method is also applicable to three dimensional structures.

In addition, the optimal actuator locations may vary with Q and R matrices. Also since convexity of the objective function is proved in binary space of actuator locations, it may not be strictly convex in this space and for constant Q and R matrices there may be more than one optimal position for actuators. This is the case for symmetric base structures with non-symmetric optimal actuator locations.

Chapter 3

Optimal Actuator Placement in Vibration Control

In vibration control it is desired to maintain the structure in its equilibrium position. Consequently, the actuator locations should be optimized to reject disturbances with minimum control energy. The optimization scheme presented in Chapter 2 is applied to optimize the location of piezoelectric actuator patches on beam and plate structures. The results are compared with a genetic algorithm.

This chapter also studies the relation between the optimal actuator locations and modal strain energies of the base structure. It might be desired to model the structure with a limited number of its structural modes. The number of modes required to model the structure in order to achieve accurate results for optimal actuator placement is briefly studied.

3.1 Vibration Control with piezoelectric actuator patches

To suppress the disturbances in a structure, the linear quadratic regulator (LQR) is applied as a control measure. The actuators are piezoelectric patches. It is assumed that the actuators are perfectly bonded to the top surface of the structure as shown in Figure 3.1. The figure shows an elastic structure. One layer of piezoelectric material is bonded to its top surface.

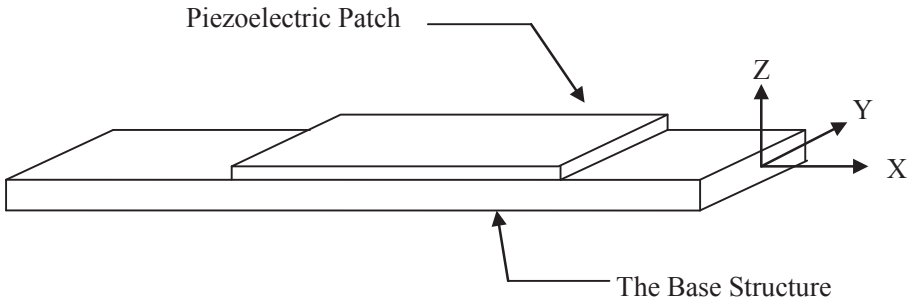

Figure 3.1: Structure with a piezoelectric patch

Letting σ indicate the stress tensor, f the body force vector, D the electric displacement vector, q the electric charge density, ρ mass density and w the structural deflection, the electrostatic field in piezoelectric materials is modeled by

$$\nabla\cdot\sigma + f = \rho\ddot{w},$$

$$\nabla\cdot D + q = 0.$$

The first equation is the elasticity equilibrium equation and the second equation is Gauss's law of electrostatics [8]. The constitutive equations of piezoelectric materials are

$$\sigma = C_e S + e\nabla\phi \tag{3.1a}$$

$$D = eS - \epsilon\nabla\phi, \tag{3.1b}$$

where, σ is the stress vector, S is the strain vector, ϕ is the electric potential, C_E is the matrix of elastic constants under constant electric field (dependent on modulus of elasticity and Poisson's ratio), ϵ is the electric permittivity matrix under constant mechanical strain, $e = dC$ contains the piezoelectric coupling constants, d is the dielectric constant matrix, and D is the electric displacement vector [8].

In this study, the structure and the bonded piezoelectric materials are modeled applying the finite element discretization. For voltage driven actuators, the finite element equations take the form

$$M\ddot{s}(t) + C_D\dot{s}(t) + Ks(t) - K_{s\phi}\phi(t) = F(t) \tag{3.2}$$

where $s(t)$ is the generalized nodal displacement vector. It includes the displacement and rotational degrees of freedom at each element node. The matrices M and K are the mass and stiffness matrices respectively and C_D is the damping matrix. Also $K_{s\phi}$ is the (symmetric) electro-mechanical coupling matrix, while $F(t)$ is the vector of external forces. Details for finite element modeling of piezo-laminated smart structures and M, K and $K_{s\phi}$ can be found in [106]. Next, the finite element equations in equation (3.2) which form the structural dynamic equations of motion are transferred into state space form

$$\dot{x}(t) = Ax(t) + B\phi(t).$$

The vector $x(t)$ can be defined in a number of ways. In this study, the state vector, x is as

$$x(t) = \begin{Bmatrix} s(t) \\ \dot{s}(t) \end{Bmatrix}.$$

Consequently, the A and B matrices take the form

$$A = \begin{bmatrix} 0 & I \\ -M^{-1}K & -M^{-1}C_D \end{bmatrix}; B = \begin{bmatrix} 0 \\ M^{-1}K_{s\phi} \end{bmatrix}.$$

It is important that the optimal cost and location of actuators obtained from the finite element formulation converge as the size of the finite elements decreases [71]. For damped structures with a finite number of actuators where B in the partial differential formulation is bounded, this is ensured for finite element approximations if Q in the LQR equation is compact. For details, see [71]. When piezoelectric actuators are used however, the B operator is only bounded in a space larger than the state space [107]. In this study, since the aim is to control the position, which includes the first part of the state vector,

$$Q^{1/2} = \begin{bmatrix} I & 0 \end{bmatrix},$$

which is compact on the state space [71]. The R matrix in LQR equation is the identity matrix and its size is equal to the number of actuators. Numerical tests in [108, 109] indicate convergence of the optimal cost and actuator locations for vibration control of beams and plates. The examples solved in [110] for shape control of beams present the same idea.

3.2 Energy Realization

In some cases, especially for very thin structures, the A matrix may become ill-conditioned or numerical problems may arise while solving ARE equation. Such problems may also arise during optimization of actuator locations.

To avoid numerical difficulties due to poor scaling of the A matrix, in this thesis, energy realization is used for the state vector. Hence, the state vector x is as

$$x(t) = \begin{Bmatrix} K^{0.5} s(t) \\ \dot{s}(t) \end{Bmatrix}.$$

Consequently, the A and B matrices take the form

$$A = \begin{bmatrix} 0 & K^{0.5} \\ -M^{-1}K^{0.5} & -M^{-1}C_D \end{bmatrix}; B = \begin{bmatrix} 0 \\ M^{-1}K_{s\phi} \end{bmatrix}.$$

3.3 Optimal Actuator Placement in Structures

Consider now the problem of optimizing the locations of piezoelectric patch actuators on structures. The optimization scheme to optimize the actuator locations was discussed in detail in Chapter 2.

Each structure is discretized into finite elements. To optimize actuator locations, a grid of possible positions should be selected. With the fact that each actuator occupies a specific area, the dimensions for each finite element are considered same as the dimensions of the actuators so that they have the same area. Hence, each finite element can be a possible location for an actuator and the number of possible actuator locations equals the number of finite elements. This assumption does not affect the generality of the introduced optimization scheme. However, when relatively large patches are to be used the finite element meshing needs to be modified to achieve accurate structural stiffness and mass matrices. One solution can be using higher order elements to model the structure.

In the following sections, the optimal location of piezoelectric actuators are calculated for beam and plate structures. Various boundary conditions are considered for the beams and plates. In all these models the actuators are made of PZT 5A material and they have a 40 μm thickness.

The base structures are made of steel. Material properties of Steel and PZT 5A are shown in Table 3.1. In all the models a very small Rayleigh structural damping, $C_D = 1 \times 10^{-8}K$, is assumed.

Properties	Piezoelectric	Base Structure
Elastic Modulus (Nm^{-2})	61×10^9	21×10^{10}
Density ρ (kgm^{-3})	7700	7810
Dielectric Constant d_{31} (mv^{-1})	171×10^{-12}	
Poisson's Ratio	0.3	0.3

Table 3.1: Material Properties

Optimal actuator locations on beams are calculated for beams with pinned-pinned, fixed-free and fixed-pinned boundary conditions. Two different beam sizes are considered. The relation between optimal locations and modal strain energies of the beams is also studied. The beams are modeled in ANSYS using 'BEAM3'elements. This beam element type is based on Euler-Bernoulli beam theory. In this theory the beam cross-sections are assumed to remain perpendicular to centerline of the beam after deformation. The equation of motion for Euler-Bernoulli beam can be written as

$$EI\frac{\partial^4 w}{\partial x_1^4} + \rho A\frac{\partial w}{\partial t} = F,$$

where w is the displacement, x_1 is the position on th beam, E is the modulus of elasticity, I is the beam's cross-section moment of inertia, A is the cross-section area, t is time F is the external force. When the beam is augmented with piezoelectric patches, F is the PZT patches' force. The finite element equations for Euler-Bernoulli beams with attached piezoelectric patches can be found in [107] and [106].

To model the plates in ANSYS, 'SHELL181'elements are used which are based on Reissner

Mindlin plate theory. Equation of motion for a plate augmented with piezoelectric patches is

$$\rho h \frac{\partial^2 w}{\partial t^2} + C_D \nabla^4 \frac{\partial w}{\partial t} + D\nabla^4 w = \frac{\partial^2 M_{px}}{\partial x_1^2} + \frac{\partial^2 M_{py}}{\partial y_1^2},$$

$$D = \frac{Eh^3}{12(1-\nu^2)},$$

where, w is the deformation of the plate in z direction, C_D is the damping in the plate, M_{px} and M_{py} are the bending forces imposed by PZT actuators around x_1 and y_1 axes.

The finite element equations for plates with attached piezoelectric patches can be found in [107]. Plate dimensions are 500 mmx500 mmx1 mm and it is divided into 100 finite elements. The structure is augmented with actuators on its top surface and actuators are 50mm x50mm x40 μ m each which have the same area as the finite elements.

3.3.1 Beams with pinned end conditions

In the first model, the beam dimensions are 500 mm x 30 mm x 2 mm and it is divided into 15 finite elements. The stiffness and mass matrices are formed and the optimal actuator locations are calculated using the presented optimization scheme. Figure 3.2 shows the optimal location of one actuator on the beam. As is clear from this figure, the actuator location is close to the middle of the beam, but is approximately 45 per cent of the beam length from either of the beam ends.

To check the validity of this observation, the beam is subjected to a single impulse at one fourth of the beam's length from the pinned support and the beam's vertical response is calculated at the beam's mid-point as shown in Figure 3.3. The results are compared when the actuator is at 45 per cent of the beam's length and when it is in the middle. It should be mentioned that the optimal location in this case is not unique. It can be at 45 percent of the beam's

Figure 3.2: Optimal location of 1 actuator on a 0.5 m long beam with pinned end conditions

length from either side of the beam's supports. Both locations are effective in suppressing the disturbance, but still the actuator is more effective when it is optimally placed. Note that, if the actuator is placed at the beam mid-point, it can only be effective on disturbances which excite odd-numbered modes of vibration in the beam. Similar results are presented in [64]. In [64], the optimal size and location of piezoelectric actuator patches are studied on a 1.5m long simply supported beam based on controllability. The authors showed that when only the first mode of a simply supported beam is considered, the optimal location of one actuator is at mid-span of the beam. However, when considering more than one mode in modeling, the optimal actuator location will not be in the beam's midpoint.

Next, the optimal location of 5 actuators is calculated on the same beam. The result is shown in Figure 3.4. All actuators are concentrated in the middle part of the beam, which covers one third of the beam span.

To determine whether the optimal location is sensitive to the aspect of the state to be controlled, instead of minimizing the entire state, we choose to minimize the displacement at one third of the beam's length from one of the supports, and the weighting matrix Q is modified appropriately. Calculations reveal that the optimal location of one and five actuators in this case did not change and were the same as Figure 3.2 and 3.4 respectively.

The optimal location of actuators need to be calculated on higher order models as well. Consequently, the beam dimensions are changed to 3 m x 0.03 m x 0.002 m with the same material properties and the actuator locations are calculated on this beam. The beam is divided

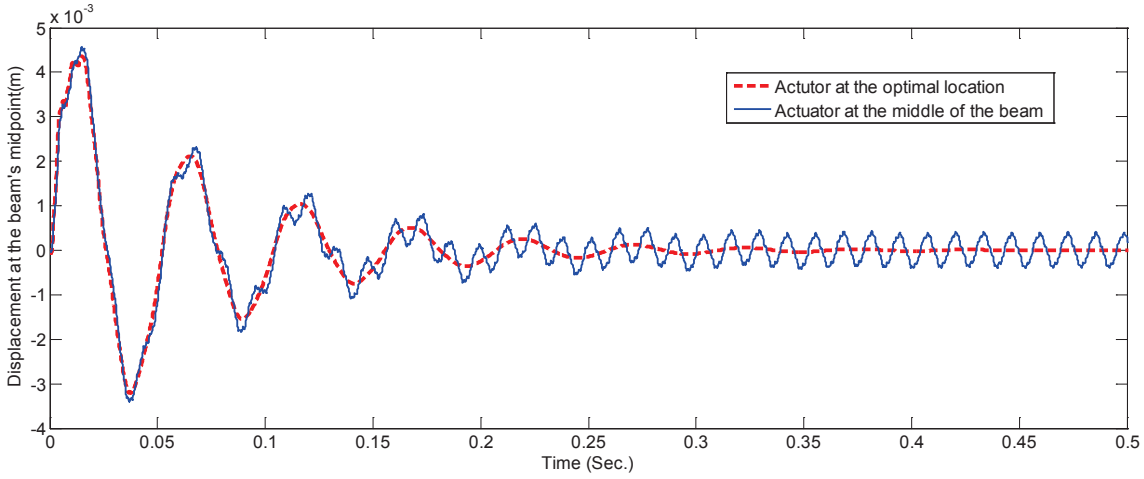

Figure 3.3: The beam's response at the mid-point to an impulse at one fourth of the beam's length for optimal and non-optimal actuator locations on a 0.5m long beam with pinned end conditions

Figure 3.4: Optimal location of 5 actuators on a beam with pinned end conditions

into 100 finite elements. The optimal locations for 1, 2 and 5 actuators was calculated for this beam. The results are shown in Table 3.2. The locations are shown based on the element number. Since the beam model is symmetric, either of the beam ends can be the start of element numbering. The optimal locations are close to the mid-section of the beam, however, the optimal locations are not symmetric with respect to the mid-section of the beam. The reason is the same as what discussed about Figure 3.2. When the number of actuators is relatively small, locating them in the middle of the beam, minimizes their control over a wide range of disturbances.

It is worth to mention that in Figure 3.4 each actuator covers seven percent of the beam lengths and five actuators cover one third of the beam's length. That is why they have covered the middle one third of the beam. In the three meter long beam each actuator covers one per cent of the beam's length and the possible arrangements that five actuators can have are far more than in Figure 3.4.

Number of actuators	Optimal Actuator Locations
1	46 or 55
2	49,56
5	44,46,50,52,55

Table 3.2: Optimal actuator locations on a beam with pinned end conditions

The optimal location is close to the location of maximum modal strain energy for the first mode as shown in Figure 3.5. Using only the first mode results in the beam's mid-point as the optimal actuator location. However, since as shown in Figure 3.6, the strain energy for even-numbered modes is zero at this point the optimal location is moved to element 46. Using any higher number of modes leads to similar results.

Returning to the shorter beam in Figure 3.2, regardless of the values on the vertical axis, the strain energy for the first mode has the same shape as the first modal strain energy for the longer beam as in Figure 3.5, and in both structures, the locations of high strain energies for the first mode are in the middle section of the beam. The ANSYS finite element software is applied to calculate modal strain energies. The actuators are optimally located at high strain energy locations for the first mode.

The relationship between modal strain energy and optimal actuator locations was first suggested in [48]. In an example of optimal location of sensor/actuator pairs on a cantilever undamped beam, the pairs were located in areas of high modal strain energy on the beam. The

Figure 3.5: First Modal Strain Energy for the beam with pinned ends

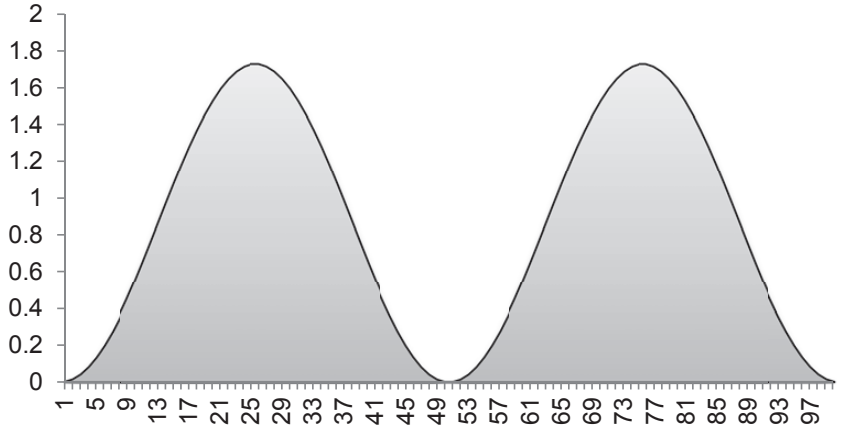

Figure 3.6: Second Modal Strain Energy for the beam with pinned ends

authors also studied the same problem on a cantilever plate [5].

For two actuators one is located in the middle of the beam and the other is at 45 percent of the beam's length. Using the first three vibration modes of the beam leads to the same results.

As Table 3.2 shows the locations for 3, 4 and 5 actuators are also close to the middle section of the beam. Based on Figure 3.5, these locations are all close to high strain energy points of the first mode. However, since strain energies of the even-numbered modes are zero in the middle, the actuators are not at this location. This discussion can be verified by Figure 3.7. This figure shows the number of modes needed to converge to the accurate results for various numbers of actuators. Although one mode is not enough, use of the first five modes provides convergence. This shows that the high strain energy locations of first few modes have a major effect on the optimal actuator locations.

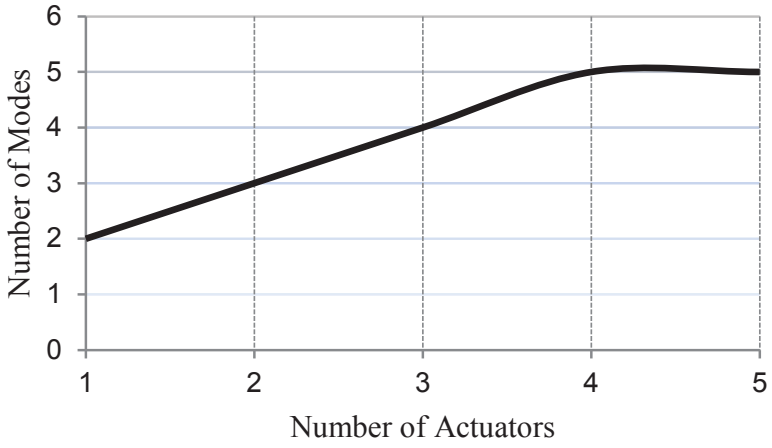

Figure 3.7: Number of modes required to accurately calculate the optimal location of actuators

3.3.2 Optimal Actuator Locations on Cantilever Beams

The locations of one and five actuators are calculated on a 0.5 m x 0.03 m x 0.002 m cantilever beam which is divided into 15 finite elements. The results are shown in Figures 3.8 and 3.9, respectively. The results reveal that the actuators should be placed close to the fixed end of the

beam.

Figure 3.8: Optimal location of one actuator on a 0.5 m long cantilever beam

Figure 3.9: Optimal location of one actuator on a 0.5 m long cantilever beam

The state weight matrix Q was also changed, so that only the vertical motion at the beam's tip is to be controlled and the optimal locations of one and five actuators were calculated for this case. The optimal locations remain the same as in Figures 3.8 and 3.9.

Next, the beam dimensions are changed to 3 m x 0.03 m x 0.002 m with the same material properties. The beam is divided into 100 finite elements. Table 3.3 shows the optimal location of one, two and ten actuators. In all the cases the actuators are concentrated close to the fixed end of the beam.

Figure 3.10 shows the modal strain energy of the first mode. Clearly, the actuators are distributed on locations of maximum strain energies for the first mode. Moreover, the first mode of vibration is enough to calculate the optimal location of actuators.

3.3.3 Optimal Actuator Locations on the beam with fixed-pinned boundary conditions

In the first step, the location of one and five actuators are calculated on a 0.5 m x 0.03 m x 0.002 m beam which is divided into 15 finite elements. The beam is fixed at one end and simply

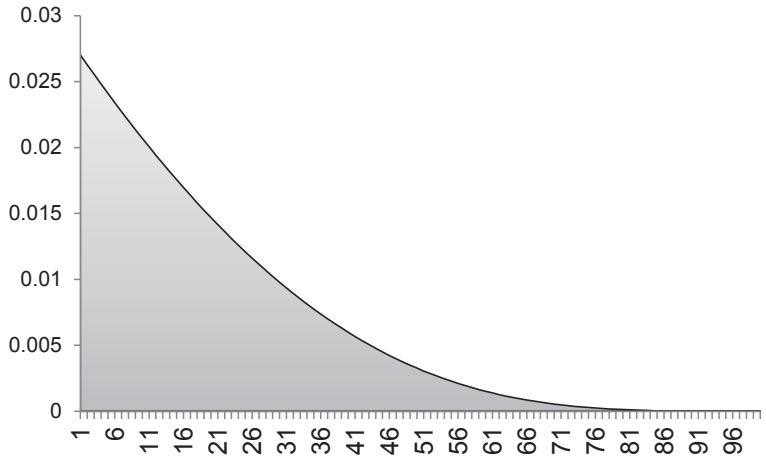

Figure 3.10: First Modal Strain Energy for a cantilever beam

Number of actuators	Optimal Actuator Locations
1	1
2	1,2
10	1,2,3,4,5,6,7,8,9,10

Table 3.3: Optimal actuator locations on a beam with pinned end conditions

supported at the other end. The results are shown in Figures 3.11 and 3.12, respectively.

In the next step, the Q matrix is modified to control only the vertical motion at one third of the beam's length. The optimal location of one and five actuators remains unchanged.

Next, the beam dimensions are changed to 3m x 0.03m x 0.002m with the same material properties. The beam is divided into 100 finite elements. Table 3.4 shows the optimal location of 1, 2, 5, 10 and 20 actuators on the beam. In all these cases it is observed that the actuators are concentrated close to fixed end, until they cover 9 percent of the beams length. The remainder of actuators are placed approximately less than 40 percent of the beam's length from the pinned

end. Figure 3.13 shows the first modal strain energy, for this beam. Close to the fixed end 9 percent of the beam's length has the highest strain energy. The results show that the actuators are distributed throughout the beam's length at points of the highest strain energies of the first mode. As for the cantilever beam example only the first mode of vibration is needed to calculate the optimal actuators locations even for higher number of actuators.

Since for the beam in Figures 3.11 and 3.12, the first modal strain energy has the same form, in this beam also the first modal strain energy is enough to locate the actuators.

Figure 3.11: Optimal location of one actuator on a beam with pinned-fixed end conditions

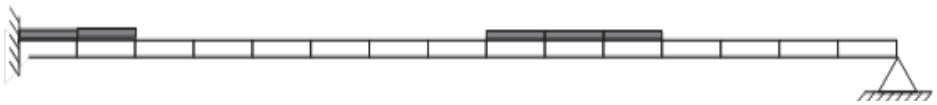

Figure 3.12: Optimal location of 5 actuators on a beam with pinned-fixed end conditions

3.3.4 Comparison with a genetic algorithm

The developed method and a genetic algorithm were both used to calculate the optimal locations of 10 actuators on a 3m x 0.03m x 0.002m beam with pinned end conditions. The elapsed time for optimization and the results are compared for both methods. The results are shown in Table 3.5. For genetic algorithm, the population size is taken as 100, to get results as accurate as possible. A random initial population is chosen and the optimization constraint on the number

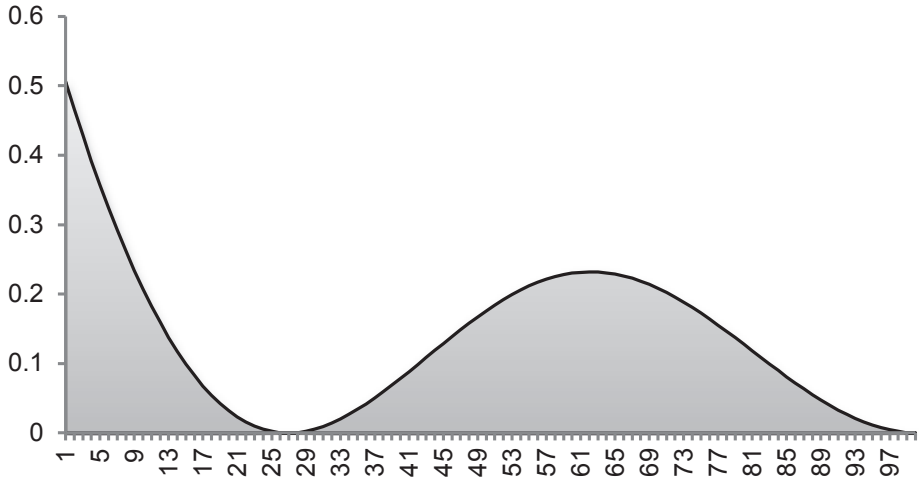

Figure 3.13: First Modal Strain Energy for a beam with pinned-fixed end conditions

Number of actuators	Optimal Actuator Locations
1	1
2	1,2
5	1,2,3,4,5
10	1,2,3,4,5,6,7,8,9,62
20	1-9,58-68

Table 3.4: Optimal actuator locations on a fixed-pinned beam

of actuators is taken into account by assigning a very large number to the fitness value when the number of ones in binary genes of each chromosome goes higher than 10. The introduced method converges much faster than the genetic algorithm and the result is more accurate.

Algorithm	Optimal Actuator Locations	Elapsed Time (Sec.)	Objective Value
Current Method	43,45,46,47,48,49,50,52,53,56	478.4837	71.9857
GA	43,44,45,47,48,49,50,51,54,58	4.1385e4	72.1688

Table 3.5: Optimal location of 10 actuators on a beam with pinned end conditions

3.3.5 Optimal actuator locations in plates and comparison with a genetic algorithm

First, the location of one actuator is optimized on a cantilever plate. The result is shown in Figure 3.14. To verify the accuracy of the optimization code, we calculated the value of objective function for each element, and observed that in the optimized location, the objective function has its minimum value. Moreover, two other positions are considered for the actuator as shown in Figure 3.15 and the plate is subjected to a vertical impulse at the tip. Figure 3.16 shows the vertical deformation at the same point with the three actuator locations. Clearly, when the actuator is optimally placed, the disturbances are suppressed much faster.

Next, the optimal placement for 10 actuators is calculated on the same plate and Figure 3.17(a) shows the result.

Genetic algorithm was also applied to calculate the optimal placement of actuators on this plate as shown in Figure 3.17(b). Applying GA, a random initial population is chosen and as for previous examples the optimization constraint is taken into account by assigning a very large number to the fitness value when the number of ones in binary genes of each chromosome goes higher than 10.

The results for both methods are compared in Table 3.6. In addition to being much faster in computation, the current applied method is more exact than genetic algorithm.

To verify the optimization results, the plate is subjected to a vertical impulse at its tip.

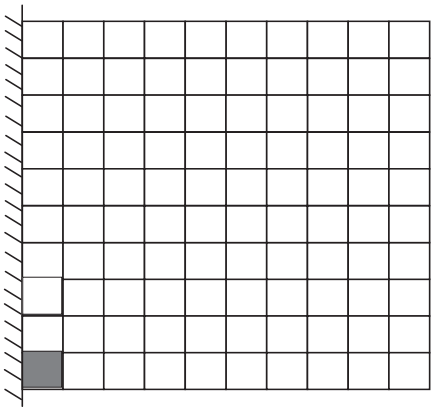

Figure 3.14: Optimal Location of one Actuator on a cantilever steel plate

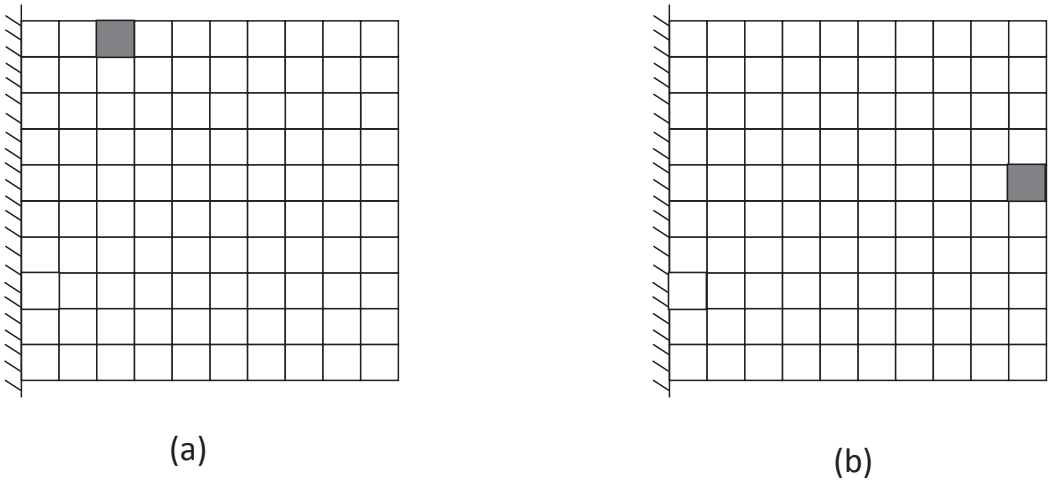

Figure 3.15: Non-optimal actuator locations

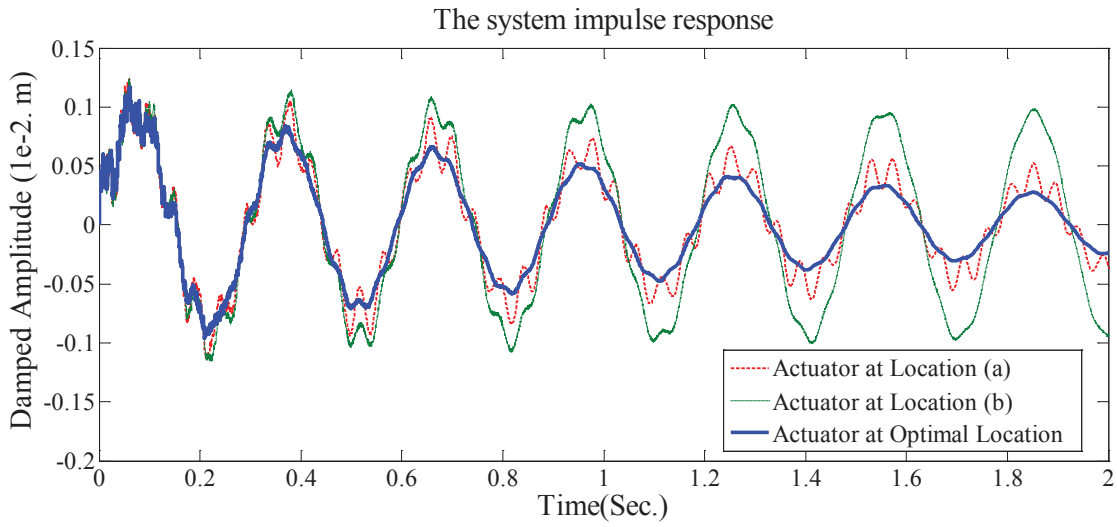

Figure 3.16: Displacements at the plate tip subjected to a vertical impulse at its tip

	Objective value	Elapsed time(sec.)
Current Method	1.5845	491.9577
Genetic algorithm	1.7483	4.4433E4

Table 3.6: Comparison of GA and the introduced algorithm for the cantilevered plate

The response at the free end of the plate is shown in Figure 3.19 for the optimal placements from genetic algorithm and the presented method. The responses from two non-optimal actuator placements are also included in this figure. The non-optimal placements are shown in Figure 3.18. Figure 3.19 shows that with the optimal placement the vibrations are suppressed much faster than the other non-optimal locations. Also comparing with the GA results, the results from the presented scheme are slightly more effective in vibration suppression.

In the next step, the boundary conditions of the cantilever plate are changed to pinned con-

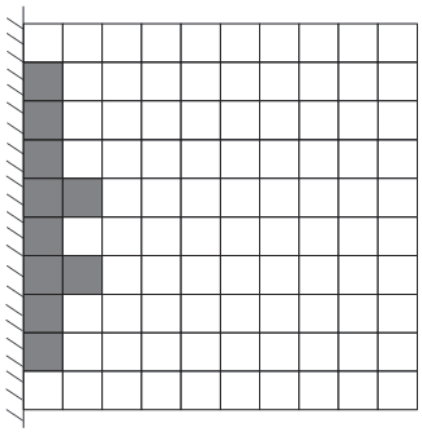

(a) Based on the presented method

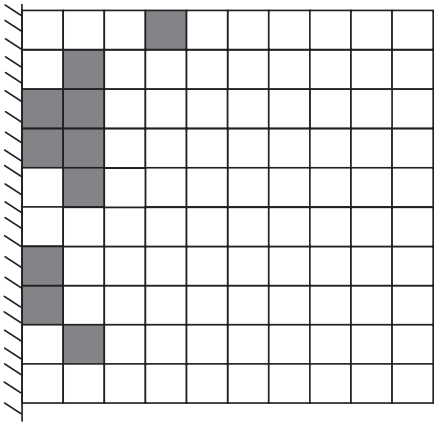

(b) Based on Genetic Algorithm

Figure 3.17: Optimal Location of 10 actuators on a cantilever plate

ditions on the two opposite sides, instead of a fixed side as shown in Figure 3.20. Consequently, the nodes on these two sides are free to rotate but restricted to move. Figure 3.20 shows the optimal location of these actuators on the plate. The same problem is also solved with GA and the

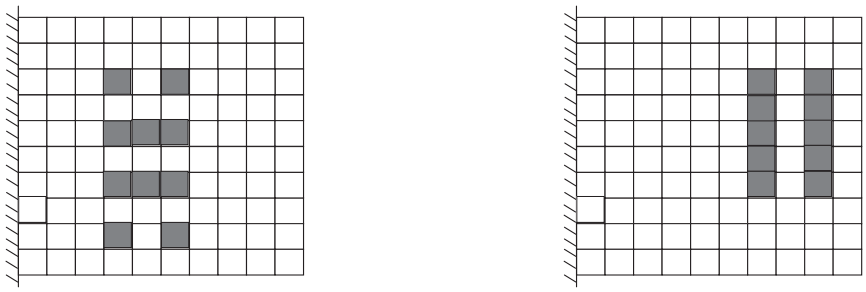

(a) (b)

Figure 3.18: Non-optimal Actuator Locations

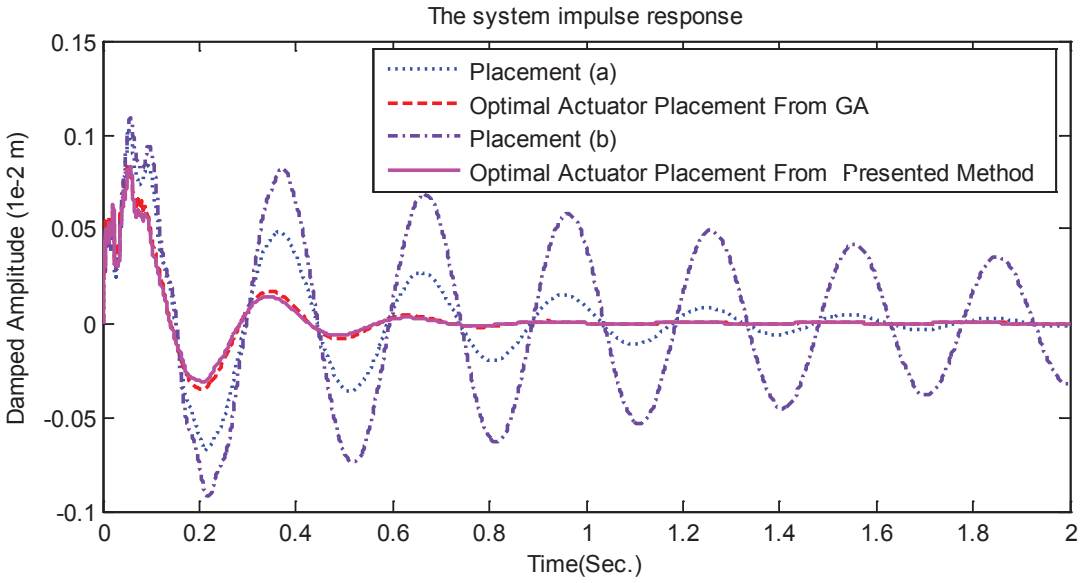

Figure 3.19: Displacements at the plate tip for ten actuators

results are compared in Table 3.7. Figure 3.21 shows the optimal location of actuators achieved by GA. Same as previous examples, Table 3.7 shows that the proposed method is much faster

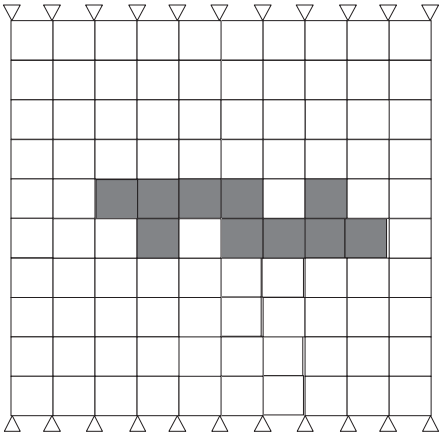

Figure 3.20: Optimal location of actuators on a plate with pinned end conditions

and more accurate than genetic algorithm.

	Objective value	Elapsed time(sec.)
Current Method	2.4115	9.1625E3
Genetic algorithm	2.4433	1.553E5

Table 3.7: Comparison of GA and the introduced algorithm for the plate with pinned end conditions

The optimal location of actuators is close to locations of high strain energies for the first three modes of vibration, see Figures 3.22, 3.23, and 3.24. The optimal actuator locations for the first three modes of vibration in the plate are shown in Figure 3.25. Applying the first three structural modes of vibration also leads to locations very close to the full model as in Figure 3.20. The plate's modes of vibration are calculated using ANSYS finite element software. There is only 6 percent error in the optimal objective value when the truncated model with three modes is applied.

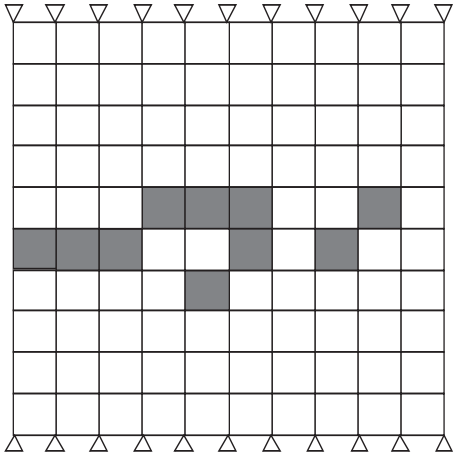

Figure 3.21: Optimal location of actuators on a plate with pinned end conditions applying GA

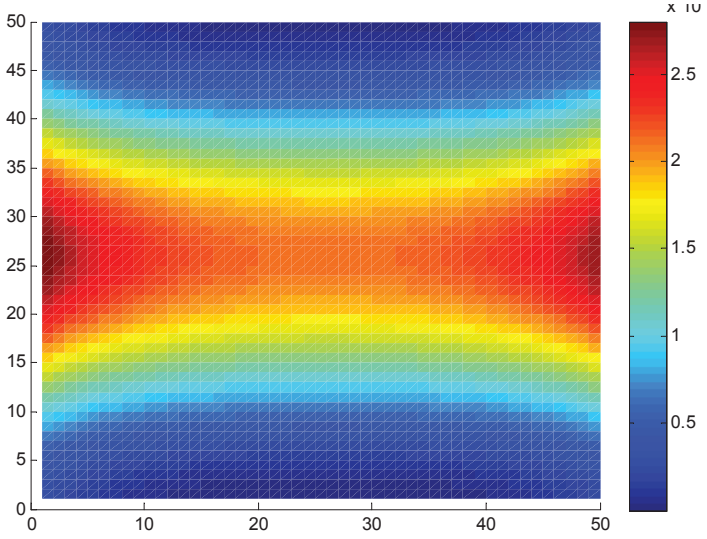

Figure 3.22: First modal strain energy of the plate with pinned end conditions on its two opposite edges

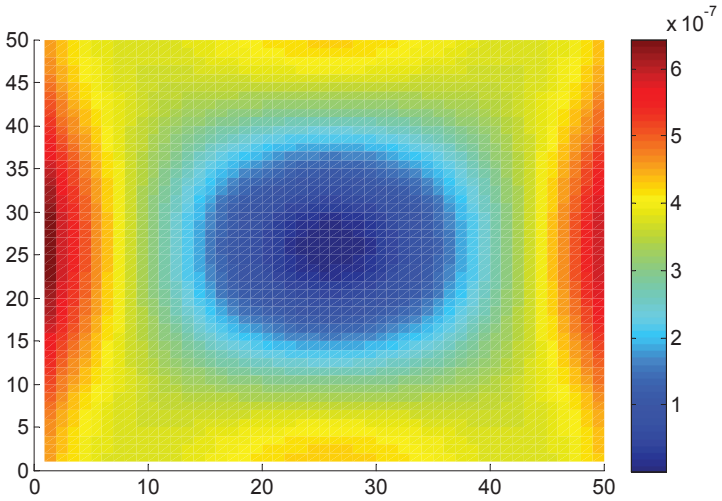

Figure 3.23: Second modal strain energy of the plate with pinned end conditions on its two opposite edges

3.4 Summary

In summary the presented optimization scheme is an efficient and accurate algorithm in optimal actuator placement even for structures with a large number of elements. It was observed that the optimal locations of actuators in vibration control are related to the location of the maximum strain energies of the first few structural modes. The sufficient number of modes to determine actuator locations for a given problem, and the weight that should be assigned to each mode depends on the type of structure. The examples solved in this chapter suggested that rigid structures require fewer number of modes than flexible structures.

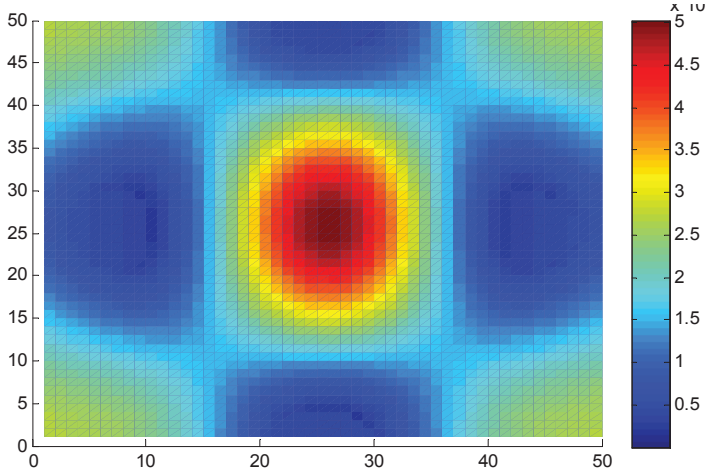

Figure 3.24: Third modal strain energy of the plate with pinned end conditions on its two opposite edges

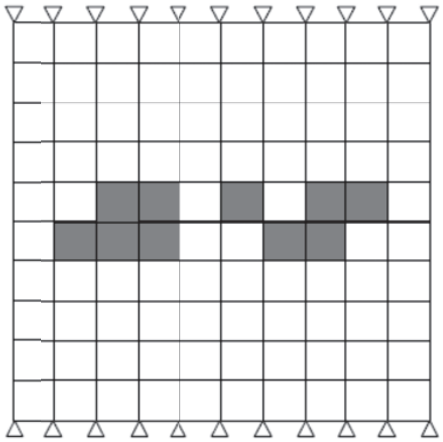

Figure 3.25: Optimal location of actuators on a plate with pinned end conditions applying only the first three modes of plate to model it

Chapter 4

Optimal Actuator Placement in Shape Control

This chapter investigates shape control of flexible structures. Optimal actuator locations are calculated for flexible structures. To optimize actuator placement the optimization scheme introduced in Chapter 2 is applied. In Section 4.1 shape control of flexible structures is formulated. The shape control formulation is then implemented in a finite element discretization of structural models. In Section 4.2, the presented optimization scheme is applied to optimize actuator locations on structures. The actuator placement is optimized in shape control of beams and plates with various boundary conditions. This section suggests a lower bound in the number of actuators and studies the importance of optimal actuator placement when a limited number of actuators are available for shape control.

4.1 Shape Control Method

For shape control, the shape of a structure is regulated to a position which may be different from its equilibrium position. Consider the structure as a linear time invariant system.

$$\begin{aligned} \dot{x}(t) &= Ax(t) + Bu(t), \quad x(0) = x_0, \\ y(t) &= Cx(t). \end{aligned} \tag{4.1}$$

where $x(t)$ is the state vector and is a function of displacements and velocities in the structure and $u(t)$ is the input vector. The vector $y(t)$ is the output vector which is related to the structure's shape.

The aim in a shape control problem is to minimize the error between the current state $x(t)$ and the desired state x_d. The structure is required to remain in a fixed position in space, which is time independent. Let's name this position vector as s_d and the structure's position at each time instant $s(t)$.

To solve the shape control problem an augmented state, $z(t)$ is applied, defined as in [111],

$$z(t) = \begin{bmatrix} x(t) \\ q(t) \end{bmatrix}. \tag{4.2}$$

The vector $q(t)$ is an error function and is defined by

$$\dot{q}(t) = Cx(t) - y_d, \tag{4.3}$$

where

$$y_d = Cx_d. \tag{4.4}$$

The augmented state $z(t)$ can be applied to rewrite equation 4.1 in the form of an augmented state equation for shape control,

$$\dot{z}(t) = A_z z(t) + B_z u(t) + \gamma, \tag{4.5}$$

where

$$A_z = \begin{bmatrix} A & 0 \\ C & 0 \end{bmatrix}, \tag{4.6}$$

$$B_z = \begin{bmatrix} B \\ 0 \end{bmatrix}, \qquad \gamma = \begin{bmatrix} 0 \\ -y_d \end{bmatrix}. \tag{4.7}$$

The term γ can be treated as a constant disturbance and the problem turns into a disturbance rejection problem. In terms of the augmented state z, the quadratic cost function is

$$J = \int_0^\infty [z(t)^T Q z(t) + u(t)^T R u(t)] dt,$$

where

$$Q = \begin{bmatrix} 0_{n\times n} & 0_{n\times m} \\ 0_{m\times n} & I_{m\times m} \end{bmatrix}, \qquad R = I_{n_p \times n_p}.$$

The number of states in (4.1), the number of outputs and the number of actuators are indicated by n, m and n_p, respectively. We must confirm stabilizability of (A_z, B_z).

The pair (A_z, B_z) is stabilizable if there exists a feedback F such that the system $\dot{z}(t) = (A_z + B_z F)z(t)$ is asymptotically stable, which means all eigenvalues of $A_z + B_z F$ are in the open left-half plane.

Theorem 1 [112]: The pair (A_z, B_z) is stabilizable if and only if

$$rank[A_z - \lambda I \quad B_z] = n + m \qquad for \quad all \quad \lambda \in sp^+(A_z),$$

where $sp^{+}(A_z)$ is the set of eigenvalues of A_z matrix with non-negative real parts .

Theorem 2: The pair (A_z, B_z) is stabilizable if and only if $rank(\begin{bmatrix} A & B \\ C & 0 \end{bmatrix}) = n + m$.

Proof: To prove stabilizability, first it is required to calculate the eigenvalues of A_z. To find the eigenvalues of A_z matrix,

$$det(A_z - \lambda I) = 0,$$

needs to be solved which leads to

$$det(\begin{bmatrix} A - \lambda I & 0 \\ C & -\lambda I \end{bmatrix} = 0. \tag{4.8}$$

Equation (4.8) has a solution only when $\lambda I = 0$ or else $A - \lambda I$ is not a full rank matrix which leads to $det(A - \lambda I) = 0$. The solution of $det(A - \lambda I) = 0$ results in eigenvalues of A. Consequently, the eigenvalues of A_z are either zero or a solution of $det(A - \lambda I) = 0$, which are the eigenvalues of the A matrix.

Hence the rank condition needs to be satisfied at eigenvalues of A and also $\lambda = 0$,

$$[A_z - \lambda I \quad B_z] = \begin{bmatrix} A - \lambda I & 0 & B \\ C & -\lambda I & 0 \end{bmatrix}.$$

Since (A, B) is stabilizable, this matrix has a rank $m+n$ for all eigenvalues of A. Now considering $\lambda = 0$, the matrix becomes

$$\begin{bmatrix} A & 0 & B \\ C & 0 & 0 \end{bmatrix}.$$

Hence, to have a stabilizable (A_z, B_z) pair it is required that

$$rank(\begin{bmatrix} A & B \\ C & 0 \end{bmatrix}) = n + m. \tag{4.9}$$

To achieve a rank $n + m$ for the matrix in Equation (4.9), the number of columns in B must be equal to or larger than the number of rows in C. The number of columns in B equals the number of actuators. The number of rows in C equals the number of desired outputs. This means that the number of actuators must be larger than or equal to m which is the number of elements in the output vector, y or the number of desired outputs, y_d.

It is worth to mention that all practical structures experience a natural structural energy dissipation or damping during vibration. Normally, depending on the type and material of the structures a natural viscous damping ratio of 2 to 15 percent can be recommended in structural modeling [113]. In the presence of structural damping, all eigenvalues of A have negative real parts.

To calculate J_{opt}, the algebraic Riccati equation should be solved [114],

$$A_z P_z + P_z^T A_z - P_z B_z R^{-1} B_z^T P_z + Q = 0. \tag{4.10}$$

The optimal input voltage is

$$u_{opt}(t) = -R^{-1} B_z^T P_z z(t) = -K_z z(t). \tag{4.11}$$

Replacing $u_{opt}(t)$ in Equation 4.5, the closed loop system equation will be

$$\dot{z}(t) = A_{cz} z(t) + \gamma, \tag{4.12}$$

where

$$A_{cz} = A_z - B_z K_z.$$

Theorem 3 [111]: For detectable $(A_z, Q^{1/2})$ and stabilizable (A_z, B_z), the control law (4.11) asymptotically tracks the desired shape regardless of the initial state.

Proof: In Equation (4.12o), γ is time-independent. Consequently, in [111], differentiating both sides of Equation (4.12) with respect to time leads to,

$$\ddot{z}(t) = A_{cz}\dot{z}(t). \tag{4.13}$$

Stabilizability of (A_z, B_z) and detectability of $A_z, Q)$, results in a strictly stable system in equation 4.13. Hence, $\dot{z}(t)$ approaches zero regardless of the initial conditions. The vector $\dot{z}(t)$ equals

$$\dot{z}^T(t) = [\dot{x}^T(t) \quad \dot{q}^T(t)].$$

Hence as $t \to \infty$,

$$\dot{q}(t) = y(t) - y_d \to 0.$$

Therefore $y(t) \to y_d$ as $t \to \infty$.

The discussions so far, i.e., Theorems 1,2 and 3, require that the number of actuators be larger than or equal to the number of outputs. Consequently, it is required to define $y(t)$ such that while characterizing the desired shape, the number of its elements is smaller than or equal to the number of actuators. Choosing $y(t)$ is a designer's option. Different functions can be chosen depending on the type of states or the structure's degrees of freedom. In this study, $y(t)$ will be formed by writing the C matrix as a function of structural modes of vibration. It is discussed in detail in the following.

Any desired position can be expanded into the structural modes of vibration. Flexible structures with distributed mass have infinite degrees of freedom and an infinite number of modes. However, when structures are modeled with numerical methods such as finite elements or when the structural mass is considered as a lumped mass system, structural modes of vibrations reduce to a finite number. Consider a structure with N modes of vibration (eigenvectors) and N natural frequencies. The displacement vector, $s(t)$ can be expanded into its natural modes of

vibration [113]

$$s(t) = \sum_{i=1}^{N} v_i \zeta_i(t), \tag{4.14}$$

where v_i is the i^{th} mode shape and $\zeta_i(t)$ is the time variation for the i^{th} mode. If $s(t)$ equals the constant reference position s_d, equation 4.14 can be written as

$$s_d = \sum_{i=1}^{N} r_i v_i, \tag{4.15}$$

where r_i is called the participation factor of each mode in the desired position.

For each desired position s_d, normally the coefficient r_i for the first few modes is significantly higher than the others. These modes are the dominant modes for s_d. With a good approximation, s_d can be expanded into,

$$s_d \approx \sum_{i=1}^{N_1} r_i v_i,$$

where $N_1 < N$ is the number of dominant modes.

Now let's assume that the first half of elements of $x(t)$ are functions of displacements and the second half are functions of velocity. For instance if the regular state vector is used

$$x(t) = [s(t)^T \quad \dot{s}(t)^T]^T, \tag{4.16}$$

the desired state x_d is

$$x_d = [s_d^T \quad 0]^T. \tag{4.17}$$

And if the energy realization is used

$$x(t) = [(K^{0.5} s(t))^T \quad \dot{s}(t)^T]^T, \tag{4.18}$$

the desired state x_d is

$$x_d = [(K^{0.5} s_d)^T \quad 0]^T. \tag{4.19}$$

Define the C matrix as

$$C = [V \qquad 0_{N\times N_1}],$$

where V is formed by the first N_1 modes of the structure,

$$V = \begin{bmatrix} v_1' \\ \vdots \\ v_{N_1}' \end{bmatrix}, \tag{4.20}$$

Consequently, $\dot{q}$ is

$$\dot{q}(t) = [V \qquad 0_{N_1\times N}]x(t) - [V \qquad 0_{N_1\times N}]x_d, \tag{4.21}$$

The function $\dot{q}(t)$ can be defined more effectively in some situations by assigning weights to elements of y and y_d. The weights are also the designer's choice; however, it is better to assign larger weights to the modes that have larger participation in the desired shape. This way larger control effort will be dedicated to these modes. Hence a wise option is to choose the weights as functions of the participation factor of each mode in s_d. Then V is

$$V = \begin{bmatrix} w_1 v_1^T \\ \vdots \\ w_m v_m^T \end{bmatrix},$$

where w_1 and w_m are the assigned weights. These weights can simply be the modal participation factors r_i in s_d.

4.2 Optimal Actuator Placement in Structures

Consider now the problem of optimizing the locations of piezoelectric patch actuators on structures. It is assumed that the actuators are perfectly bonded to the top surface of the structure as

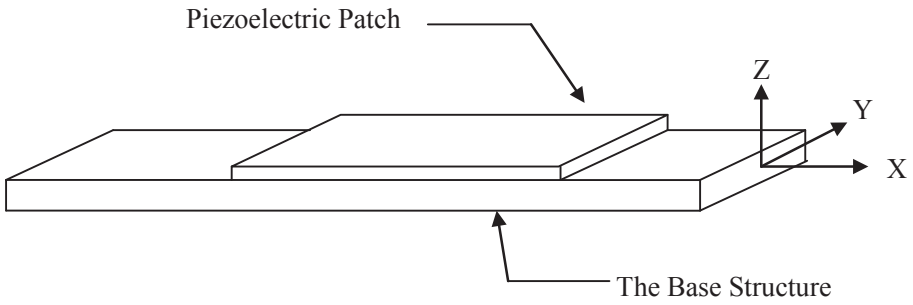

Figure 4.1: Structure with a piezoelectric patch

shown in Figure 4.1. Finite element approximation is used to model the base structures, and the actuators are assumed to have the same area as the finite elements.

For voltage-driven actuators, the finite element equations take the form

$$M\ddot{s}(t) + C_D\dot{s}(t) + Ks(t) - K_{s\phi}\phi(t) = Ks_d + F(t),$$

where M and K are the mass and stiffness matrices respectively and C_D is the damping matrix. A very small Rayleigh structural damping, $C_D = 10^{-8}K$ is assumed. Also $K_{s\phi}$ is the (symmetric) electro-mechanical coupling matrix, while $F(t)$ is the vector of external forces. Details for finite element modeling of piezo-laminated smart structures and M, K and $K_{s\phi}$ can be found in [106]. Next, the finite element equations are transferred into state space form by defining the state variable x with the energy realization

$$x(t) = \begin{Bmatrix} K^{0.5}s(t) \\ \dot{s}(t) \end{Bmatrix}.$$

The system dynamics can be written as

$$\dot{x}(t) = Ax(t) + B\phi(t),$$

where

$$A = \begin{bmatrix} 0 & K^{0.5} \\ -M^{-1}K^{0.5} & -M^{-1}C_D \end{bmatrix}; B = \begin{bmatrix} 0 \\ M^{-1}K_{s\phi} \end{bmatrix}.$$

Applying this state vector, the error function $\dot{q}$ can be defined as

$$\dot{q} = [V \qquad 0_{N_1 \times N}]x(t) - VK^{0.5}s_d. \tag{4.22}$$

Consequently, as $\dot{q} \to 0$,

$$(K^{0.5}s(t) - K^{0.5}s_d) \to 0. \tag{4.23}$$

The matrix K is the structural stiffness matrix and it is positive definite. Hence, in general $K^{0.5}$ has non-zero eigenvalues. This means that when equation (4.23) is true, then $s(t) - s_d \to 0$. Consequently, applying the energy realization will also result in the desired shape for the structure.

It should be mentioned that by choosing the V matrix as a function of structural modes, in fact the intention will be to minimize the modal errors. Hence, the weightings in V should be chosen in a way to minimize the error for modes that are participating more in the desired shape regardless of the components of state vector. As an example when state vectors are formed using the energy realization, in fact the purpose is to minimize the error between strain energies. Now the strain energies for the modes that are participating more in the desired shape should be minimized and V should be composed of the first few dominant modes in s_d and the weightings should be chosen as the participation factors of these modes in s_d. Using the weights based on the participation factors in $K^{0.5}s_d$ may assign very small weights to some of the dominant modes in s_d and make them completely ineffective. This reduces the accuracy and efficiency of the system.

Using energy realization results in optimal actuator positions very close to the positions

Properties	Piezoelectric	Base Structure
Elastic Modulus (Nm^{-2})	61×10^9	21×10^{10}
Density ρ (kgm^{-3})	7700	7810
Dielectric Constant d_{31} (Mv^{-1})	171×10^{-12}	
Poisson's Ratio	0.3	0.3

Table 4.1: Material properties of steel and piezoelectric materials

achieved with regular state space formulation. For some structures such as beams and some desired shapes, these two realizations result exactly the same. For example the optimal locations on a cantilever beam are the same for the two realizations for desired shape s_{d2} discussed later in this chapter.

For the augmented states, A_z and B_z are the same as was discussed in previous sections. In addition detectability of (A_z, Q) needs to be verified before each optimization procedure. This is checked for all the models in the following examples.

We considered patches 40 μm thick and made of PZT 5A. The base structures are made of steel. Material properties of Steel and PZT 5A are shown in Table 4.1. The optimal locations of actuators for shape control of flexible structures are calculated using the presented optimization scheme. Optimal actuator locations on beams are calculated for beams with pinned-pinned and fixed-free boundary conditions. 'BEAM3'finite elements which are based on Bernoulli-Euler beam theory are used to model the beams in ANSYS finite element software. The equations of motion for Bernoulli-Euler beams with attached piezoelectric patches can be found in [107].

Optimal actuator locations are also calculated on plates with two different boundary conditions. To model the plates in ANSYS, 'SHELL181'elements are used which are based on Reissner Mindlin plate theory. The equations of motion for Reissner Mindlin plates with attached piezoelectric patches can be found in [107].

4.2.1 Optimal Actuator Locations on a Cantilever Beam

A cantilever beam is shown in figure 4.2. The beam dimensions are 0.5 m x 0.03 m x 0.002 m and it is divided into 15 finite elements.

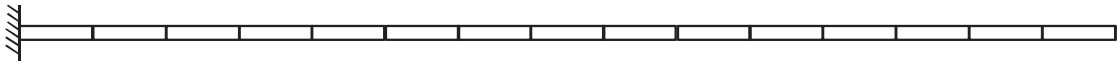

Figure 4.2: A 0.5m long cantilever beam divided into 15 finite elements

The desired position for this beam, s_{d1} is

$$s_{d1} = 10v_3 + 6v_5, \tag{4.24}$$

where v_3 and v_5 are the third and fifth modes of vibration for the beam as shown in Figure 4.3. Only the third and fifth modes are present for the reference position. The V matrix is

$$V = \begin{bmatrix} 10v_3^T \\ 6v_5^T \end{bmatrix},$$

and y_d is formulated accordingly.

In Figure 4.5, the results for 2, 4, and 5 actuators are compared with the desired shape. These actuators are optimally located. With 2 and 4 actuators the error is significant.In fact with 2 actuators there is no control over the desired shape. Consequently, it is required to apply at least 5 actuators. Despite the fact that only 2 modes are involved in the reference shape, applying fewer actuators than 5, leads to inaccurate results and considerable errors. The reason is that N_1 in Equation (4.15) equals 5. Figure 4.4(a) shows the optimal location for 2 actuators. Figure

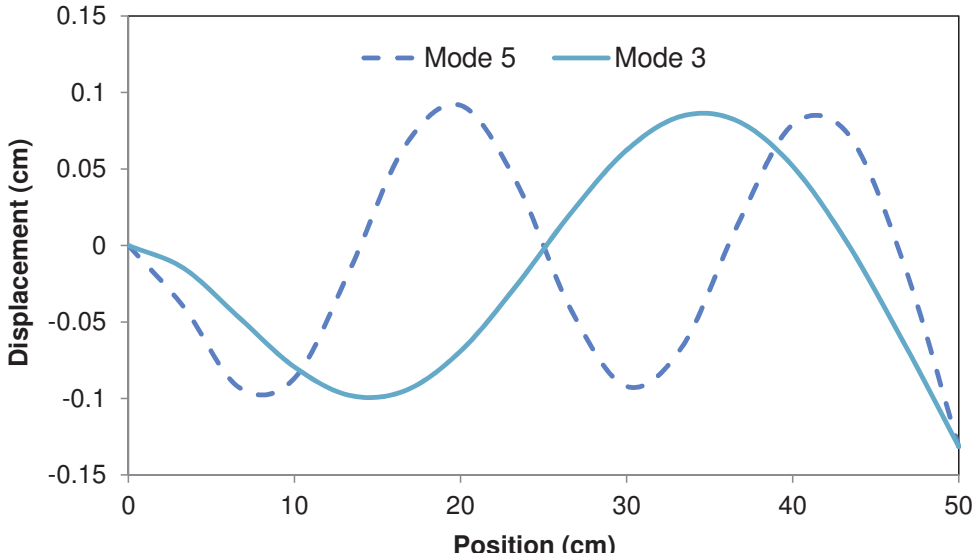

Figure 4.3: Third and fifth modes of vibration for a cantilever beam

4.4(b) shows the optimal location for four actuators. The optimal location of five actuators are shown in Figure 4.4(c).

It should be mentioned that accuracy is not only dependent on the number of actuators, but also on the desired shape. As another example, the optimal location of actuators is studied on the same beam with a different reference shape. The desired shape for this problem is

$$s_{d2}(\xi) = 0.0948\left[\left(\frac{\xi}{50}\right)^3 - \left(\frac{\xi}{50}\right)^4\right], \tag{4.25}$$

where ξ is the distance from the fixed end in centimeters. The dominant modes for this shape are modes 1, 2, 3, 33 and 35 of the beam. The optimal location of 3, 4 and 5 actuators are calculated for this problem. The number of actuators is smaller than the number of highest dominant mode. For n_p actuators, C is chosen as a matrix with n_p rows. The rows are the first n_p modes of the structure, multiplied by their participation factor in the reference shape. Figures 4.6(a), 4.6(b) and 4.6(c) show the optimal locations of 3, 4 and 5 actuators, respectively. In Figure 4.7,

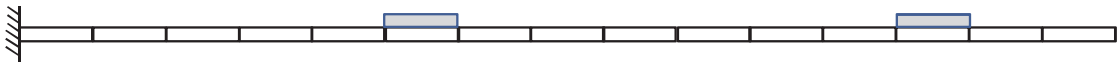

(a) 2 actuators

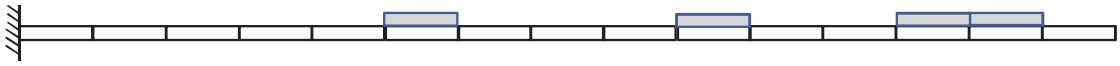

(b) 4 actuators

(c) 5 actuators

Figure 4.4: Optimal actuator locations for a 0.5m long cantilever beam for desired shape s_{d1}

the achieved shapes with 3, 4 and 5 actuators are compared with the reference position. The small existing error is because 4 and 5 actuators cannot compensate for the missing part of deformation related to modes 33 and 35.

As the number of actuators increases, the residual error becomes smaller. Figure 4.6(d) shows the optimal location of 6 actuators. The achieved shape with 6 actuators as shown in Figure 4.8, is slightly more accurate than those in Figure 4.7. However, to reach complete accuracy a larger number of actuators is required.

The required accuracy in a shape control problem depends on the application and operation

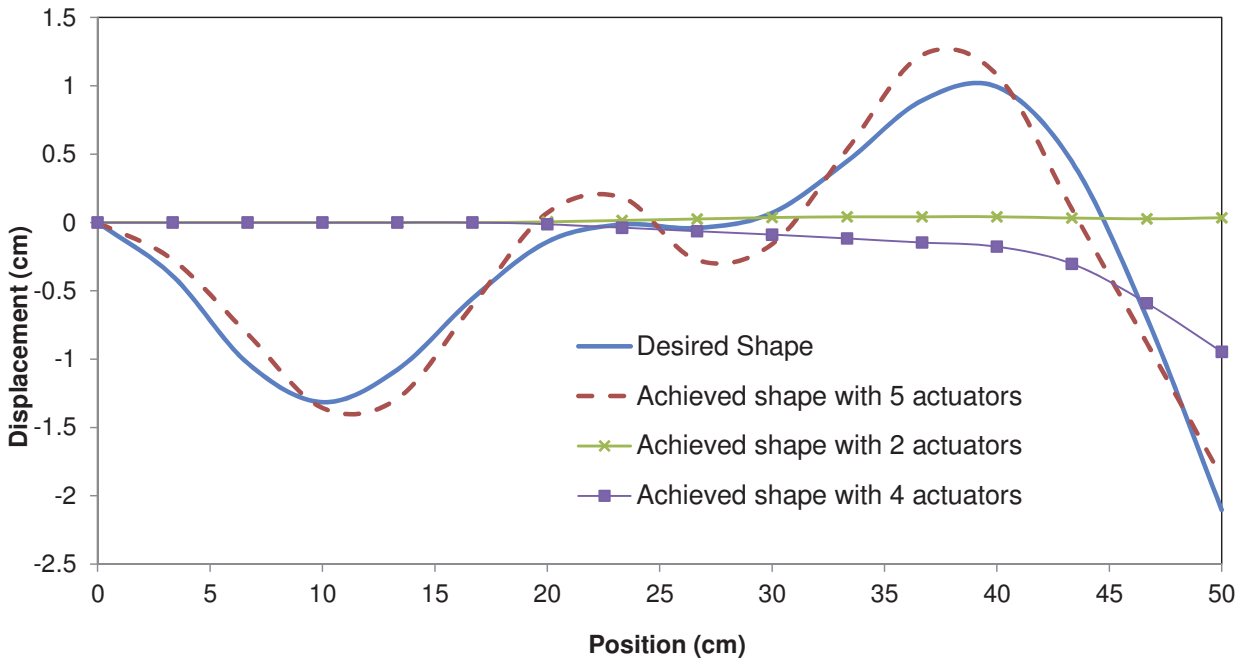

Figure 4.5: Comparison between achieved shapes and desired shape s_{d1} for a 0.5m long cantilever beam

requirements of the structure. According to the results so far, the minimum number of required actuators depends on the type of structure and desired shape.

To study the efficiency of the introduced optimization method, the optimal locations of actuators need to be calculated on structures with more elements. Consequently, the beam dimensions are changed to 3 m x 0.03 m x 0.002 m with the same material properties as previous models. The actuator locations are calculated on this beam. The beam is divided into 100 finite elements. The desired position is,

$$s_{d3}(\xi) = 0.948\left[\left(\frac{\xi}{300}\right)^3 - \left(\frac{\xi}{300}\right)^4\right], \tag{4.26}$$

where d is the displacement in cm from the fixed end. The dominant modes for this shape are

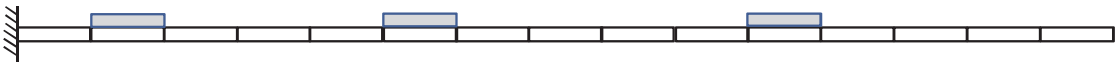

(a) 3 Actuators

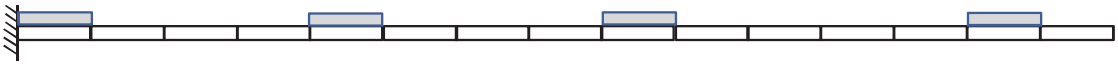

(b) 4 Actuators

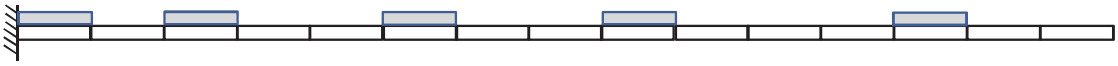

(c) 5 Actuators

(d) 6 Actuators

Figure 4.6: Optimal actuator locations for a 0.5m long cantilever beam for desired shape s_{d2}

modes 1, 2, 3, 4, 5 and modes 224 and 232. The last two modes have large modal stiffnesses and require large control energies. Consequently, despite the fact that these are dominant modes compared with the others, they might be less important in controlling position than the first modes. This idea can be studied through calculating optimal actuator locations by considering

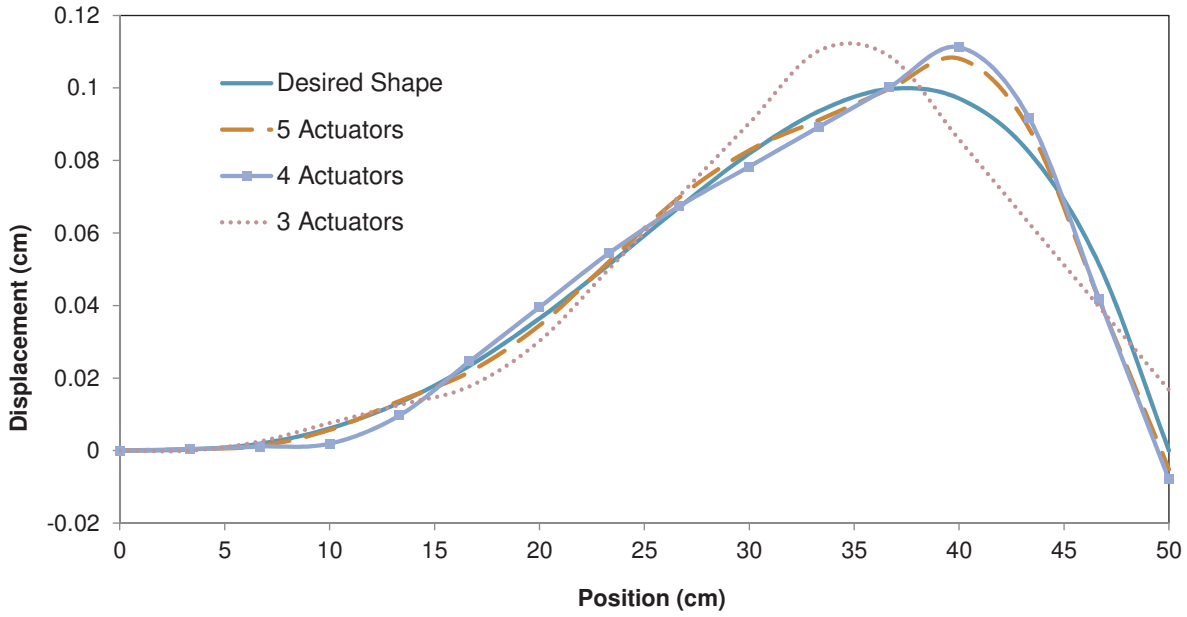

Figure 4.7: Comparison between achieved shapes and desired shape s_{d2} on a 0.5m long cantilever beam

the effect of the first five modes in y_d. Hence V in equation 4.22 is

$$V = \begin{bmatrix} r_1 v_1^T \\ \vdots \\ r_5 v_5^T \end{bmatrix},$$

where r_1 to r_5 are the participation factors for modes 1 to 5. Table 4.2 shows the optimal locations for 10 actuators. The desired and achieved shapes are compared in Figure 4.9. This figure shows that both shapes match reasonably well.

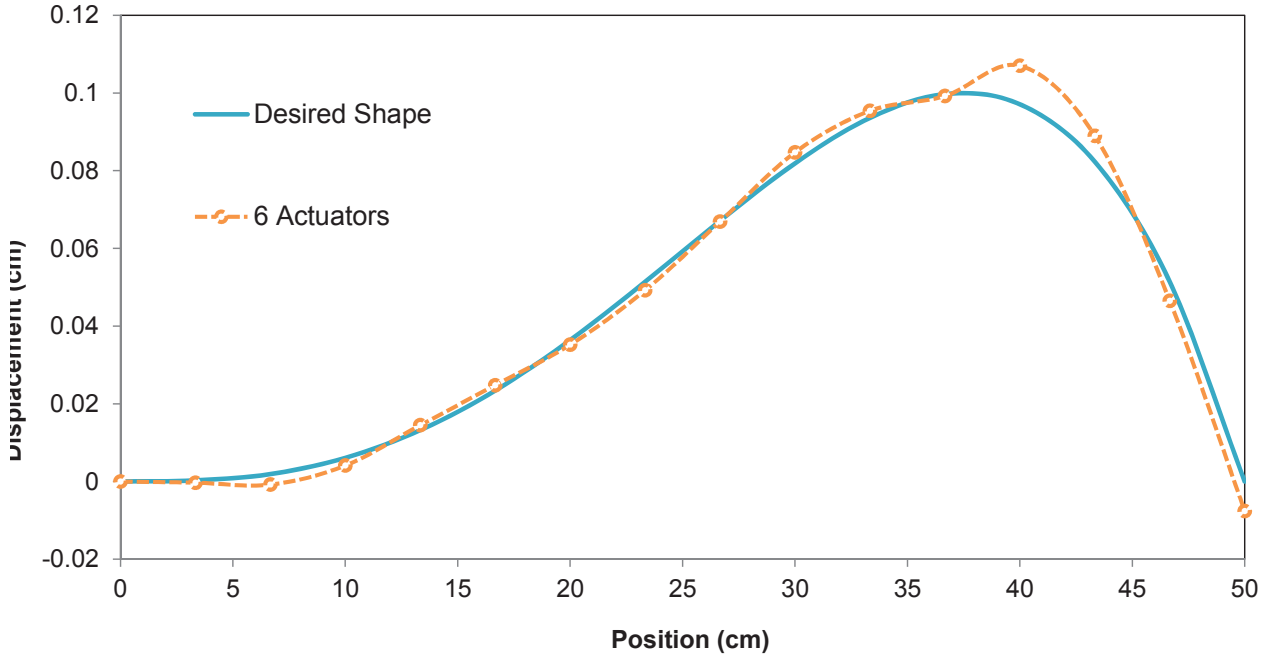

Figure 4.8: Comparison between desired shape s_{d2} and achieved shapes with 6 actuators on a 0.5m long cantilever beam

Number of actuators	Optimal Actuator Locations
10	2,5-8,92,94-97

Table 4.2: Optimal actuator locations on a 3m long cantilever beam for desired shape s_{d3}

4.2.2 Optimal Actuator Locations on a Simply Supported Beam

A simply supported beam is shown in Figure 4.10. The beam dimensions are 0.5 m x 0.03 m x 0.002 m and it is divided into 15 finite elements. The desired shape for this beam is

$$s_{d4}(\xi) = 0.05(1 - \cos 2\pi\xi/50), \tag{4.27}$$

where ξ is the distance in *cm* from either of the pinned end conditions. This shape is symmetric.

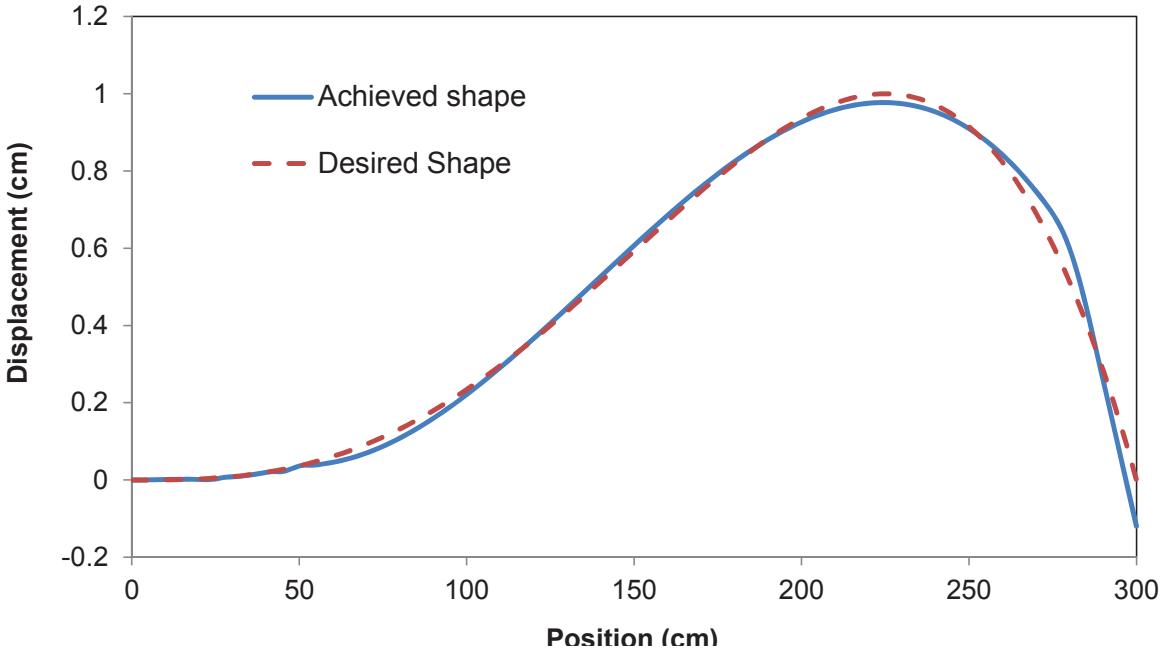

Figure 4.9: Comparison between desired shape s_{d3} and achieved shapes on a 3m long cantilever beam with 10 actuators

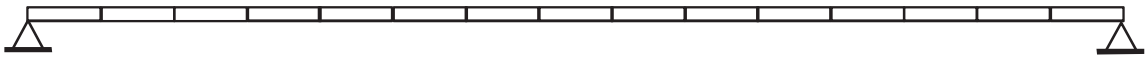

Figure 4.10: A simply supported beam

For this reference position, the dominant modes are 1,3,5, 30 and 32. The modal participation factors for these modes in the desired shape are

$$r_1 = 0.599, \quad r_3 = 0.133, \quad r_5 = 0.023, \quad r_{30} = 0.228, \quad r_{32} = 0.402.$$

The participation factors for odd-numbered modes are zero for this shape, since all these modes are anti-symmetric and the desired shape is symmetric. Although the modes 30 and 32 have

large participation factors, it is not economical to apply actuators all over the beam's length. Hence, the optimal location of 3 and 5 actuators are calculated for this shape on the beam. The desired output, y_d, as discussed in the previous section is formed by only including the effects of first, third and fifth modes. According to the presented formulation, the highest structural mode involved in y_d poses conditions for the minimum number of actuators. The vector y_d is not dependent on the number of actuators as long as this number is larger than the minimum required. The matrix V in Equation (4.22) is

$$V = \begin{bmatrix} r_1 v_1^T \\ r_3 v_3^T \\ r_5 v_5^T \end{bmatrix},$$

(a) 3 Actuators

(b) 5 Actuators

Figure 4.11: Optimal actuator locations for a 0.5 m long simply supported beam for desired shape s_{d4}

The optimal locations of 3 and 5 actuators for this beam are shown in figures 4.11(a) and 4.11(b). The achieved shapes are compared with the desired shape in figure 4.12. For 3 actuators the achieved shape does not match the desired shape. The V matrix includes up to the fifth

structural mode. This means that to be able to control the fifth mode at least 5 actuators are required to achieve the desired shape. It supports the idea that although V includes 3 modes and y_d has three elements, 3 actuators are not capable of deforming the beam to its desired position. The highest mode involved in the desired shape is the key factor in specifying the minimum number of actuators not the number of elements in y_d. When 5 actuators are applied the achieved shape is close to the reference position.

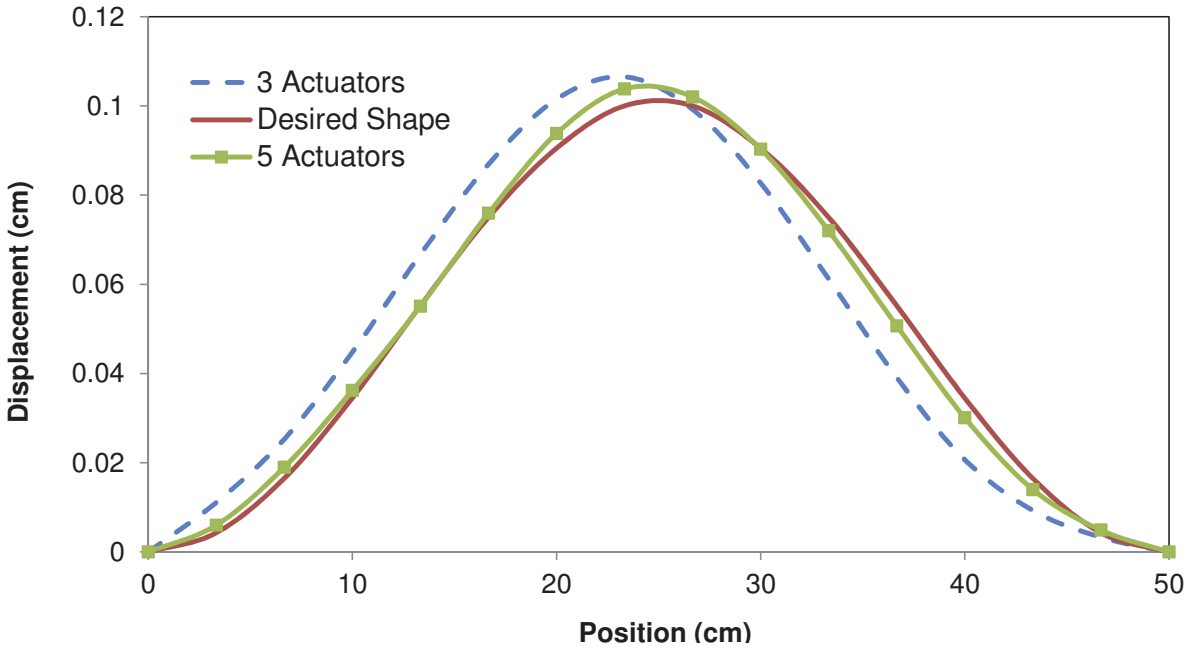

Figure 4.12: Comparison between desired shape s_{d4} and achieved shapes on a 0.5m long simply supported beam

Next, the beam dimensions are changed to 3m x 0.03m x 0.002m . The beam is divided into 100 finite elements. The desired shape for the beam is

$$s_{d5}(\xi) = \frac{1}{2}(1 - \cos 2\pi\xi/300), \tag{4.28}$$

Number of actuators	Optimal Actuator Locations
10	17-19,49-52,82-84

Table 4.3: Optimal locations of 10 actuators on a 3m long simply supported beam for desired shape s_{d5}

where ξ is the distance in *cm* from either of the pinned ends of the beam. For this shape, the first, third and fifth modes are the dominant modes. The optimal location of 10 actuators is calculated for the beam. The results are shown in Table 4.3. In Figure 4.13 the achieved shape when actuators are optimally located on the beam is compared with the desired position.

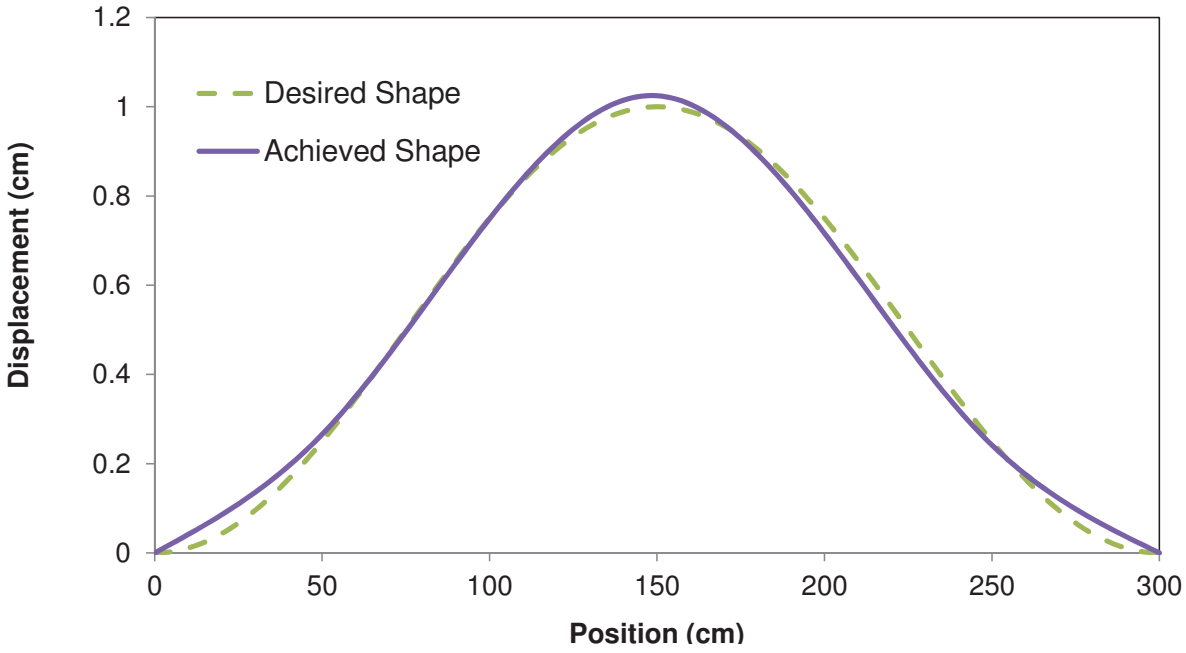

Figure 4.13: Comparing desired shape s_{d5} and achieved shapes on a 3m long simply supported beam with 10 actuators

4.2.3 Optimal Actuator Locations on Plates

In this section the optimal location of 10 actuators is calculated for shape control of a plate with two different boundary conditions. Plate dimensions are 500 mmx500 mmx1 mm and it is divided into a 10x10 grid of finite elements. The structure is augmented with actuators on its top surface and actuators are 50 mm x50 mm x40 μm each, which is the same area as the finite elements.

The optimization results are also compared with a genetic algorithm. For genetic algorithm, the population size is taken as 100, to get results as accurate as possible. A random initial population is chosen and the optimization constraint on the number of actuators is taken into account by assigning a very large number to the fitness value when the number of ones in binary genes of each chromosome goes higher than 10.

Cantilever Plate

In the first model, the plate is fixed at one of its edges as shown in Figure 4.14. The desired shape is

$$s_{d6} = 10v_1 + 10v_4, \tag{4.29}$$

where v_1 and v_4 indicate the first and forth mode shape, respectively. Figure 4.16(a) shows this reference position.

To optimize actuator locations on this plate V in Equation 4.22 can be written as

$$V = \begin{bmatrix} 10v_1^T \\ 10v_4^T \end{bmatrix}. \tag{4.30}$$

Figures 4.15(a) and 4.15(b) show the optimal locations of 10 actuators on this plate when the presented optimization scheme and a genetic algorithm (GA) are applied, respectively. Let's call

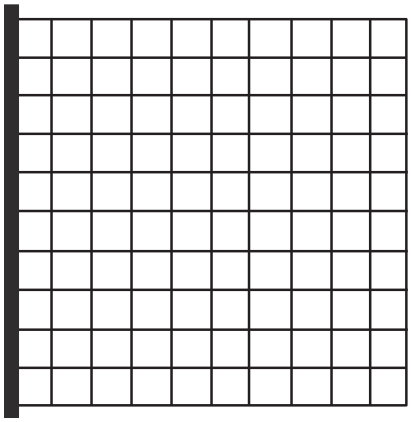

Figure 4.14: A cantilever plate

the placement in Figure 4.15(a), placement (a) and the placement in Figure 4.15(b), placement (b). The calculated optimal locations from the two methods are very close. However, the objective value with the presented method is slightly smaller. The objective value for actuator placement (a) is 1.8943 and this value for placement (b) is 1.921. This verifies the accuracy of the presented optimization scheme.

Besides verifying the results, GA is applied to show how important it is to optimally place actuators for a shape control problem when limited number of actuators are applied. The results from GA present a near optimal solution for this problem. Figures 4.16(b) and 4.16(c), show the achieved vertical displacements for placements (a) and (b) respectively. Figures 4.17(a) and 4.17(b) show the error percentage for the deformations in Figures 4.16(b) and 4.16(c) respectively. Despite the fact that placement (b) is a near optimal solution, it does not result in an accurate achieved position for the plate. The results for actuator placement (a) is much more accurate that the results from placement (b).

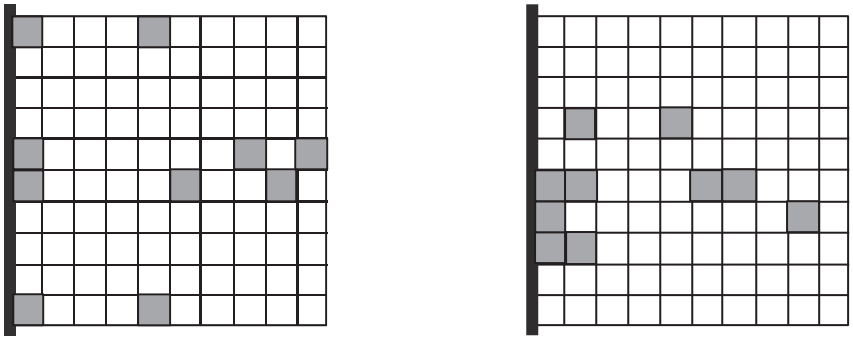

(a) Presented Optimization Scheme, Objective value=1.8943 (b) Genetic Algorithm, Objective value=1.921

Figure 4.15: Optimal actuator locations on a cantilever plate for desired shape s_{d6} applying two different optimization schemes

Plate with Pinned-Pinned Boundary conditions

The boundary conditions on the plate are changed to pinned condition on two opposite sides of the plate. This model is shown in Figure 4.18. The desired shape is

$$s_{d7} = 10v_1 + 10v_4, \tag{4.31}$$

where v_1 and v_4 are the plate's first and forth modes of vibration. Consequently, the V matrix, takes the same form as Equation 4.30. The desired shape is shown in Figure 4.20(a).

Figures 4.19(a) and 4.19(b) show the optimal locations of 10 actuators on this plate when the presented optimization scheme and when a genetic algorithm are applied respectively. Let's call the placement in Figure 4.19(a), placement (c) and the placement in Figure 4.19(b), placement (d). Genetic algorithm results in an objective value of 8.9733. The presented optimization scheme results in an optimum objective value of 8.8905 . The difference between the calculated optimums by both methods is very small. Almost no difference between the errors in achieved

shapes is.

Figures 4.20(b) and 4.20(c) show the achieved plate shapes from placement (c) and (d), respectively. Figures 4.21(a) and 4.21(b) show the error percentage for the deformations in Figures 4.20(b) and 4.20(c) respectively. Despite the fact that the objective values for both placements are almost identical, the maximum shape error for placement (d) is significantly larger than the maximum shape error for placement(c). Although the matrix V includes only modes one and four of the structure, 4 actuators is a lower bound for the number of actuators and may not lead to an accurate shape for the plate. To achieve an accurate shape for the plate, a higher number of actuators is required.

It can be concluded that the minimum number of actuators required to achieve accurate results depends on the desired shape and type of the structure. A lower band is the number of desired outputs. However, this is required to achieve stabilizability in the system.

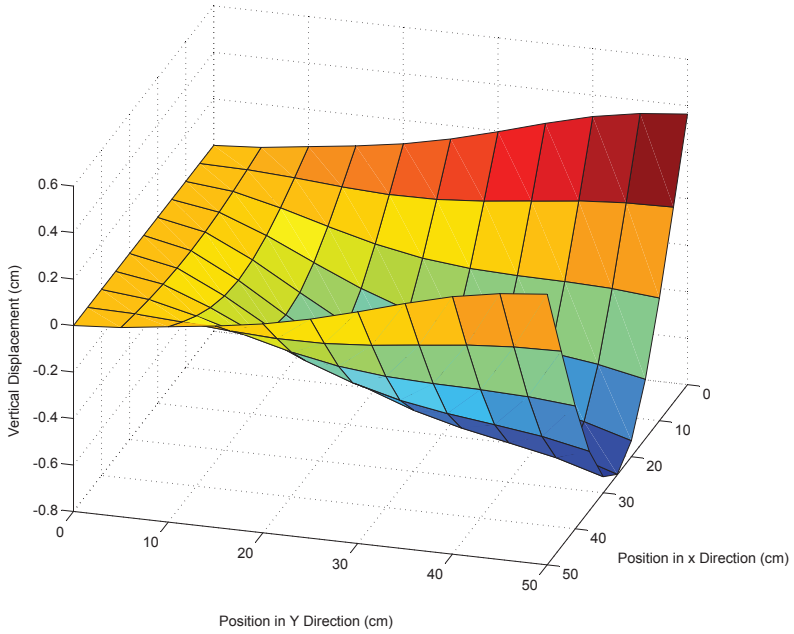

(a) Desired shape s_{d6} for the cantilever plate

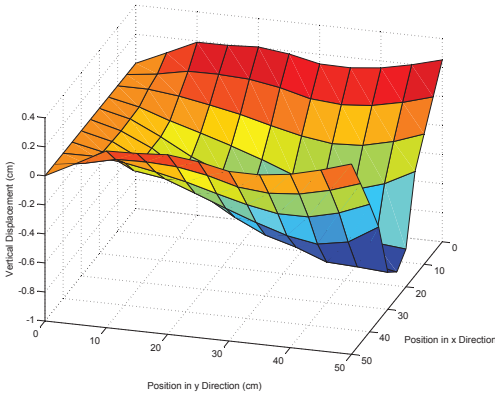

(b) Presented optimization scheme

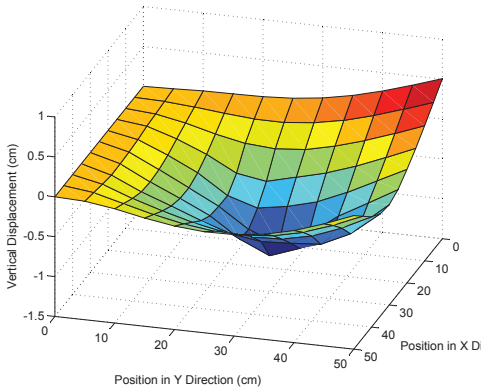

(c) A Genetic algorithm

Figure 4.16: The achieved and desired shapes with 10 actuators on a cantilever plate

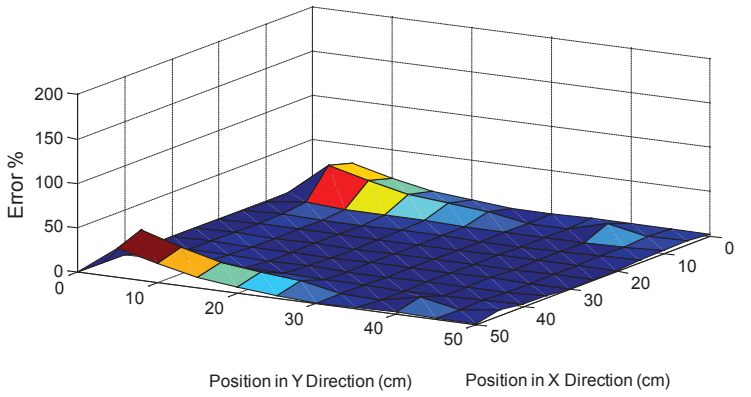

(a) Presented optimization scheme

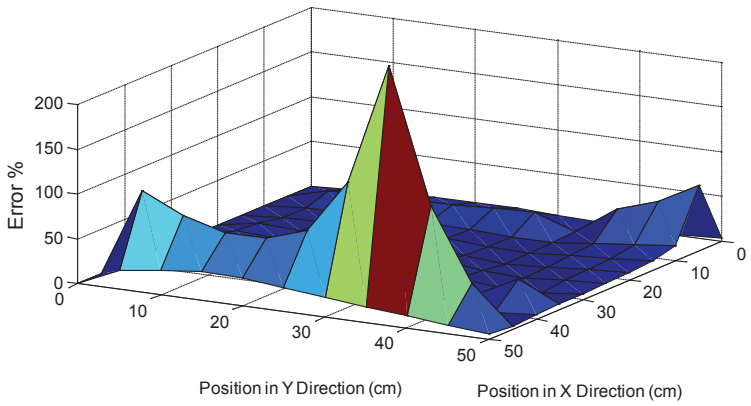

(b) A Genetic algorithm

Figure 4.17: The errors between achieved and desired shape s_{d6} on a cantilever plate

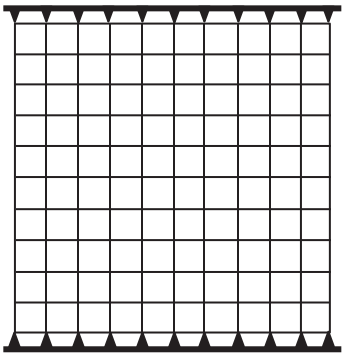

Figure 4.18: A plate with pinned boundary conditions on its two opposite edges

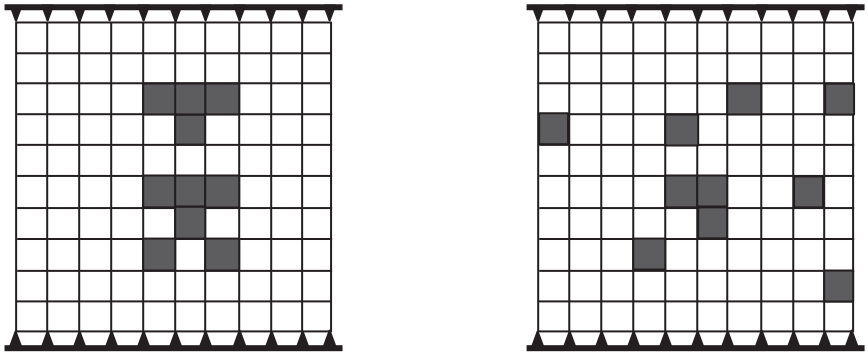

(a) Presented Optimization Scheme, Objective value=8.8905 (b) Genetic Algorithm, Objective value=8.9733

Figure 4.19: Optimal actuator locations for desired shape s_{d7} on a cantilever plate applying two different optimization schemes

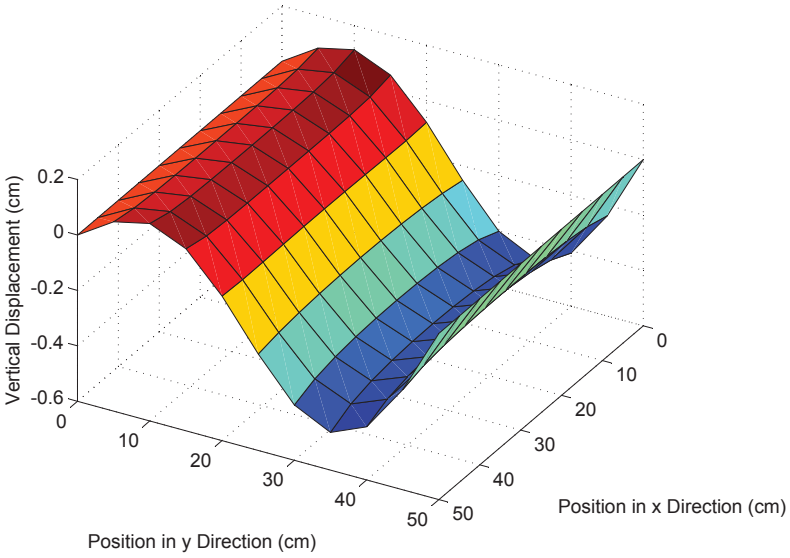

(a) Desired shape

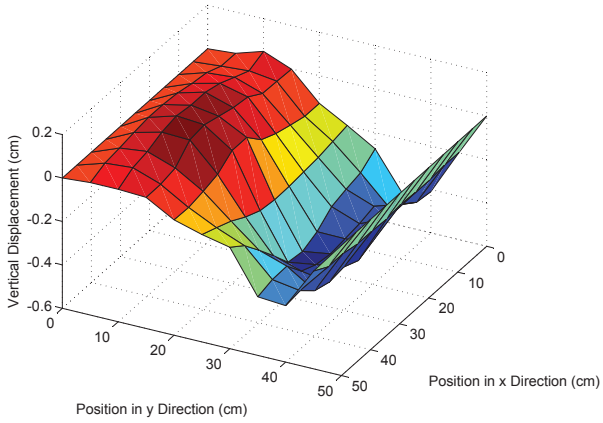

(b) Presented optimization scheme

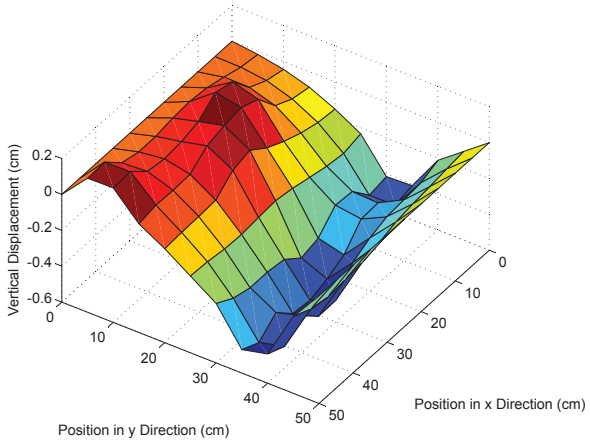

(c) A Genetic algorithm

Figure 4.20: The achieved and desired shape s_{d7} on a plate with pinned boundary conditions on its two opposite edges

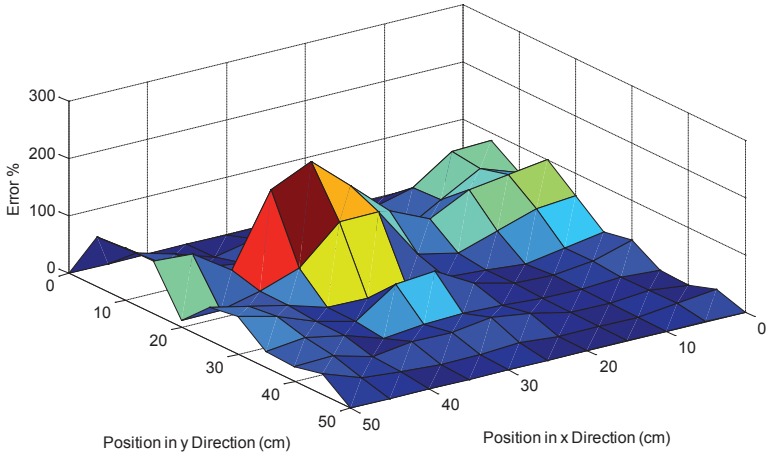

(a) Presented optimization scheme

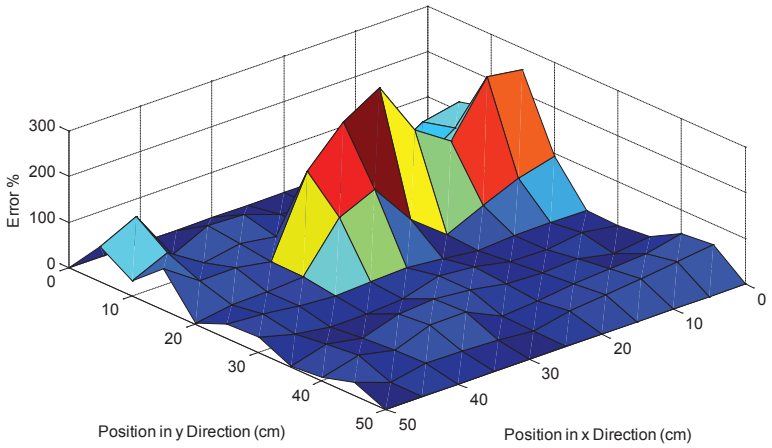

(b) A Genetic algorithm

Figure 4.21: The errors between achieved and desired shape s_{d7} on a plate with pinned boundary conditions on its two opposite edges

Chapter 5

Experimental Study of Optimal Shape and Vibration Control

In this chapter optimal location of piezoelectric patches in vibration control and shape control of a steel cantilever beam is experimentally studied. The linear quadratic regulator (LQR) is the state feedback control law. Because of the limitations in the number of sensors, the states need to be estimated. The state estimation approach is discussed in Section 5.4.

The stiffness and mass of the actuator patches are assumed to be negligible. Moreover, the feedback control is calculated based on finite element estimation of the beam. The finite element modeling and the aforementioned assumption need to be verified. Section 5.3 explains the experiments carried out to verify these two criteria.

Moreover, two non-contact laser sensors are used in these experiments. Consequently, it is important to locate the sensors in optimal positions so that they can read displacements efficiently. The optimal sensor placement is studied in Section 5.5. The same optimization method is applied to find the optimal sensors locations.

5.1 Experimental Setup

To study the actual effect of optimal actuator placement, experiments were performed on a cantilever beam. The experimental setup is shown in Figure 5.1. A thin steel beam is hung from the top of an aluminum frame. The beam has a fixed boundary condition at the top and is free at the bottom. The optimal location of two actuators on this cantilever beam is studied for both vibration and shape control. To study the optimal actuator location problem, 4 patches are attached to the beam surface with superglue as shown in Figures 5.2 and 5.3. In each experiment only two of these actuators are activated to suppress the beam's vibration or regulate it to the desired shape.

Figure 5.1: Experimental setup for vibration control and shape control of a steel cantilever beam

Table 5.1 shows the beam and piezoelectric patch dimensions. The beam material properties are shown in Table 5.2. The actuators are PSI-5A4E piezo sheets from Piezosystems. These actuators are made of Lead Zirconate Titanate and are Industry Type 5A or Navy Type II.

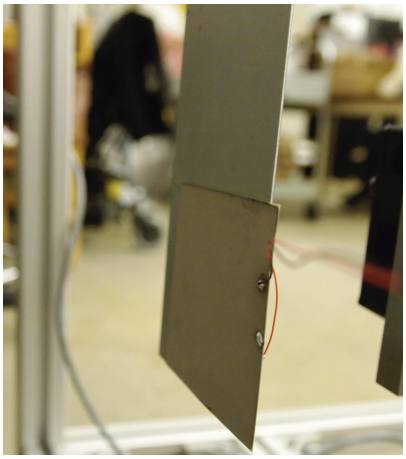

Figure 5.2: Piezoelectric patch bonded to the beam's surface

Material properties of piezo-patches are shown in Table 5.2. For this material, the relative dielectric constant, $K_3 = 1800$ for 1 KHz frequency [3]. Relative dielectric constant is applied to calculate the capacitance of piezoelectric patches. The capacitance is

$$C_p = \frac{K_3 \epsilon_0 A}{t_p},$$

where $\epsilon_0 = 8.9 \times 10^{-12}$ farads/meter is the permittivity of the free space, A is the area of electrodes and t_p is the thickness of patches [3]. For the piezo-patches used in these experiments, both top and bottom surfaces are covered by electrode layers . Consequently, A is equal to the surface area of each patch. For the patch dimensions in Table 5.1 , $C_p = 660 \times 10^{-9}$ F.

	Beam	Piezoelectric Patch
Length(cm)	70	7
Width(cm)	7	7
Thickness(mm)	0.85	0.127

Table 5.1: Dimensions of the beam and the piezoelectric patches

Figure 5.3: The beam, actuators and sensors

Properties	Piezoelectric	Base Structure
Elastic Modulus (Nm^{-2})	66×10^9	21×10^{10}
Density ρ (kgm^{-3})	7800	7810
Dielectric Constant d_{31} (mv^{-1})	190×10^{-12}	
Poisson's Ratio	0.3	0.3

Table 5.2: Material Properties

SA11 power amplifier is used for input voltages of actuators. This amplifier is modified to have 3 input and 3 output channels. It is capable of providing up to 270 V peak to peak, when it is provided by 115 VAC 60 Hz or 220 VAC 50 Hz. It accepts an input voltage range of ±9 VCD

or peak AC. Its output current range is from 0 to ±300 mA DC or peak AC. The maximum input voltage of actuators is dependent on the amplifier's output current range and the capacitance of piezoelectric patches. Consequently, the maximum voltage that can be supplied to the actuators is

$$V_{max} = \frac{I_{max}}{2\pi f C_p},$$

where I_{max} is the maximum current which in this case equals 300mA, f is the frequency which equals 1 KHz [3]. The maximum voltage that the amplifier provides for actuators is 72 Volts. Keyence LK081 and LK031 non-contact laser sensors are applied to read the deformations and estimate the states. Each laser sensor comes with its own controller. Table 5.3 shows the specifications of these sensors. Hence sensor location 1 in Figure 5.4 is LK-031 since the range of displacements is smaller in this position. It is located at a 30 mm horizontal distance from the beam. Sensor location 2 is LK-081 and it is located 80 mm away from the beam. The data acquisition system (DAQ), includes Sensory 626 data acquisition card and a computer. This DAQ card is compatible with MATLAB. The controller is programmed using simulink in MATLAB. Figure 5.4 shows the experimental beam model. The block diagram of the experimental setup is shown in Figure 5.5. In these experiments, the feedback control and input voltages of actuators are calculated based on a discrete time system. The time step is one millisecond.

The next step is to identify the optimal location of actuators. To find the optimal location of the two actuators on the beam, the beam is modeled with 10 'BEAM3' finite elements in ANSYS finite element software. Each element has the same dimensions as the actuator patches. To complete the finite element modeling, the damping of the beam's material also needs to be estimated. Moreover, the finite element modeling and the estimated damping must be verified by comparing the experimental and analytical natural frequencies of the beam.

Sensor Head	LK-031	LK-081
Controller	LK-2001	LK-2101
Reference Distance(mm)	30	80
Measuring Range(mm)	±5	±15
Sampling Rate (μs)	512	1024
Resolution (μm)	1	3

Table 5.3: Specifications of non-contact laser sensors

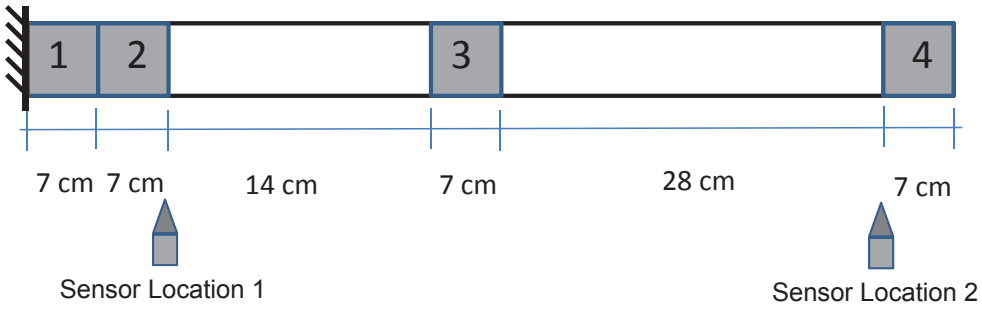

Figure 5.4: Experimental beam model and the actuator and sensor positions

5.2 Damping Estimation

To estimate the damping of the beam, the beam is released to vibrate from an initial displacement at its end point. The beam's displacement is recorded by sensor 2. A Rayleigh damping model is assumed for the beam. The beam is also modeled with finite element discretization. Vibration of the model beam is then simulated with the same initial conditions as the experiments. The damping in the model is varied until the vibrations of the model beam match the vibrations from the experiment. To assure the accuracy of the damping matrix estimation, the

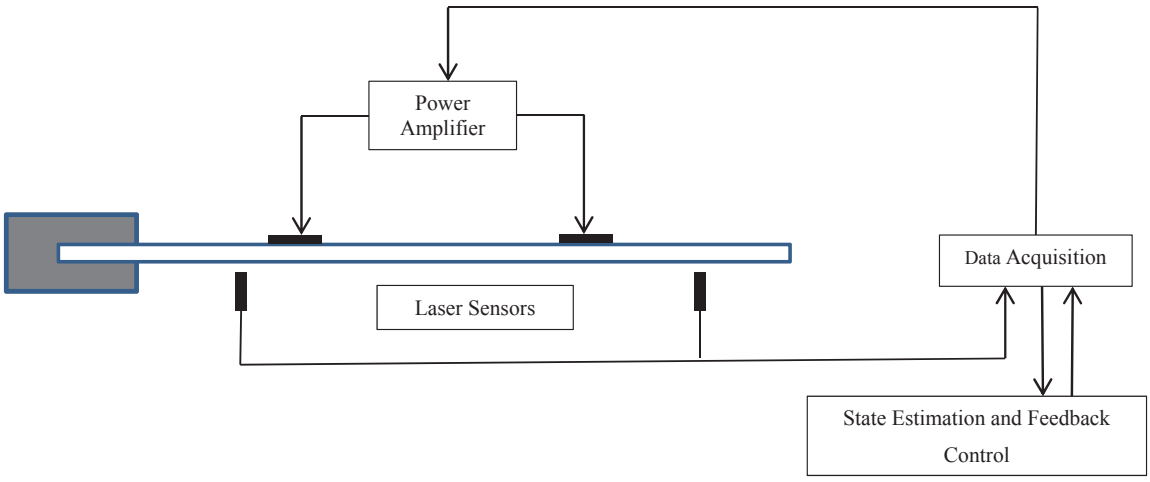

Figure 5.5: Block diagram of the experimental setup

experiments are repeated for various initial displacements at the beams tip. The analytical and experimental results are then compared to assure accuracy.

The beam's damping is estimated as

$$C_d = 5 \times 10^{-4} K,$$

where K is the stiffness matrix of the beam which is calculated by finite element modeling. Table 5.4 shows a sample comparison of the decay ratio in vibration amplitude in 10 seconds at the end of the beam. For this table the initial condition is 7 mm at the end of the beam.

	Decay Ratio (Percent)
Experimental Beam	25
Analytical Beam	24.7

Table 5.4: Decay ratio in the beam's vibration amplitude in 10 seconds

5.3 Verification of Finite Element Model

The beam is modeled with a finite element method. It is divided into 10 elements and the size of each element is 7cm×7cm. These elements are relatively coarse. Since the state space equations of the beam and the feedback control are dependent on the number and size of elements, it is required to verify that the finite element modeling captures the dynamics of the beam with an acceptable accuracy. On the other hand, since piezo-patches have a very small thickness, in the optimization of actuator locations, the stiffness and mass of actuators were neglected. In this section, experiments are carried out to verify the validity of this assumption.

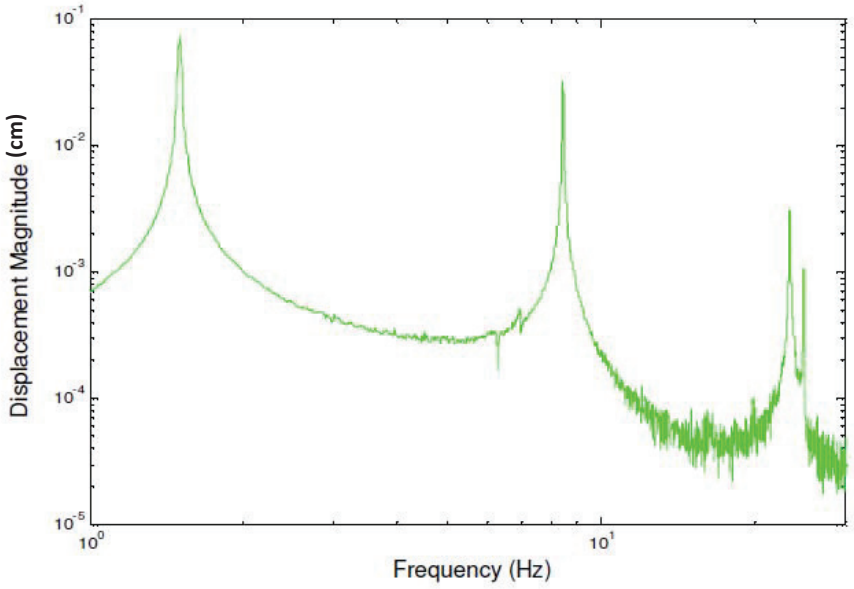

Figure 5.6: Frequency response of the beam without actuators

Before attaching the actuators, the beam is subjected to an impulse at one third of its length from the top. Figure 5.6 shows the frequency response function of the beam. In the next step, the four piezoelectric patches are bonded to the beam and the beam is subjected to an impulse at the same location as before. Figure 5.7 shows its frequency response. In both Figures 5.6 and 5.7

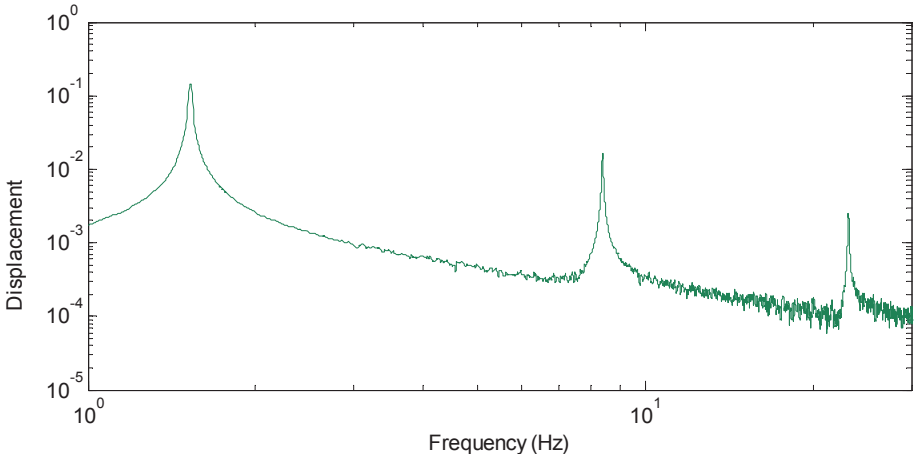

Figure 5.7: Frequency response of the beam with actuators

Natural Frequencies(Hz)	First	Second	Third
Finite Element modeling	1.56	8.480	23.887
Beam without Actuators	1.499	8.438	23.400
Beam With Actuators	1.526	8.385	23.16

Table 5.5: The first three natural frequencies of the beam with and without actuators

the first 3 natural frequencies of the beam are captured. Table 5.5 shows the first three natural frequencies from finite element modeling of the beam. It also compares the natural frequencies of the beam before and after bonding the patches. This table shows that the modeling results are in good agreement with the experimental results. It also shows a negligible change in the first three natural frequencies after attaching the actuators. Excluding the stiffness and mass matrices of piezoelectric actuators, leads to 1.8 percent error in the first natural frequency of the beam. This error is not significant in the optimization of actuators placement. Moreover, there

is only 4 percent error in the first natural frequency of the beam when it is compared with the first natural frequency of the beam without actuators.

5.4 State Estimation

In our system,

$$\begin{matrix} \dot{x}(t) = Ax(t) + Bu(t), \quad x(0) = x_0 \\ y(t) = Cx(t) \end{matrix},$$

the state vector is

$$x = \begin{Bmatrix} K^{0.5}\zeta \\ \dot{\zeta} \end{Bmatrix},$$

where ζ is the generalized nodal displacement vector. The elements of this vector are the deformations at the element nodes in finite element discretization. Two sensors are available for the experiments. Each sensor reads the displacement at one node on the beam. A state estimator should be designed for the experiments. A simple Luenberger observer may be applied as the estimator,

$$\dot{x}_e(t) = Ax_e(t) + Bu(t) + L[y(t) - Cx_e(t)]$$

Therefore,

$$\dot{x}_e(t) = (A - LC)x_e(t) + Ly(t) + Bu(t).$$

The gain L is the observer gain.

Defining the error as $\dot{e}(t) = x(t) - x_e(t)$, the error equation is

$$\dot{e}(t) = A_c e(t), \tag{5.1}$$

where

$$A_c = A - LC$$

.

If all the eigenvalues of A_c have negative real parts, Equation (5.1) will be asymptotically stable. If (A, C) is observable, the eigenvalues of $A - LC$ can be arbitrarily assigned. However, the assumption here is that the sensor provides the exact results free of any noise. This is not true in practice and the sensor is always contaminated by some noise. The noise inserts limitations on the extent to which the eigenvalues of A_c can be made negative. Moreover, because there is always integration between y and x_e, x_e will approach x for a full-order estimator. This is not true for reduced order estimators. There will be noise in x_e arising from that in y, because x_e is partly determined by a memoryless transformation on y. Consequently, the performance for a reduced order estimator may be worse than a full order estimator [114]. That is why one may approach the state estimation problem from stochastic point of view.

The Kalman-Bucy filter can be applied as the state estimator. It also removes the noise effect in the system. Here, the A, B and C matrices are time invariant. For now, let's assume we have disturbance noise $v(t)$, and measurement noise $w(t)$ in our system. These are additive noises and are white, Gaussian and with a zero mean. The noises are assumed white, because it implies that they are uncorrelated from instance to instance [114]. These assumptions for the noises applies to many noise occurring processes.The system can be written as

$$\begin{aligned} \dot{x}(t) &= Ax(t) + Bu(t) + v(t), \\ y(t) &= Cx(t) + w(t) \end{aligned} ,$$

where $x(t)$ and $u(t)$ are the state and input vectors respectively. Therefore, mathematically the noise covariances can be written as,

$$E[v(t)v'(\tau)] = Q_e\delta(t-\tau) \qquad E[v(t)] \equiv 0,$$

$$E[w(t)w'(\tau)] = R_e\delta(t-\tau) \qquad E[w(t)] \equiv 0.$$

The matrices Q_e and R_e are symmetric non-negative matrices. The presence of $\delta(t-\tau)$ in these equations indicates the whiteness property of the noises. The Q_e and R_e matrices should be introduced to the estimator. Since the noise information is not available at the start of the experiments, values need to be chosen for these matrices and the accuracy of the estimator should be verified in the next stages. For now, $Q_e = I$ and $R_e = I$, where I is the identity matrix. Assuming the initial time is in infinite past, for a completely observable pair $[A, C']$, the optimal estimator can be written as [114]

$$\dot{x}_e = Ax_e + Bu + K_e[Cx_e - y],$$

where K_e is called the gain of the optimal estimator and is given by

$$K_e = -P_e C^T R_e^{-1}.$$

The matrix P_e is the solution of algebraic Riccati equation

$$P_e A^T + AP_e - P_e C^T R_e^{-1} C P_e + Q_e = 0. \tag{5.2}$$

To achieve an asymptotically stable system, it is required that $A + K_e C$ has eigenvalues with negative real parts. For $Q_e = DD^T$, it can be ensured when the pair $[A, D]$ is stabilizable.

5.5 Optimal Sensor Location

It is desirable to optimally place the sensors on a structure, so that they can operate efficiently. The optimal sensor locations can be found based on estimator-regulator duality.

Consider a regulator problem defined by A, B, Q and R. Let P the associated Riccati equation solution and K the control gain. Define matrices

$$\hat{A} = A^T, \quad \hat{C} = B, \quad \hat{Q} = Q, \quad \hat{R} = R,$$

and define an estimation problem by $\hat{A}, \hat{C}, \hat{Q}$ and $\hat{R}$. Let $\hat{P}_e$ be the solution of the associated Riccati equation and K_e be the feedback gain [114]. Then

$$\hat{P}_e = P, \qquad K_e = K.$$

Consequently, an approach similar to optimal actuator placement can be applied to optimize sensor locations. What shall be aimed in an optimal estimation problem is a minimum error variance. At each time, the error variance is

$$ErrorVariance = E\left\{[x(t) - x_e(t)]^T [x(t) - x_e(t)]\right\}.$$

In [114], it is shown that

$$E\left\{[x(t) - x_e(t)]^T [x(t) - x_e(t)\right\} = P_e(t).$$

For a time invariant system, P_e is time independent. Consequently, the error variance is also time invariant. To minimize the error variance, $\|P_e\|$ can be minimized. In equation (5.2), P_e is the solution of Riccati equation. Assuming constant A, Q_e and R_e matrices, P_e is dependent on C and C is a function of sensor locations. Hence, defining a vector of possible sensor locations, π_e, the objective function for sensor location optimization can be written as

$$\sigma_e(\pi) = \|P_e(\pi)\|. \tag{5.3}$$

This is a non-convex function. However, applying the formulation in [6] the problem is re-formulated into a convex optimization problem. The formulation is exactly as mentioned in Chapter 2. Same as optimal actuator location problem, the vector π is a vector of N_e logical elements where the j^{th} entry has a 1 when a sensor exists in that location and a value of zero otherwise. When M_e sensors are available, the optimization problem is

$$\begin{gathered} \min\{\sigma(\pi_e); \pi_e \in \Phi\}, \\ s.t. \\ \Phi = \{\pi_e \in \mathbb{R}^N \quad s.t. \quad \pi_{e_j} \in \{0,1\}; \textstyle\sum_{j=1}^{N} \pi_{e_j} = M_e\}. \end{gathered} \tag{5.4}$$

Each such vector π_e defines a possible vector of actuator locations.The optimization procedure, presented in Chapter 2 can be applied to solve Equation 5.4.

This procedure is used to optimize sensor locations. The non-contact sensors in this experiment are placed so that their laser beam is normal to the beam's surface. Each sensor can read the normal displacement at one point on the beam. Since the beam is discretized into finite elements, possible sensor locations can be chosen as the unconstrained element nodes. The beam is divided into 10 elements and it has 10 unconstrained nodes. Consequently, $N = 10$ for this problem. The possible sensor locations are shown in Figure 5.8.

Figure 5.8: Possible sensor locations

Two sensors are available. Hence, $M_e = 2$. Solving this optimization problem with the presented optimization scheme, yields the optimal location of two sensors as shown in Figure 5.9. The optimal location of one sensor is at the beam's tip. However, since we have non-contact sensors, it is not practical to place a sensor at the beam's tip. Moreover, since the measuring range for the LK031 series is small, its location is moved one element towards the beam's fixed end. Therefore, the sensors are placed as in Figure 5.4.

It should be mentioned that the matrices Q_e and R_e are functions of measurement and dis-

Figure 5.9: Optimal sensor locations

turbance noise. Some values are assumed for this matrices and the optimal sensor locations are calculated. The assumptions for this matrices should be verified and the estimator should operate properly. If the estimation does not lead to correct results , these matrices should be changed and the optimal actuator locations should be recalculated. Therefore, optimal sensor placement is a kind of trial and error problem.

5.6 Vibration Control

To study the vibration control problem, first the optimal location of 2 actuators on the experimental beam is calculated. For the optimization, Q and R matrices are assumed equal to the identity matrix. The optimal locations are positions 1 and 2 on the beam as shown in Figure 5.4. The initial condition for the beam vibration is 13 mm initial displacement at the beam's tip.

The optimal vibration control problem is studied for two different Q matrices. In each test, two of the actuators in Figure 5.4 are activated and the results are compared to each other.

The first step is to verify the state estimation. Consequently, the vibrations near the beam's tip are compared for the analytical and experimental results when the actuators are located at positions 1 and 2. The results are shown in Figure 5.11(b). It is observed that the results are in good agreement.

In the first set of experiments, Q matrix is assumed equal to identity. Figure 5.11(a) shows

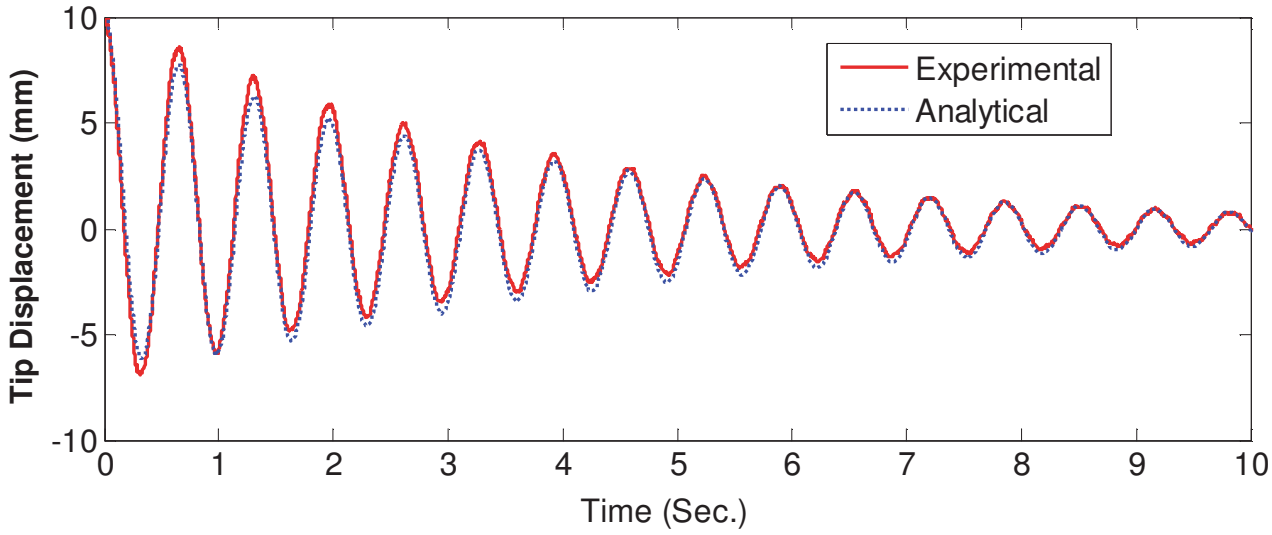

Figure 5.10: Beam's tip displacement to compare experimental and analytical results

	1,2	1,3	1,4	2,3	2,4
Suppression Time (Sec.)	8.5	10.46	13.76	13.72	14.42

Table 5.6: Suppression time for various actuating positions

the uncontrolled and controlled responses which are read near the beam's tip. The controlled responses in this figure are for 3 combinations of actuators. The actuator numbers are shown in Figure 5.4. As in Figure 5.11(a), the optimally located actuators, suppress the effect of vibrations in a shorter amount of time.

Table 5.6 shows the suppression time for all the existing actuator locations in this problem. It is observed that when actuators are placed optimally, the disturbances are suppressed faster.

To also study the difference in actuators' voltages for various position combinations, Figure 5.12(a) shows the actuators' voltages when they are at positions 1 and 2. Figure 5.12(b)

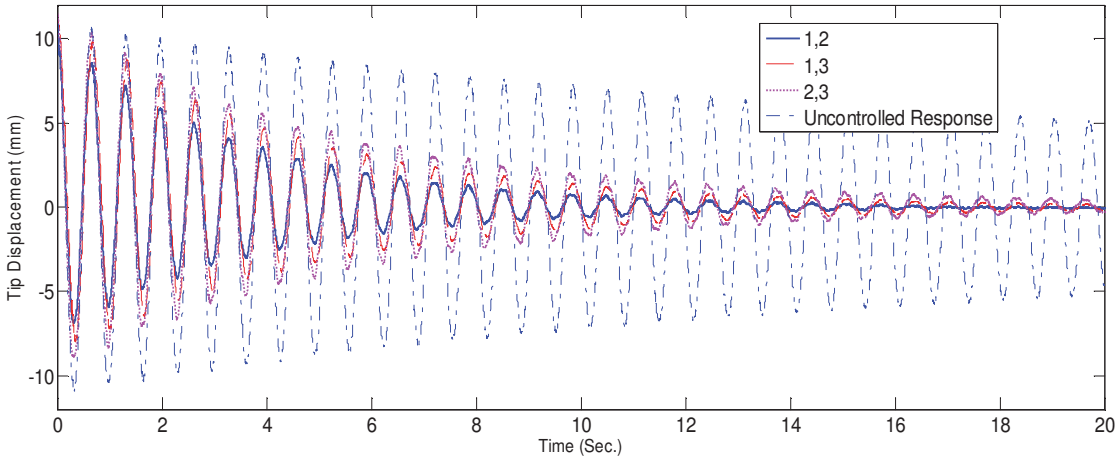

(a) Vibrations in 20 seconds

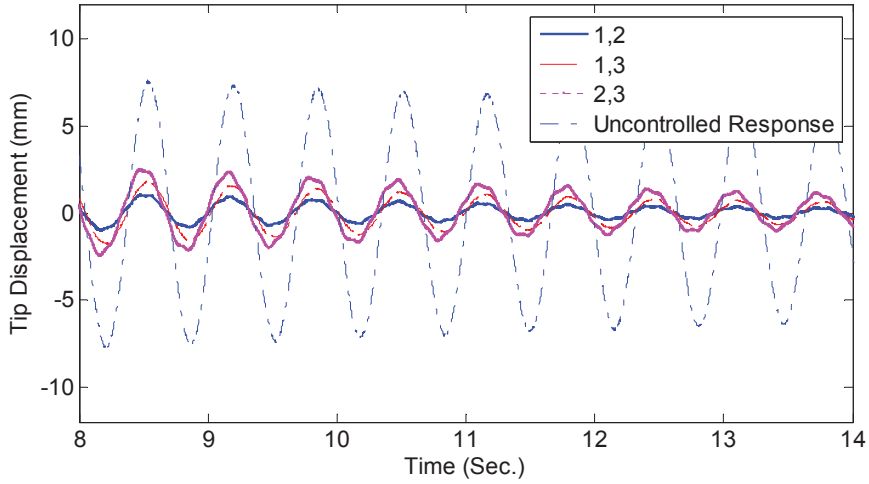

(b) Magnified beam vibrations

Figure 5.11: Beam's near tip displacement with different actuating locations in vibration control experiment

shows actuators' voltages when they are located at positions 2,3. It can be observed that when actuators are optimally located, smaller voltages are applied to the actuators to suppress distur-

bances.

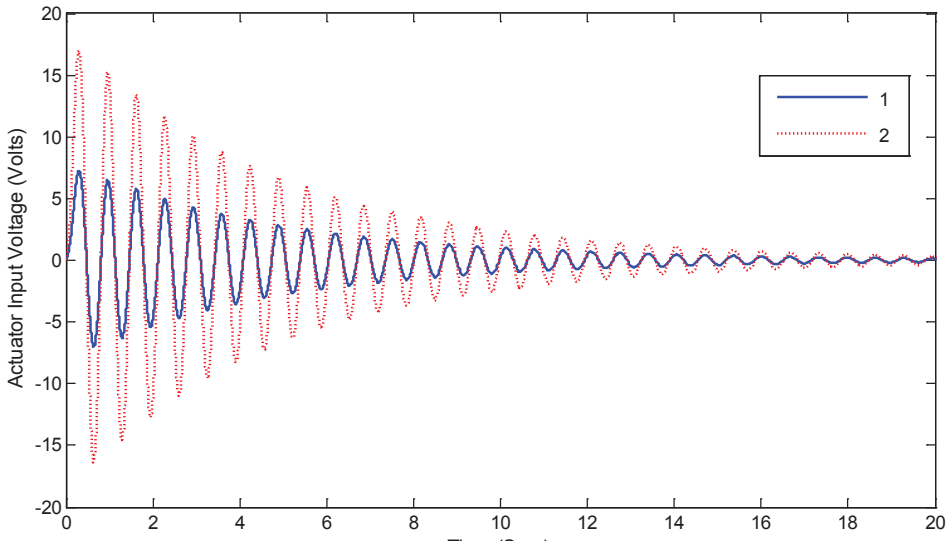

(a) Actuators at positions 1 and 2

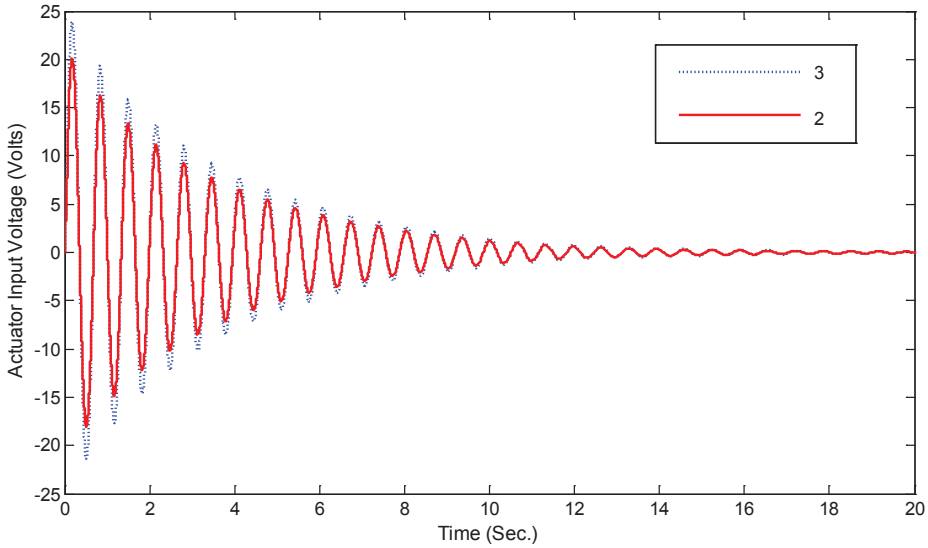

(b) Actuators at positions 2 and 3

Figure 5.12: Input voltage of actuators

For larger values of Q elements, smaller suppression times can be achieved. Consequently, in the next set of experiments, the same procedure is followed, except that $Q = 10000I$, where I is the identity matrix. Figure 5.13 shows the controlled and uncontrolled responses read by sensor 2. Same as before, the controlled responses in the figure are for the same 3 combinations as in Figure 5.11(a). Table 5.7 shows the suppression times for all the existing actuator combinations. Comparing these results with Table 5.6, shows that the suppression times decrease considerably by increasing the diagonal elements of Q.

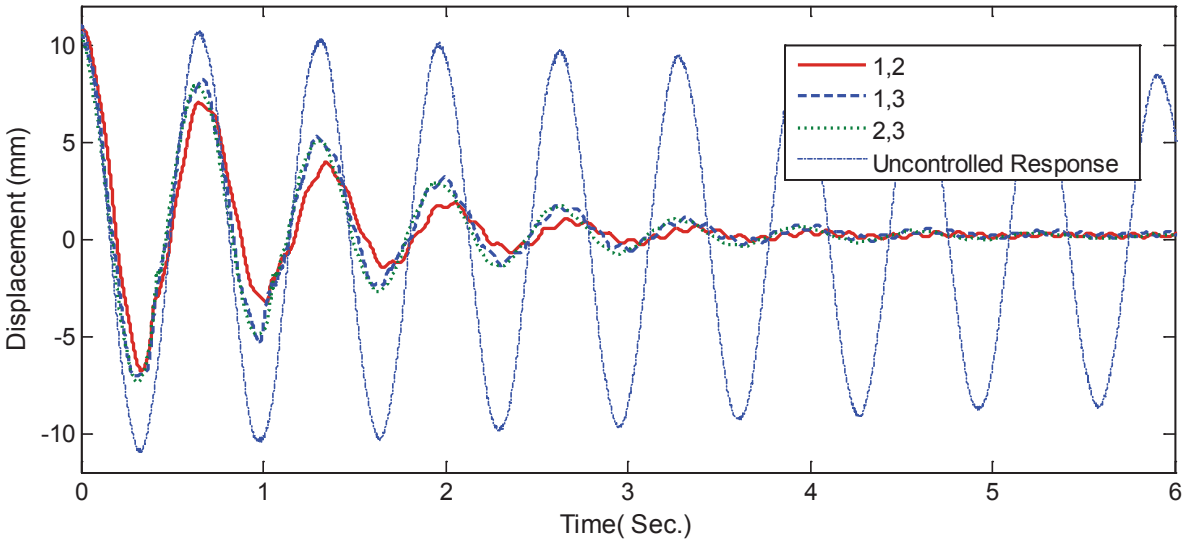

Figure 5.13: Beam's tip displacement with different actuating locations in vibration control

	1,2	1,3	1,4	2,3	2,4
Suppression Time (Sec.)	5.45	6.44	7.20	7.803	8.056

Table 5.7: Suppression time for various actuating positions

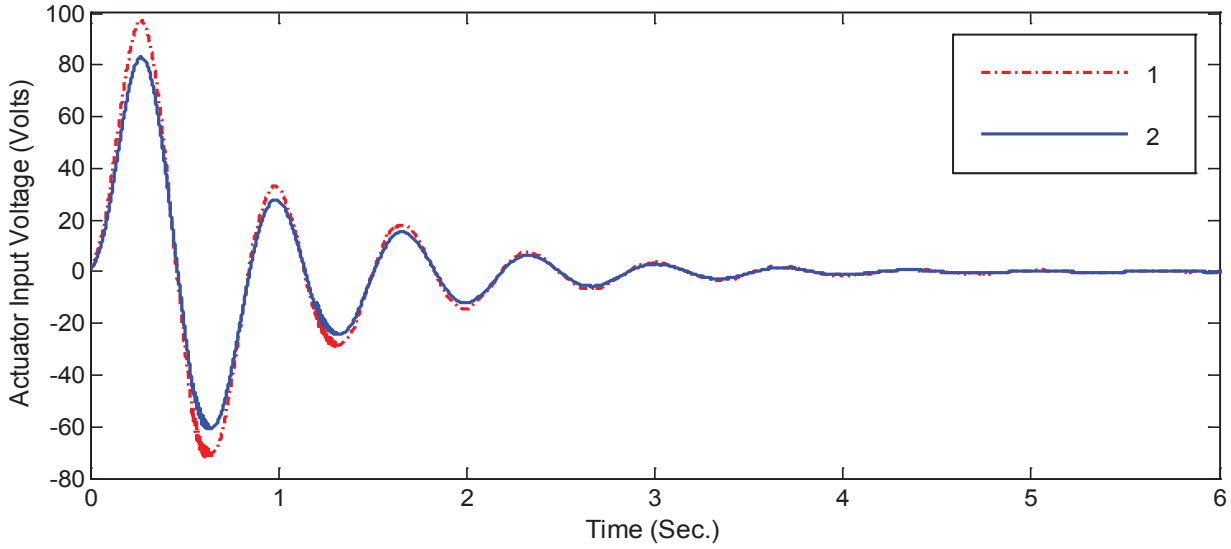

Figure 5.14: Input voltage of actuators at positions 1 and 2

5.7 Shape Control

To study the optimal shape control problem, the optimal location of 2 actuators on the beam is calculated. The optimal locations are dependent on the desired shape. The desired shape is the beam's first mode of vibration with a 2.3 mm deformation at its tip. Consequently, 2 mm displacement at sensor 2 location and 0.19 mm displacement at sensor 1 location is expected. The desired shape is shown in Figure 5.16. The range of displacements is small in this study and this increases the error ratio. As a result of the 72 volt limitation in the supply voltage of the actuators, it is impossible to go beyond this limit. However, according to Table 5.3, the applied sensors in this study can read small range displacements with a good accuracy.

It is desired to compare the achieved beam displacement and actuators' input voltages when they are located at different positions. Analyses show that the optimal actuator locations are at positions 1 and 2 in Figure 5.4.

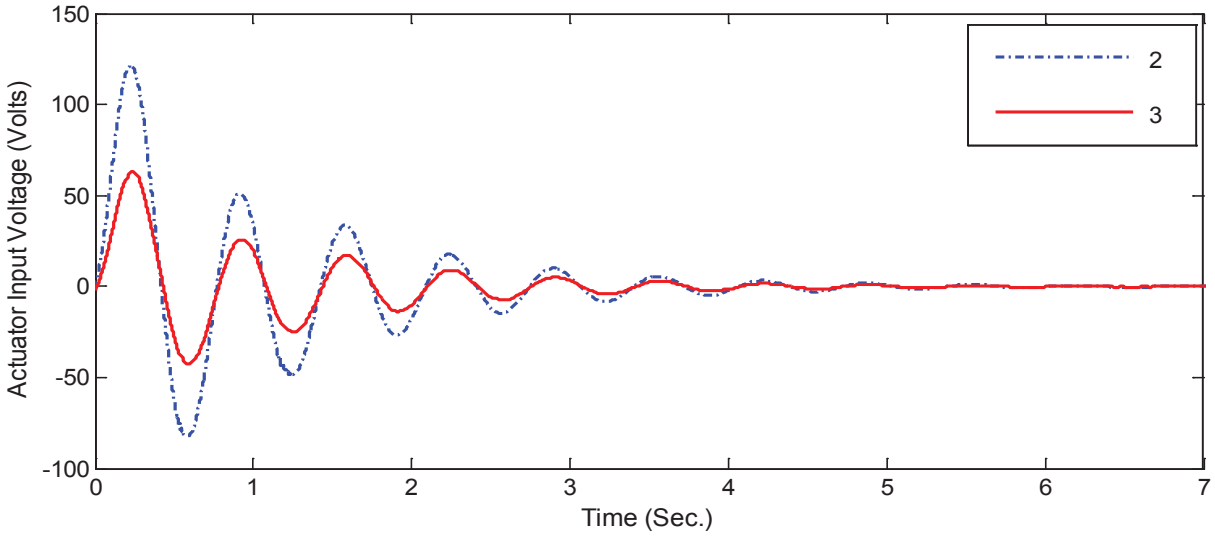

Figure 5.15: Input voltage of actuators at positions 1 and 2

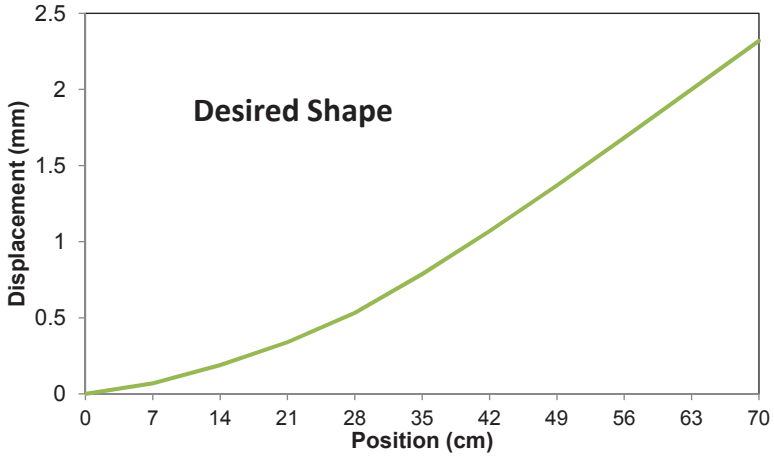

Figure 5.16: The desired shape for the beam

The shape control experiments are repeated for 3 sets of actuator locations. In the first set, actuators 1 and 2 are activated. In the second set, actuators 1 and 3 and in the third set, actuators

2 and 3 are activated. Due to the 72 volts limitation in actuators' voltages as discussed previously, it was impossible to repeat the experiments for the other possible actuator combinations, since they needed much higher input voltages.

The beam displacements recorded by sensors include measurement noises. Figure 5.17 shows the actual displacements at sensor locations 1 and 3. These results are not filtered and include noise effect. These displacement curves are smoothed using the moving average method in Matlab for the other results.

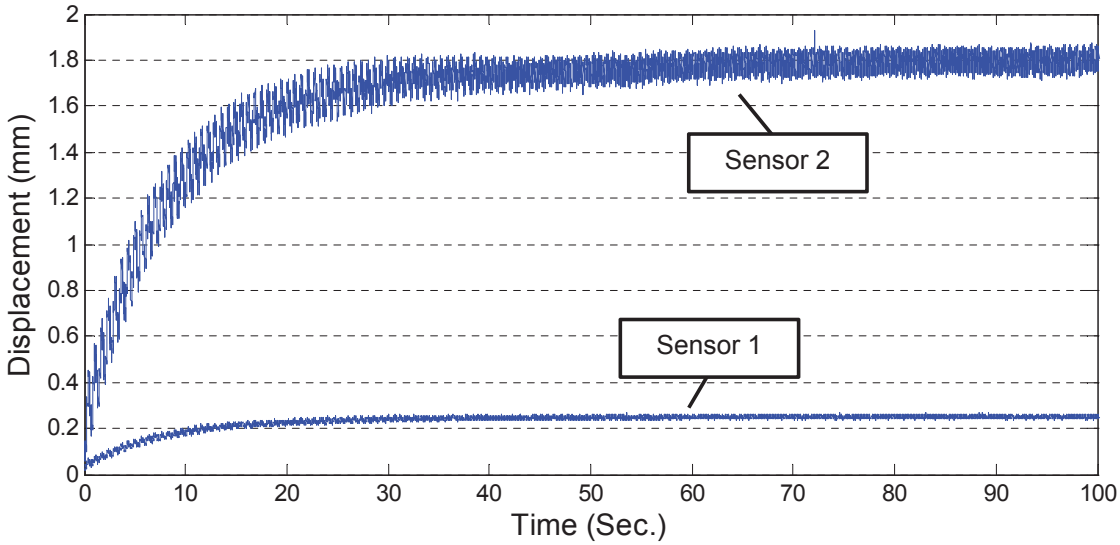

Figure 5.17: Unfiltered displacement with actuators at positions 1 and 3

Figure 5.18(a) shows the displacements of the beam at sensor 1 and sensor 2 positions. At Sensor 1 location (Position 1) the deformation reaches 0.203 mm and at Sensor 2 location (position 2) it reaches 1.967 mm. The error is 6.8 per cent at Position1 and 1.65 per cent at

Position 2. Figure 5.18(b) shows the input voltages of actuators. The steady state input voltage for Actuator 1 is 54 volts and this value for Actuator 2 is 51 volts. The average voltage is 52.5 volts.

To verify repeatability of the experiments, the results for three tests are compared together. In these tests the actuators are located at positions 1 and 2. Figures 5.19(a) and 5.19(b) show the results at sensor locations 1 and 2, respectively. It is observed that repeating the experiment results in the same displacements for the beam.

Next, actuators 1 and 3 are activated to achieve the desired shape. Figure 5.20 shows the structure deformations at positions 1 and 3. At sensor position 1 the beam's displacement reaches 0.249 mm and it reaches 1.76 mm at sensor position 2. The error is 31 percent at Position 1 and 12 percent at Position 2. Clearly, the errors are higher than when the actuators are optimally located. Figure 5.21 shows the actuators' input voltages. The steady state input voltage for actuator 1 is 70 volts and for actuator 3 is 43 volts. The average voltage is 56.5 volts. It is observed that the average voltage is higher than when the actuators are optimally located.

In the next step actuators 2 and 3 are activated. Figure 5.22 shows the deformations at sensor positions 1 and 2. At Position 1 the displacement reaches 0.0996 mm and it reaches 1.774 mm at Position 2. The error is 50.2 percent at Position 1 and it is 11.3 percent at Position 2. On average the errors are higher than the previous actuator locations. Figure 5.23 shows the steady state input voltages of actuators. The input voltage of actuator 2 is 73 volts and for actuator 3 is 50 volts. The average voltage is 61.5 which is higher than previous locations.

Figure 5.24 compares the deformations with the desired shape. When actuators 1 and 2 are activated the results accurately match the desired shape. This is not happening when actuators at the other positions are activated and as they get further from the optimal locations, the result becomes more inaccurate.

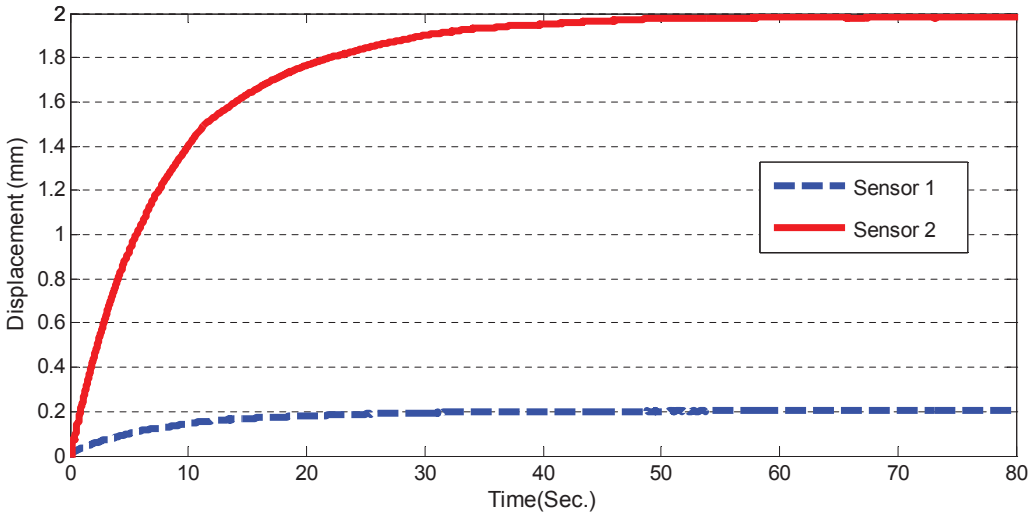

(a) Displacement at sensor locations

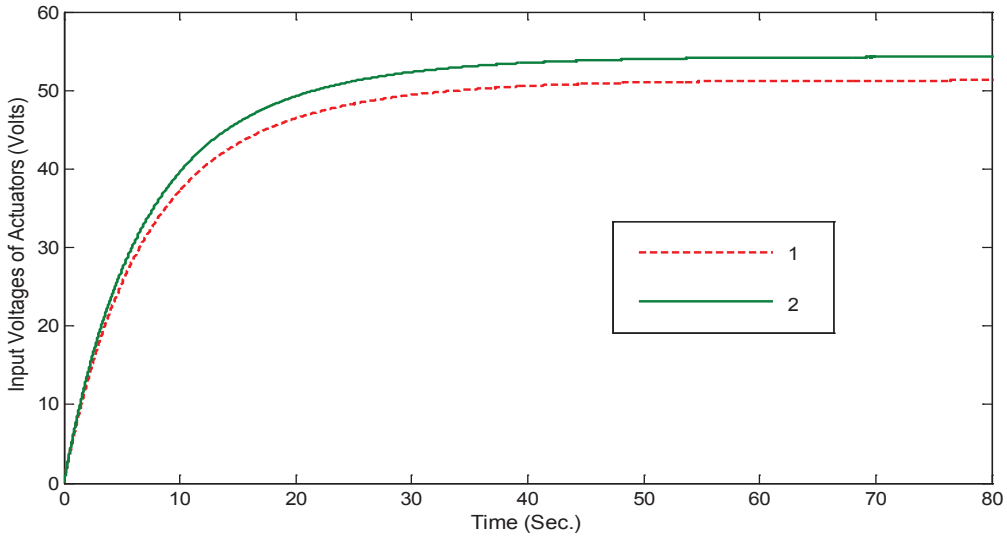

(b) Input voltages of actuators

Figure 5.18: Actuators at positions 1 and 2 in shape control

It is observed that when actuators are optimally located, the input voltages of actuators are optimal as well. Table 5.8 compares the maximum and minimum actuator voltages for various actuator placements. As the actuators are located further from the optimal locations the maximum voltage increases dramatically. This increases the cost of providing input voltages for actuators.

Actuator locations	Maximum Input Voltage	Minimum Input Voltage
1,2	54	51
1,3	70	43
2,3	73	50

Table 5.8: Actuator input voltages for various actuator locations

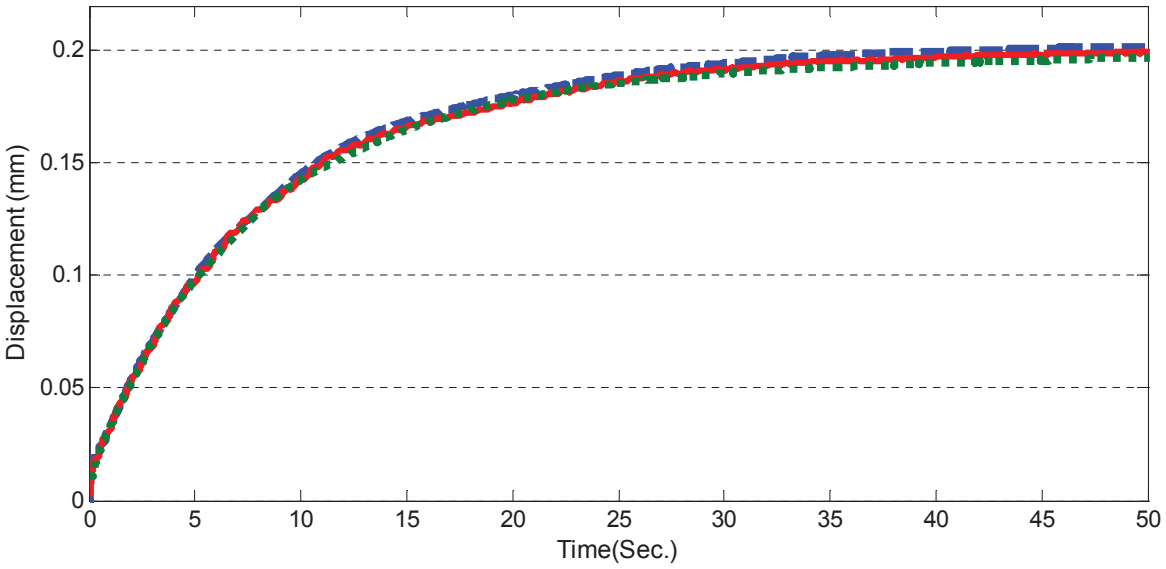

(a) Sensor 1 Position

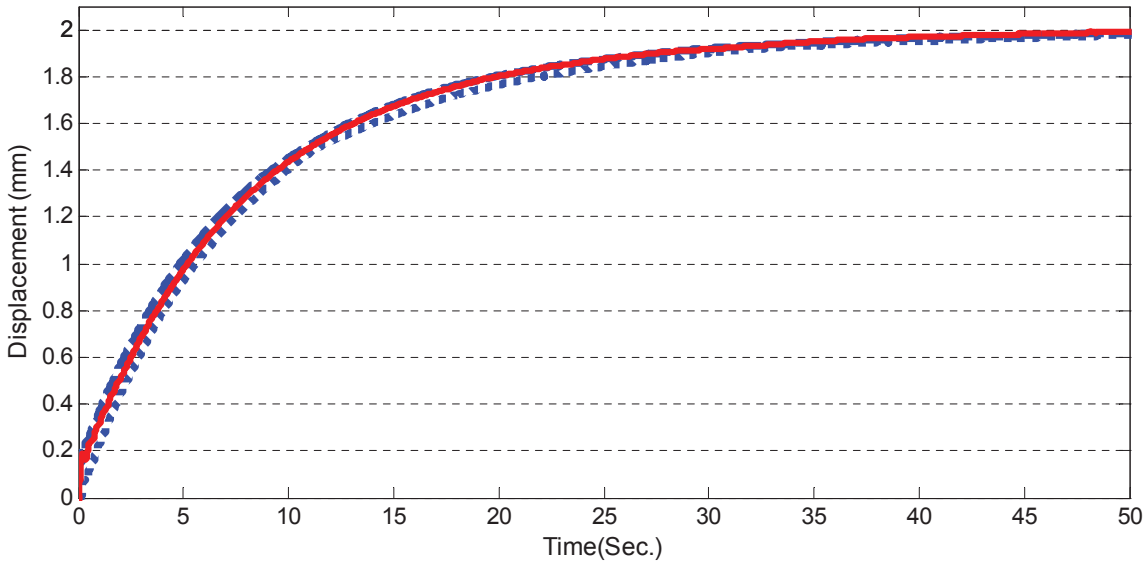

(b) Sensor 2 Position

Figure 5.19: Achieved displacement in repeated experiments

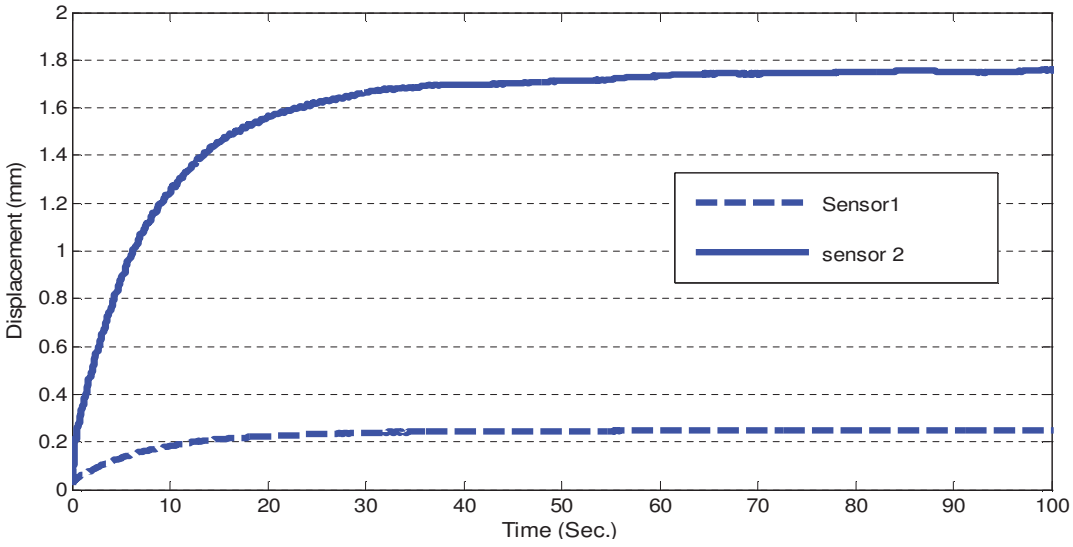

Figure 5.20: Displacement with actuators at positions 1 and 3 in shape control

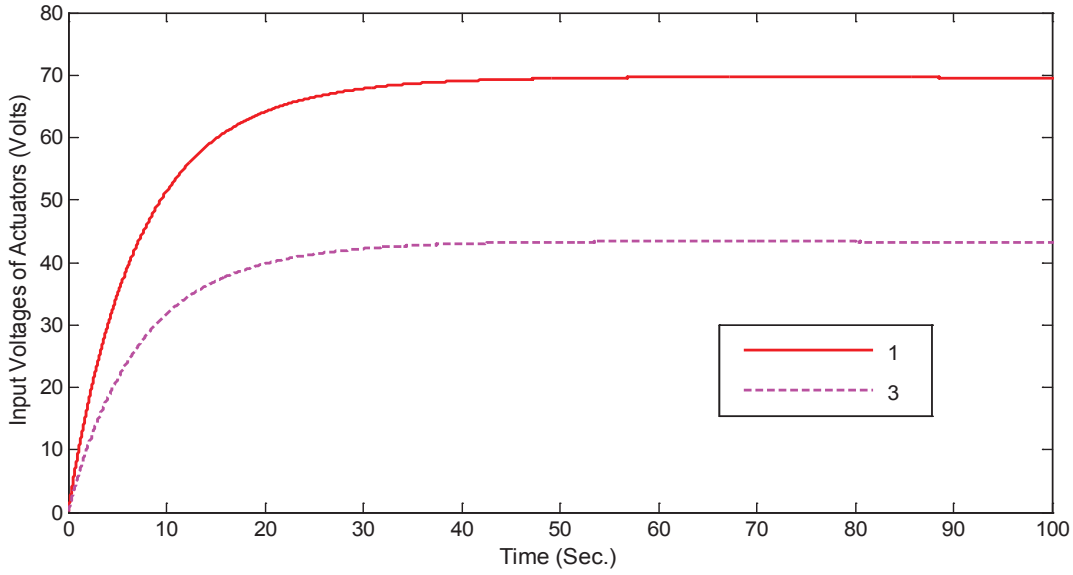

Figure 5.21: Input voltages of actuators at positions 1 and 3 in shape control

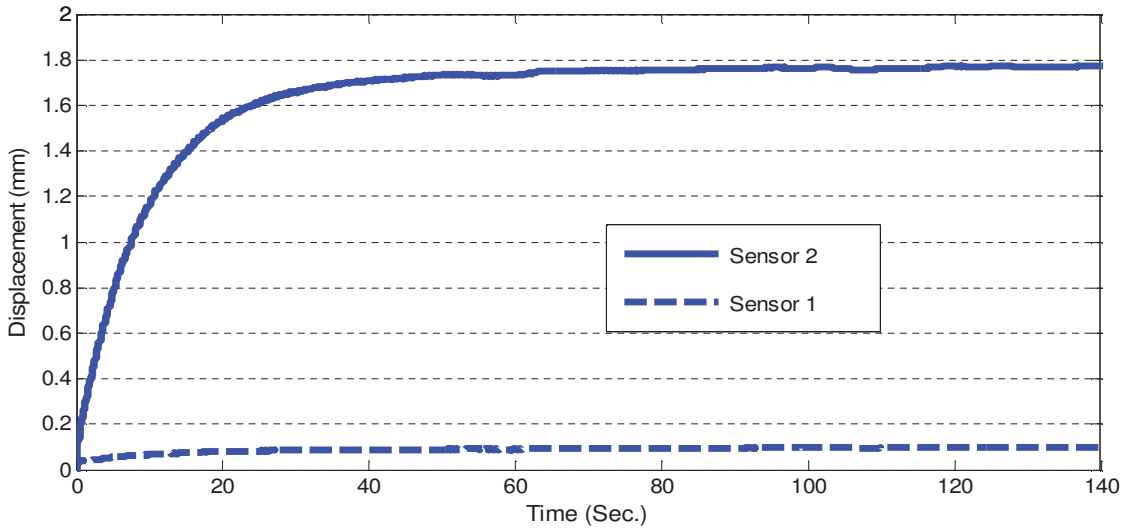

Figure 5.22: Displacement with actuators at positions 2 and 3 in shape control

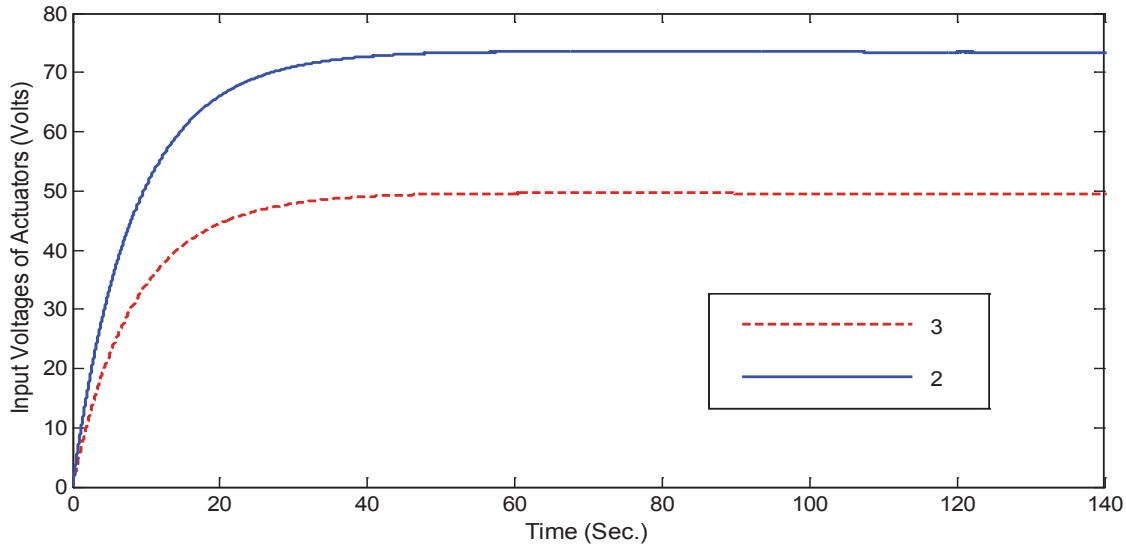

Figure 5.23: Input voltages of actuators at positions 2 and 3 in shape control

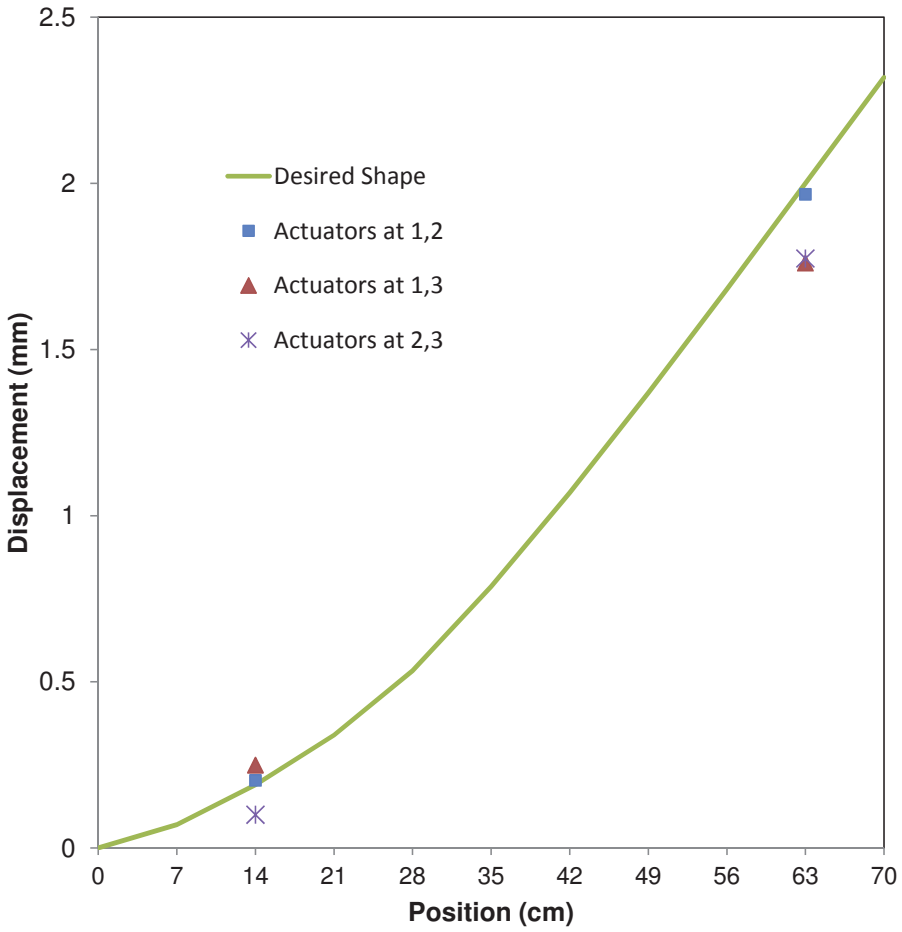

Figure 5.24: Comparison of displacements for various actuator placements

Chapter 6

Summary and Future Work

With the advent of new ultra-large ultra-lightweight flexible structures, the topic of optimal actuator placement has absorbed attention during the last few years. The main goal of this dissertation was to prepare an optimization scheme to determine optimal actuator placement in control of flexible structures.

6.1 Key Contributions

During the past few years considerable research has been dedicated to optimal actuator placement in flexible structures. This dissertation introduced an optimization algorithm to optimize the location of multiple control devices. The main contributions of this study can be summarized as follows:

- **Developing a new optimization scheme**: Various objective functions and a number of different optimization techniques are introduced in the literature. However, the main difficulty in optimal actuator placement has always been in non-convexity of the objective

functions. Mainly evolutionary algorithms are applied to solve the problem. A large drawback of these methods is that they do not utilize the gradient information of the objective function and consequently, for large structures, might be computationally expensive or lead to inaccurate results. Gradient-based techniques on the other hand are prone to resulting in local optima. The optimization may require a number of repetitions to yield reliable results.

In this study, the linear quadratic regulator is chosen as the control law for the control system. The actuator placement is optimized to minimize the optimal quadratic cost. The main advantage of the developed optimization algorithm is that based on a formulation presented in [6], the objective function is mapped into a convex space of actuator locations. The optimization is then a convex integer optimization problem. An integer optimization, composed of branch and bound and minimax optimizations is used to solve the optimization problem. This optimization method is considerably faster than the existing evolutionary algorithms.

It is worth mentioning that this method is not only applicable to optimal actuator placement but can also be applied to solve optimal sensor location problems.

- **Optimal actuator placement in vibration control**: Utilizing the proposed optimization scheme, the optimal location of actuators is calculated on beam and plate structures. The computation times and the results are compared to a genetic algorithm and it is observed that the proposed scheme is faster and more accurate. One main conclusion is that the modal strain energies are relevant to the optimal actuator locations.

- **Optimal actuator placement in shape control** Despite the many studies on optimal actuator placement in vibration control, very few of them are focused on actuator placement optimization in shape control. Optimal shape control is important in many high precision

structures and ultra light-weight, large-scale structures. Since these structures are mainly composed of very thin membranes, a limited number of light-weight actuators can be used as control devices. Hence, optimal location of actuators in shape control is an important issue for future research.

This dissertation formulates the shape control problem of a structure by expanding the desired shape into the structure's modes of vibration. The equations of motion for the structure are all in time domain. Based on the number of dominant modes in the desired shape a lower bound for the number of required actuators is suggested. The optimal location of actuators is then calculated on beam and plate structures and the results are also compared with a genetic algorithm.

- **Experimental study of optimal shape and vibration control**: Relatively few studies exist on experimentally studying the optimal actuator placement and their effects on the required control effort in an active control system. This issue has not been studied for shape control to the author's knowledge. However, it is important to have a knowledge of how changing actuator locations may effect the input efforts even in a small structure. This dissertation studies this issue both for shape control and vibration control. It is shown that, when the actuators are optimally located , not only does the control system work more accurately, but the input voltages are also significantly reduced. Moreover, the introduced optimization scheme was applied to optimized the sensors' locations in the experiments.

6.2 Future Work

The optimization method presented in this dissertation, is formulated based on the number of finite elements in the structure's modeling. Piezoelectric patches are assumed to have the same size as the finite elements. However, when the size of patches exceeds the accuracy limits, this might not be a realistic model of the structure, since large finite elements might lead to large modeling errors. Hence, there is need for a code that covers any size of patch with a reliable accuracy. A future objective is to develop an adaptive mesh refinement procedure. Since during the optimization process the number of finite elements needs to be kept constant, a p-refinement or an element subdivision h-refinement method may be applicable. The former method locally increases the order of polynomials in inaccurate elements [115]. In the latter method, if the existing elements show too much error, they are simply divided into smaller ones, keeping the original element boundaries intact [115]. However, this process is cumbersome and leads to a number of hanging points.

Further, the location of actuators is studied in this dissertation. There has been a brief discussion on the minimum number of required actuators in shape control. However, it was later shown that this only presents a lower bound on the number of actuators and it does not always lead to desirable results, specially in plate structures. It is shown how sensitive the shape control results are to the number of actuators. The proposed optimization scheme can be modified to also optimize the number of actuators. This is a future topic for research in both shape and vibration control.

Chapter 5 includes a brief discussion on optimal sensor placement. The presented optimization scheme is also applicable to sensor placement. In damage detection problems sensor placement has a significant importance. One future topic is to apply the presented optimization scheme to an in-depth study of optimal sensor placement.

References

[1] A. Preumont. *Vibration Control of Active Structures: An Introduction*. Springer, 2002.

[2] JM. Renno. *Dynamics and Control of Membrane Mirrors for Adaptive Optic Applications*. PhD thesis, Virginia Polytechnic Institute and State University, 2008.

[3] Piezo System, Inc., 65 Tower Office Park Woburn, MA 01801 USA. *Catalog No.8*, 2011.

[4] E.J. Ruggiero. Lqr control and judicious sensor placement derived from functional gain analysis for a 1d active membrane. *Smart Materials and Structures*, 16:2398–2407, 2007.

[5] K.R. Kumar and S. Narayanan. The optimal location of piezoelectric actuators and sensors for vibration control of plates. *Smart Materials and Structures*, 16:2680–91, 2007.

[6] J. Geromel. Convex analysis and global optimization of joint actuator location and control problems,. *IEEE Transactions on Automatic Control*, 34:711–720, 1989.

[7] V. Piefort and A. Preumont. Modeling of smart piezoelectric shell structures with finite elements. In *Proceedings of the 25th International Conference on Noise and Vibration Engineering, ISMA*, 2000.

[8] J. Lee and L. Jiang. Exact electrostatic analysis of piezoelectric laminate via state space approach. *International Journal of Solids and Structures*, 33:977–990, 1996.

[9] J. Pan, CH. Hansen, and SD. Snyder. A study of the response of a simply supported beam to excitation by a piezoelectric actuator. *Journal of Intelligent Material Systems and Structures*, 3:3–16, 1992.

[10] JF. Rivory, CH. Hansen, and J. Pan. Further studies of the dynamic response of a simply supported beam excited by a pair of out-of-phase piezoelectric actuators. *Journal of Intelligent Material Systems and Structures*, 5:654–664, 1994.

[11] S.M. Yang and Y.J. Lee. Modal analysis of stepped beams with piezoelectric materials. *Journal of Sound and Vibration*, 176:289–300, 1994.

[12] S.J. Kim and J.D. Jones. Influence of piezo-actuator thickness on the active vibration control of a cantilever beam. *Journal of Intelligent Material Systems and Structures*, 6:610–623, 1995.

[13] S. Basak, A. Raman, and S.V. Garimella. Dynamic response optimization of piezoelectrically excited thin resonant beams. In *Transactions of the ASME. Journal of Vibration and Acoustics*, 2005.

[14] A.M. Khalatkar, R.H. Haldkar, and V.K. Gupta. Finite element analysis of cantilever beam for optimal placement of piezoelectric actuator. In *2nd International Conference on Mechanical and Aerospace Engineering*, 2011.

[15] J.C. Lin and M.H. Nien. Adaptive modeling and shape control of laminated plates using piezoelectric actuators. *Journal of Materials Processing Technology*, 189(1-3):231–236, 2007.

[16] J. Bruch Jr, J. Sloss, S. Adali, and I. Sadek. Optimal piezo-actuator locations/lengths and applied voltage for shape control of beams. *Smart Materials and Structures*, 9:205–211, 2000.

[17] S.K. Agrawal, D. Tong, and K. Nagaraja. Modeling and shape control of piezoelectric actuator embedded elastic plates. *Journal of Intelligent Material Systems and Structures*, 5:514–521, 1994.

[18] A. Vidhya, D. Maheswari, and S.K. Patnaik. Active vibration control of piezo actuated cantilever beam using PSO. In *IEEE Students' Conference on Electrical, Electronics and Computer Science: Innovation for Humanity*, 2012.

[19] K.D. Dhuri and P. Seshu. Multi-objective optimization of piezo-actuator placement and sizing using genetic algorithm. *Journal of Sound and Vibration*, 323:495–514, 2009.

[20] A. Zabihollah, R. Sedagahti, and R. Ganesan. Active vibration suppression of smart laminated beams using layerwise theory and an optimal control strategy. *Smart Materials and Structures*, 16:2190–201, 2007.

[21] T. Roy and D. Chakraborty. Genetic algorithm based optimal design for vibration control of composite shell structures using piezoelectric sensors and actuators. *International Journal of Mechanics and Materials in Design*, 5:45–60, 2009.

[22] A. Benjeddou. Advances in piezoelectric finite element modeling of adaptive structural elements: a survey. *Computers and Structures*, 76:347–364, 2000.

[23] K. Chandrashekhara and K. Bhatia. Active buckling control of smart composite plates-finite-element analysis. *Journal of smart Materials and Structures*, 2:31–39, 1993.

[24] A. Islam and K. Craig. Damage detection in composite structures using piezoelectric materials (and neural net). *Journal of smart Materials and Structures*, 3:318–328, 1994.

[25] I. Bruant, F. Pablo, and O. Polit. Active control of laminated plates using a piezoelectric finite element. *Mechanics of Advanced Materials and Structures*, 15:276–90, 2008.

[26] V. Balamurugan and S. Narayanan. Shell finite element for smart piezoelectric composite plate/shell structures and its application to the study of active vibration control. *Finite Elements in Analysis and Design*, 37(11):713–738, 2001.

[27] F. Casciati, J. Rodellar, and U. Yildirim. Active and semi-active control of structures-theory and applications: A review of recent advances. *Journal of Intelligent Material Systems and Structures*, 23(11):1181–1195, 2012.

[28] T.W. Kim and J.H. Kim. Optimal distribution of an active layer for transient vibration control of a flexible plate. *Smart Materials and Structures*, 14(11):904–916, 2005.

[29] A. Zabihollah. Effects of structural configuration on vibration control of smart laminated beams under random excitations. *Journal of Mechanical Science and Technology*, 24(5):1119–1125, 2012.

[30] E.J. Ruggiero and D.J. Inman. Modeling and vibration control of an active membrane mirror. *Smart Materials and Structures*, 18(9):1–10, 2009.

[31] I. Kucuk, IS. Sadek, and E. Zeini. Optimal vibration control of piezolaminated smart beams by the maximum principle. *Computers and Structures*, 89(9-10):744–749, 2011.

[32] M.K. Kwak, H. Seok, and J. Moonsan. Dynamic modeling and active vibration controller design for a cylindrical shell equipped with piezoelectric sensors and actuators. *Journal of Sound and Vibration*, 321(3-5):510–524, 2009.

[33] T. Nestorovic Tamara, N. Durrani, and M. Trajkov. Experimental model identification and vibration control of a smart cantilever beam using piezoelectric actuators and sensors. *Journal of Electroceramics*, 29(1):42–55, 2012.

[34] Y. Li, Y.Y. Qiu, and F.J. Peng. Active vibration control for the flexible spacecraft structure based on an ATMD/PPF strategy. *Applied Mechanics and Materials*, 105-107:668–674, 2012.

[35] F. Botta, N. Marx, S. Gentili, C.W. Schwingshackl, L. Di Mare, G. Cerri, and D. Dini. Optimal placement of piezoelectric plates for active vibration control of gas turbine blades: Experimental results. In *Proceedings of SPIE - The International Society for Optical Engineering*, 2012.

[36] H. Irschik. A review on static and dynamic shape control of structures by piezoelectric actuation. *Engineering Structures*, 24:5–11, 2002.

[37] P. Binette, M.L. Dano, and G. Gendron. Active shape control of composite structures under thermal loading. *Journal of Intelligent Material Systems and Structures*, 18(2):1–12, 2009.

[38] A. Chellabi, Y. Stepanenko, and S. Dost. Optimal active control of a deformable mirror. *Journal of Vibration and Control*, 15(3):415–438, 2009.

[39] M. Shaik Dawood, L. Iannucci, and E. Greenhalgh. Three-dimensional static shape control analysis of composite plates using distributed piezoelectric actuators. *Smart Materials and Structures*, 17:1–10, 2008.

[40] Y.R. Hu and G. Vukovich. Active robust shape control of flexible structures. *Mechatronics*, 15:807–820, 2005.

[41] Q. Luo and L. Tong. A sequential linear least square algorithm for tracking dynamic shapes of smart structures. *International journal for numerical methods in engineering*, 67:66–88, 2006.

[42] A. Punhani. *Shape and vibration control of smart laminated plates*. PhD thesis, Ohio State University, 2008.

[43] R. Kudikala, D. Kalyanmoy, and B. Bhattacharya. Multi-objective optimization of piezoelectric actuator placement for shape control of plates using genetic algorithms. *Journal of Mechanical Design*, 131:091007, 2010.

[44] V. Gupta, M. Sharma, and N. Thakur. Optimization criteria for optimal placement of piezoelectric sensors and actuators on a smart structure: A technical review. *Journal of Intelligent Material Systems and Structures*, 21:1227–1243, 2010.

[45] S.L. Padula and R.K. Kincaid. *Optimization strategies for sensor and actuator placement*. Citeseer, 1999.

[46] M.I. Frecker. Recent advances in optimization of smart structures and actuators. *Journal of Intelligent Material Systems and Structures*, 14:207–216, 2003.

[47] S. Liu, L. Tong, and Z. Lin. Simultaneous optimization of control parameters and configurations of PZT actuators for morphing structural shapes. *Finite Elements in Analysis and Design*, 44(417-424), 2008.

[48] K. Ramesh Kumar and S. Narayanan. Active vibration control of beams with optimal placement of piezoelectric sensor/actuator pairs. *Smart Materials and Structures*, 17, 2008.

[49] A.H. Daraji and J.M. Hale. Active vibration reduction of a flexible structure bonded with optimized piezoelectric pairs using half and quarter chromosomes in genetic algorithms. *Journal of Physics: Conference Series*, 382:1–6, 2012.

[50] W. Li, X. Li, Z. Zhao, Y. Wang, and Y. Zhao. Optimal piezoelectric sensors and actuators deployment for active vibration suppression of satellite antenna reflector. *Advanced Materials Research*, 479-481(7):1490–1494, 2012.

[51] M. Tianbing and D. Fei. Simultaneous optimization of smart beam structure for vibration control based on chaos particle swarm algorithm. *Applied Mechanics and Materials*, 101-102:356–359, 2012.

[52] D. Marinova. Finite element formulation for analysis and shape regulating of plates with laminated piezoelectric material. *Mechanics of Advanced Materials and Structures*, 16:224–235, 2009.

[53] Q. Luo and L. Tong. High precision shape control of plates using orthotropic piezoelectric actuators. *Finite Elements in Analysis and Design*, 42:1009–1020, 2006.

[54] C. Chee, L. Tong, and G.P. Steven. Piezoelectric actuator orientation optimization for static shape control of composite plates. *Composite Structures*, 55:169–184, 2002.

[55] F. Andoh, G. Washington, and V. Utkin H.S. Yoon. Efficient shape control of distributed reflectors with discrete piezoelectric actuators. *Journal of Intelligent Material Systems and Structures*, 15(1):3–15, 2004.

[56] Y. Yu, X.N. Zhang, and S.L. Xie. Optimal shape control of a beam using piezoelectric actuators with low control voltage. *Smart Materials and Structures*, 18:1–15, 2009.

[57] D. Sun and L. Tong. Design optimization of piezoelectric actuator patterns for static shape control of smart plates. *Smart Materials Structures*, 14:1353–1362, 2005.

[58] S. Liu and Z. Lin. Integrated design optimization of voltage channel distribution and control voltages for tracking the dynamic shapes of smart plates. *Smart Materials and Structures*, 19:1–8, 2010.

[59] V.K. Gupta. Modified approach for optimum position and sizing of piezoelectric actuator for steering of parabolic antenna. *Structural Longevity*, 6(2):65–75, 2011.

[60] Z. Kang and L. Tong. Topology optimization-based distribution design of actuation voltage in static shape control of plates. *Computers and structures*, 86(19):1885–1893, 2008.

[61] A. Sadri, J. Wright, and R. Wynne. Modeling and optimal placement of piezoelectric actuators in isotropic plates using genetic algorithms. *Smart Materials and Structures*, 8:490–498, 1999.

[62] A. Hac and L. Liu. Sensor and actuator location in motion control of flexible structures. *Journal of Sound Vibration*, 167:239–261, 1993.

[63] K.D. Dhuri and P. Seshu. Piezoactuator placement and sizing for good control effectiveness and minimal change in original system dynamics. *Smart Materials and Structures*, 15:1661–1672, 2006.

[64] Q. Wang and C.M. Wang. Optimal placement and size of piezoelectric patches on beams from the controllability perspective. *Smart Materials and Structures*, 9:558–567, 2000.

[65] Z.C. Qiua, X.M. Zhang, H.X. Wub, and H.H. Zhang. Optimal placement and active vibration control for piezoelectric smart flexible cantilever plate. *Journal of Sound and Vibration*, 301:521–543, 2007.

[66] F. Peng, A. Ng, and YR. Hu. Actuator placement optimization and adaptive vibration control of plate smart structures. *Journal of Intelligent Material Systems and Structures*, 16:263, 2005.

[67] X. Zhang and A.G. Erdmann. Optimal placement of piezoelectric sensors and actuators for controlled flexible linkage mechanisms. *Journal of Vibration and Acoustics- Transactions of the ASME*, 128(22):56–60, 2006.

[68] R. Dutta, R. Ganguli, and V. Mani. Swarm intelligence algorithms for integrated optimization of piezoelectric actuator and sensor placement and feedback gains. *Smart Materials and Structures*, 20:1–14, 2011.

[69] C. Nam, Y. Kim, and TA. Weisshaar. Optimal sizing and placement of piezo-actuators for active flutter suppression. *Smart Materials and Structures*, 5:216, 1996.

[70] M.A. Demetriou. A numerical algorithm for the optimal placement of actuators and sensors for flexible structures. In *American Control Conference (ACC)*, 2000.

[71] K.A. Morris. Linear-quadratic optimal actuator location. *IEEE Transactions on Automatic Control*, 56:113–124, 2011.

[72] H.H. Ning. Optimal number and placements of piezoelectric patch actuators in structural active vibration control. *Engineering Computations*, 21:651–665, 2004.

[73] R. Barboni, A. Mannini, E. Fantini, and P. Gaudenzi. Optimal placement of PZT actuators for the control of beam dynamics. *Smart Materials and Structures*, 9:110–120, 2000.

[74] Y.K. Kang, H.C. Park, W. Hwang, and K.S. Han. Optimum placement of piezoelectric sensor/actuator for vibration control of laminated beams. *AIAA Journal*, 34:1921–1926, 1996.

[75] Y. Yang, Z. Jin, and C. Kiong Soh. Integrated optimal design of vibration control system for smart beams using genetic algorithms. *Journal of Sound and Vibration*, 282:1293–1307, 2005.

[76] F. Seeger and U. Gabbert. Optimal placement of distributed actuators for a controlled smart elastic plate. *PAMM*, 2:262–263, 2003.

[77] S. Da Silva, V.L. Junior, and M.J. Brennan. Design of a control system using linear matrix inequalities for the active vibration control of a plate. *Journal of Intelligent Material Systems and Structures*, 17:81–93, 2006.

[78] D. Kasinathan and K. Morris. Convergence of h_∞ optimal actuator locations. In *ADecision and Control and European Control Conference (CDC-ECC)*, 2011.

[79] F. Bachmann, A.E. Bergamini, and P. Ermanni. Optimum piezoelectric patch positioning: A strain energy-based finite element approach. *Journal of Intelligent Material Systems and Structures*, 23(14):1575–1591, 2012.

[80] J.S. Moita, P.G. Martins, C.M. Mota Soares, and C.A. Mota Soares. Optimal dynamic control of laminated adaptive structures using a higher order model and a genetic algorithm. In *II ECCOMAS THEMATIC Conference on Smart Structure and Materials*, 2005.

[81] Y.J. Cha, A.K. Agrawal, Y. Kim, and A.M. Raich. Multi-objective genetic algorithms for cost-effective distributions of actuators and sensors in large structures. *Expert Systems with Applications*, 39:7822–7833, 2012.

[82] S. Hanagud, M.W. Obal, and A.J. Calise. Optimal vibration control by the use of piezoceramic sensors and actuators. *Journal of Guidance, Control, and Dynamics*, 15(5):1199–1206, 1992.

[83] I. Bruant, L. Gallimard, and S. Nikoukar. Optimal piezoelectric actuator and sensor location for active vibration control, using genetic algorithm. *Journal of Sound and Vibration*, 329:1615–1635, 2010.

[84] I. Bruant, L. Gallimard, and Sh. Nikoukar. Optimization of piezoelectric sensors location and number using a genetic algorithm. *Mechanics of Advanced Materials and Structures*, 18:469–475, 2011.

[85] E.B. Flynn and M.D. Todd. Optimal placement of piezoelectric actuators and sensors for detecting damage in plate structures. *Journal of Intelligent Material Systems and Structures*, 21:265–274, 2010.

[86] A.A. Rader, F.F. Afagh, A. Yousefi-Koma, and D.G. Zimcik. Optimization of piezoelectric actuator configuration on a flexible fin for vibration control using genetic algorithms. *Journal of Intelligent Material Systems and Structures*, 18:1015–1033, 2007.

[87] A. Montazeri, J. Poshtan, and A. Yousefi-Koma. The use of 'particle swarm' to optimize the control system in a PZT laminated plate. *Smart Materials and Structures*, 17, 2008.

[88] A.K. Rao, K. Natesan, B.M. Seetharama, and R. Ganguli. Experimental demonstration of H_∞ control based active vibration suppression in composite fin-tip of aircraft using optimally placed piezoelectric patch actuators. *Journal of Intelligent Material Systems and Structures*, 19(6):651–669, 2008.

[89] A.R. Mehrabian and A. Yousefi-Koma. A novel technique for optimal placement of piezoelectric actuators on smart structures. *Journal of the Franklin Institute*, 348:12–23, 2011.

[90] A.R. Mehrabian and A. Yousefi-Koma. Optimal positioning of piezoelectric actuators on a smart fin using bio-inspired algorithms. *Aerospace Science and Technology*, 11:174–182, 2007.

[91] T. Yi, X. Zhang, and H. Li. Modified monkey algorithm and its application to the optimal sensor placement. *Applied Mechanics and Materials*, 178:2699–2702, 2012.

[92] Xin-She Yang. Harmony search as a metaheuristic algorithm. In *Music-inspired harmony search algorithm*, pages 1–14. Springer, 2009.

[93] O.A. Vanli, C. Zhang, A. Nguyen, and B. Wang. A minimax sensor placement approach for damage detection in composite structures. *Journal of Intelligent Material Systems and Structures*, 23(8):919–932, 2012.

[94] M. Guney and E. Eskinat. Optimal actuator and sensor placement in flexible structures using closed-loop criteria. *Journal of Sound and Vibration*, 312:210233, 2008.

[95] K.K. Chen and C.W. Rowley. H_2 optimal actuator and sensor placement in the linearized complex Ginzburg-Landau system. *Journal of Fluid Mechanics*, 681:241260, 2011.

[96] K. Hiramoto, H. Doki, and G. Obinata. Optimal sensor/actuator placement for active vibration control using explicit solution of algebraic riccati equation. *Journal of Sound and Vibration*, 229(5):10571075, 2000.

[97] AC. Lee and ST. Chen. Collocated sensor/actuator positioning and feedback design in the control of flexible structure system. *Transactions of the ASME. Journal of Vibration and Acoustics*, 116:146–154, 1994.

[98] A. Suchariyono, N.S. Goo, and H.C. Park. Use of lightweight piezo–composite actuators to suppress the free vibration of an aluminum beam. *Journal of Intelligent Material Systems and Structures*, 19(1):101–112, 2008.

[99] B.N. Agrawal and K.E. Treanor. Shape control of a beam using piezoelectric actuators. *Smart Materials and Structures*, 8:729–740, 1999.

[100] M. Yocum and H. Abramorich. Static behavior of piezoelectric actuated beams. *Computers and Structures*, 80:17971808, 2002.

[101] R. Potami. *Optimal sensor/actuator placement and switching schemes for control of flexible structures*. PhD thesis, Worcester Polytechnic Institute, 2008.

[102] K.A. Morris. *An Introduction to Feedback Controller Design*. Harcourt-Brace Ltd., 2001.

[103] J. Nocedal and S.J. Wright. *Numerical Optimization*. Springer, 2nd edition, 2006.

[104] C.A. Floudas. *Nonlinear and mixed-integer programming - fundamentals and applications*. Oxford University Press, 1995.

[105] R.K. Brayton, S.W. Director, and G.D. Hachtel. A new algorithm for statistical circuit design based on quasi-newton methods and function splitting. *IEEE Transactions on Circuits and Systems*, 26(9):784–794, 1979.

[106] S. Narayanan and V. Balamurugan. Finite element modeling of piezolaminated smart structures for active vibration control with distributed sensors and actuators. *Journal of Sound and Vibration*, 262:529–562, 2003.

[107] H.T. Banks, R.C. Smith, and Y. Wang. *Smart material structures: modeling, estimation, and control*. Wiley, 1996.

[108] N. Darivandi, K.A. Morris, and A. Khajepour. LQ optimal actuator location in structures. In *American Control Conference (ACC)*, 2012.

[109] N. Darivandi, K. Morris, and A. Khajepour. An algorithm for LQ optimal actuator location. *Smart Materials and Structures*, 22(3), 2013.

[110] N. Darivandi, K. Morris, and A. Khajepour. Optimal shape control of active beams. *Submitted to IEEE Conference on Decision and Control*.

[111] N.C. Shieh, K.Z. Liang, and C.J. Mao. Robust output tracking control of an uncertain linear system via a modified optimal linear-quadratic method. *Journal of Optimization Theory and Applications*, 117:649–659, 2003.

[112] J. Klamka. *Controllability of Dynamical Systems*. Kluwer Academic Publisher, 1991.

[113] A.K. Chopra. *Dynamics of Structures*. Prentice Hall, 2001.

[114] B.D.O. Anderson and J.B. Moore. *Optimal Control: Linear Quadratic Methods*. Prentice-Hall, 1990.

[115] O.C. Zienkiewicz and R.L. Taylor and. *The Finite Element Method for Solid and Structural Mechanics*. Butterworth-Heinemann, 1934.